# Doctoral Dissertation

## Analysis of Beach Nourishment Effect using Artificial Intelligence

Hyun Dong Kim

July 2020

Graduate School of Engineering
Department of Civil Engineering

Osaka University

## ACKNOWLEDGMENTS

First and foremost, I wish to express my utmost gratitude to Professor Shin-ichi Aoki, my academic supervisor, for his remarkable guidance and moral support. He has been an advisor and mentor during my Ph.D. studies at Osaka University. His generosity helped make my time at Osaka University enjoyable. I would also like to thank Professor Araki, Professor Sasaki, Professor Nishida, and Professor Irie from Osaka University and Professor Kobayashi from the University of Delaware for their time and effort to make constructive comments researches.

My appreciation also extends to my team and colleagues from my previous company, Mirae Ocean Corporation, and Osaka University. Special thanks to President Jinho Kim and Director Kisu Kwak for their generosity and support. I also thank my successor Byungsun Cho, Jinwoo Jung, and all of my team members. Their cooperation launched a great part of this dissertation. As a team manager, I had so many great experiences and memories built with them. I also thank Muhajjir and Mon for their kindness and support at Osaka University.

Last but not least, I must thank my family for helping me become who I am now as an individual and as an aspiring scholar in this field. I am forever indebted to my parents, Kyu Han Kim and Myung Hyon Jung, for everything that they have sacrificed for and given me. I would also thank my sister Hyun Jung, brother in law Junik, and their newborn baby, Theo.

This study was partially supported by the Mirae Ocean Corporation and Waterfront and Coastal Research Center in Korea. Grand Award was awarded for part of my research by the Korea Basic Science Institute under the Ministry of Science and ICT of Korea, and the prize funds were used for the later experiments of this study.

## TABLE OF CONTENTS

## LIST OF TABLES

## LIST OF FIGURES

## ABSTRACT

Global warming causes a rise in the sea level, thereby aggravating beach erosion and overtopping on many beaches. When erosion occurs, sand beaches cannot maintain sufficient sand width, and foreshore slopes become steeper from frequent erosion effects, and beaches are trapped in a vicious circle of becoming vulnerable due to incident waves. For this reason, beach nourishment can be used as a countermeasure which simultaneously minimizes environmental impacts. However, beach nourishment is not a permanent solution and requires periodic renourishment after several years. To address this problem, minimizing the period of renourishment must be an economical alternative. In this respect, selecting the optimum grain size of the sand of the beach nourishment is essential.

Numerous previous studies have found that larger grain-sized sand is more resistant to the erosion that using gravel for the nourishment and can extend the period of renourishment. In addition to selecting the optimum grain size of the sand nourishment, determining the durability and maintaining the familiarity of the native sand users should also be considered. Thus, the gravel nourishment can be an optimum method.

Among many gravel nourished beaches, Tuvalu (one of the Pacific island nations facing the threat of disappearing from erosion) is a great example of reducing erosion from storm waves. Under extreme wave conditions, other parts of the Tuvaluan coast massively lost their shoreline; however, the section with gravel nourishment had its damage appreciably less as compared to other nourished areas. In the present study, using the Tuvaluan coast with its cross-sectional of gravel nourishment site, four different test cases with one extra test case were selected for the hydraulic model

experiment aimed at discovering an effective nourishment strategy find the effective alternative methods. Two types with different mean diameters, sand and coral gravel, were used throughout the experiments in a wave flume.

Numerical simulations were performed to reproduce the gravel nourishment; however, none of such models simultaneously simulate the sediment transport of gravel and sand. Thus, the artificial neural networks (ANN), a deep-learning model, was developed throughout the study using hydraulic model experiments as training datasets to analyze its possibility to simultaneously accomplish the sediment transport of the sand and gravel and supplement the shortcomings of the numerical models.

# Chapter 1

# INTRODUCTION

## 1.1 Background

Coastal erosion has natural causes such as sea-level rise and wave energy increase; however, it is accelerated by changes in the natural environment from various artificial structures installed on the coast. Coastal zones are significant for society's development; however, they are particularly vulnerable to the impacts of nature and man and are physically very unstable. Erosion and associated loss of land is the most evident sign of this instability. Negative shoreline trends cause secondary effects that affect society through threats to human settlement. However, most of the natural sandy beach is not sufficient to protect the beach itself against extreme wave and storm surge from the beach erosion. Thus, coastal structures can be used in these erosive beaches.

Coastal structures are generally built at the locations where beach erosion causes a severe problem. The decision to build a coastal structure should be based on a thorough analysis of the shoreline developments in the past and estimated events in the future. The physical processes causing erosion should be properly identified. For the coastal protections, there are mainly two categories: hard techniques and soft techniques. Hard methods include seawalls, revetments, or jetties that can be effective, which intercept and dissipate the wave energy and currents and associated sand transport.

Nonetheless, these hard structures may enhance erosion in such areas and collapse, which results in high construction and maintenance costs. On the other hand, soft methods aim to dissipate wave energy using natural coastal processes. In this way,

coastal defense works in sympathy with natural means of sediment erosion, storage, and transport. This results in a low maintenance coastal system that can respond to external forcing factors such as storms and sea-level rise.

The erosion of the world's coasts and sand storage to mitigate beach erosion are leading to the increasingly common use of gravel for coastal protection and beach nourishment (Lopez et al., 2017). Beach nourishment, as a soft technique, can be used as a countermeasure for the erosion problem while minimizing the environmental impacts. However, beach nourishment is not a permanent solution like most soft techniques and needs periodic renourishment after several years. Beach nourishment incorporates a series of beach renourishment over a long-time horizon or life cycle of an application. This fact poses difficulties in predicting benefits and costs because of both uncertain project performance and future markets for necessary inputs. Sand is the most critical input. And with demand for sand increasing, it is difficult to predict the cost of sand a decade or more into the future (National Research Council, 1995; Davison et al., 1992; Houston, 1991). Thus, reducing the period of renourishment is essential, and therefore, it is crucial to slow down the erosion by careful planning of the nourishment to remain prolonged period. That being said, larger grain-sized sand is more resistant to erosion (Wieser, 1953), and many beaches around the world proved the usage of these gravels as a nourishment material to a lengthen the period of renourishment.

Jinkoji coast in Japan (Figure 1.1) had gravel nourishment in April 2008, using 87,000 $m^3$ of gravel size between 2.5 to 13 mm. It was found that the nourishment gravel was deposited with a slope of 1:8 at the foot of the seawall, and provided some protection from the erosion, effective in widening the foreshore and nourishment gravel

was stably deposited without offshore discharge (Kumada et al., 2010). Another beach, Marina di Pisa, Tuscany in Italy (Figure 1.2), gravel nourishment was used in 2002 as a countermeasure to protect a seawall and provide a beach on an eroding, developed, sandy shore. Gravel beach could protect coastal infrastructure and produce a surface usable for tourist activity. The movement of gravel offshore was not likely observed; however, the beach may become re-oriented toward the direction of high-energy wave approach, resulting in a narrowing of the berm in one segment, causing waves to overtop the seawall and deposit gravel landward of it (Cammelli et al., 2006). While gravel nourishment act as a significant role as beach protection, it can be inefficient if the phenomena prediction of the gravel nourishment was not analyzed well before the nourishment like Nice bay in France (Figure 1.3). On this beach, very little significant change over the last 30 years despite massive gravel nourishment amounting to 558,000 $m^3$. It was not possible to lengthen the foreshore; however, gravel nourishment in Nice beach is an essential means of containing the beach erosion hazard, at least contributing to stabilizing the beach widths (Cohen and Anthony, 2007). Lastly, Fongafale shore in Funafuti, Tuvalu (Figure 1.4), used gravel nourishment to protect the coast from erosion. Since Tuvalu is a Pacific island nation, locally available coral gravel was procured as a nourishment material. This was the first trial of a user- and eco-friendly type of coastal conservation measure in Pacific Island nations. The executed gravel beach nourishment could maintain stability under seasonal and extreme conditions of wave actions (Onaka et al., 2017).

Figure 1.1: Gravel nourished Jinkoji coast in Japan (Kumada et al., 2010)

Figure 1.2: Gravel nourished Marina Di Pisa beach in Italy (Cammeli et al., 2010)

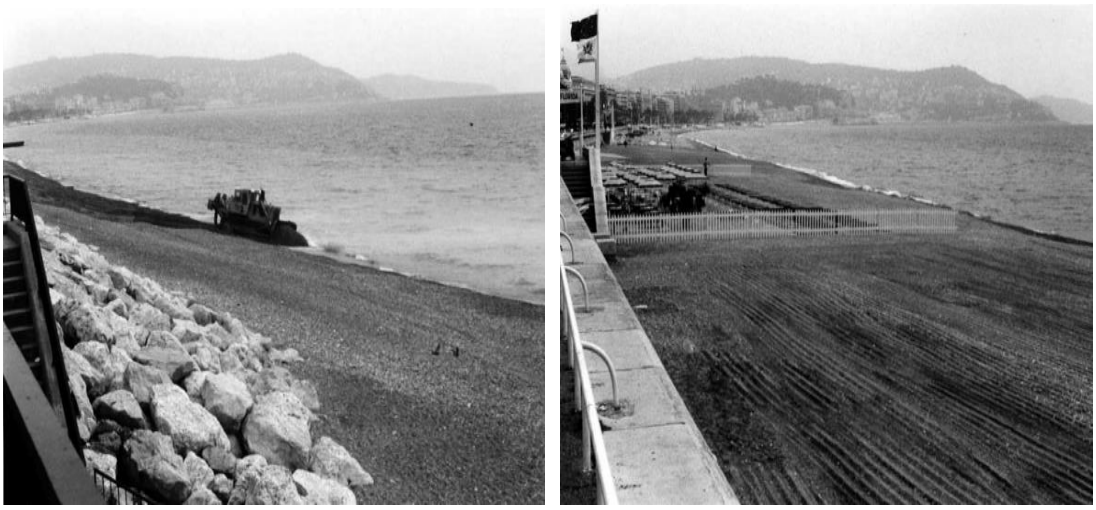

Figure 1.3: Gravel nourished Nice bay in France (Cohen and Anthony, 2007)

Figure 1.4: Gravel nourished Funafuti shore in Tuvalu (Onaka et al., 2017)

Although there are many successful cases using gravel nourishment as good protection, the gravel nourishment cannot be the permanent solution for the erosion (Daves et al., 2000; Ishikawa et al., 2012). The periodic renourishment is needed; however, lengthening the period is essential for both economic and environmental purposes. Throughout this paper, gravel nourishment will be discussed, and different placement methods and numerical simulations were used to simulate the beach profile evolution and sediment transport. Because current models cannot accurately predict the two or more-sediment usage (like gravel nourishment), these shortcomings were tried to overcome by using artificial deep learning neural networks. Thus, throughout the study, artificial neural networks have been used to simulate the nourished gravel beach with different test cases using the datasets obtained from the hydraulic model experiments to remedy numerical simulations' shortcomings.

## 1.2 Goals and objectives of the study

The flow of the research is described in this section. This thesis consists of five different chapters, chapter 1. Introduction, chapter 2. Field measurement and necessary data investigation, chapter 3. Experiment, chapter 4. Numerical simulations and artificial intelligence, and lastly, chapter 5 with conclusions and discussions.

In chapter 2, the study site was described with historical background. To understand the underlying causes of beach erosion and site-specific morphology after the nourishments to quantify the nourishment performance, bathymetric survey, topographic survey, and wave observation were conducted in the study site, Funafuti, Tuvalu. Gravel nourished areas found to be the protective sections among other sand nourished sections, and from the simple wave test using SWAN, all the sections affect similar wave heights during abnormal wind conditions (e.g., cyclones).

To elucidate the interaction processes, a hydraulic model experiment was conducted, as explained in detail in Chapter 3. Overview of experiment setup, sand profiles, and characteristics of gravel used in the experiment was explained. Four different nourishment styles (Sand berm and beach (SBB), Gravel berm and sand beach (GBS), Buried gravel layer (BGL), and Buried gravel sill (BGS)) with one extra test case (Gravel bag layer (GBL)) were conducted to find out best methods amongst.

Chapter 4 introduces existing cross-shore numerical models (CSHORE, SBEACH, and XBEACH-G) and predict sand transport in the swash zone. Because of the current model's limitation, the artificial neural networks model was introduced and developed to make it suitable to beach profile evolution prediction using various features with datasets obtained from chapter 3.

Lastly, in chapter 5, the results of the overall experimental findings and discussions were briefly summarized.

# Chapter 2

# FIELD MEASUREMENT AND BASIC DATA INVESTIGATION

## 2.1 Introduction

Tuvalu has been chosen as a study site. Sea-level rise has become increasingly evident in the Pacific, with the southwestern Pacific regarded as one of the region's most vulnerable to contemporary and future changes (Nicholls and Cazenave, 2010). Tuvalu, as shown in Figure 2.1, is one of these pacific island nations suffer from rising sea levels, which aggravate beach erosion and wave overtopping. Nonetheless, this country is faced with the threat of disappearing as rising sea levels cause beach erosion; however, it is challenging to build study constructions on Pacific islands due to their locations far from developed countries, making installation difficult. For this reason, Tuvalu has been chosen as a study site. Moreover, this country does the nourishment constantly to prevent erosion, and thus, finding the phenomena of the nourishment was one of the keys to this study.

To gain more complete understanding of the underlying causes of beach erosion and site-specific morphology after the nourishments to quantify the nourishment performance, bathymetric, topographic survey along with UAV survey have been conducted. To understand the normal conditions of wave characteristics, wave and tidal observation have been conducted as well. It is important to conduct a survey to obtain the latest information on study site to observe the recent erosion status as well as use them as input of a numerical simulation to find the erosive wave conditions (10 or 50 year return period waves) and use the wave conditions on hydraulic model experiments to reproduce the erosive wave conditions to compare each nourishment placement methods for efficiency. Surveys were conducted during November 2017 to December 2017. As shown in a Table 2.1, the scope of each survey and observation are listed.

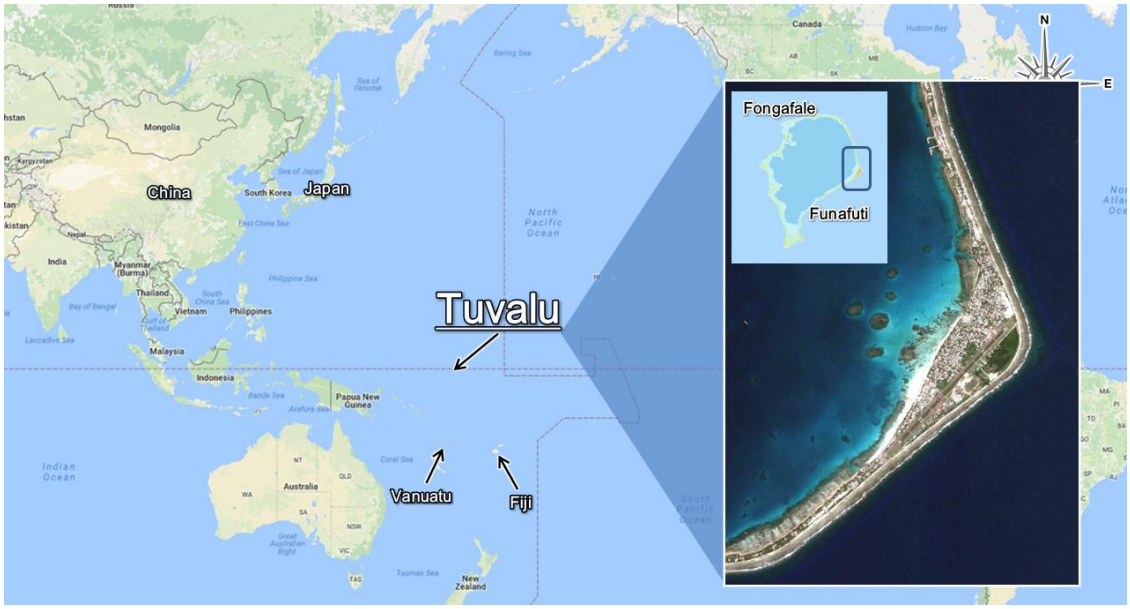


Figure 2.1: Survey location, Funafuti in Tuvalu

Table 2.1: Scope of the survey

| Division | | Target of survey | Scope | Note |
|---|---|---|---|---|
| Leveling and GCP survey | | Fongafale shore | 10 EA | Direct Leveling |
| Topographic Survey | Status Survey | Fongafale region | A=250,000 $m^2$ | Ground survey |
| | UAV Survey | Fongafale | A=250,000 $m^2$ | |
| Bathymetric Survey | | Fongafale shore | L= 280 km | Detailed: 20 m pitch |
| Wave and Tide Observation | | Fongafale shore | 20 days observation | |

## 2.2 Wave and Tide Observation

The wave and tide observations aim to verify the existing tidal data observed at the study site and analyze the characteristics of the wave at the lagoon area of Fongafale shore. Later in this chapter, results were used in SWAN model to see the normal and abnormal wave conditions (wave height and period) and its deformation. For the observations, wave pressure gauge was installed in a point located in Figure 2.2 around 2 km from the Fongafale shore on lagoon side from November 16th to December 5th, total 20 days. Throughout the observation, the wave pressure gauge manufactured by AAT in Korea was used (WTG-IC256), which is based on the IC pressure sensor. The observed data were acquired for 20 days with 30 min intervals.

Collected data were analyzed by Zerocross analysis to yield significant wave height ($H_{1/3}$), significant wave period ($T_{1/3}$), 1/10 maximum wave height ($H_{1/10}$), maximum wave period ($T_{1/10}$), mean wave height ($H_{mean}$), mean wave period ($T_{mean}$), and peak wave directions (Dp). The observation location's significant wave height was in the range of 0.09~0.25m, with an average value of 0.13m. The maximum wave height ($H_{max}$) was in the range of 0.13~0.91m, with an average value of 0.31m. The significant wave period ($T_{1/3}$) was in the range of 5.25~14.03sec with an average value of 7.77sec, and the maximum wave period ($T_{max}$) was in the range of 3.00~13.73sec with an average value 5.28 sec as shown in Table.2.3.


Figure 2.2: Wave and tide observation

Table 2.2: Specifications of the wave and tide observation

| Site (WGS84) | Duration | Depth (DL(-)m) | Device |
|---|---|---|---|
| 8° 30' 36" S<br>179° 11' 08" E | 2017. 11. 16~<br>2017. 12. 05 | 2.34 | WTG-256 |

Table 2.3: Observed wave characteristics in Fongafale

| Specifications | $H_{1/3}$ | $H_{1/10}$ | $H_{mean}$ | $H_{max}$ | $T_{1/3}$ | $T_{1/10}$ | $T_{mean}$ | $T_{max}$ |
|---|---|---|---|---|---|---|---|---|
| | (m) | | | | (sec) | | | |
| Max | 0.25 | 0.44 | 0.14 | 0.91 | 14.03 | 10.34 | 13.83 | 13.73 |
| Min | 0.09 | 0.11 | 0.04 | 0.13 | 5.25 | 4.29 | 5.26 | 3.00 |
| Mean | 0.13 | 0.20 | 0.07 | 0.31 | 7.77 | 5.75 | 8.37 | 5.28 |

The wind data of Fongafale from the Australian Bureau of Meteorology during the same period was in the range of 0.2~8.2 m/s, and the data were compared with the observed data. By comparing the two results, a similar trend was observed. The wave characteristics of the study area surrounded by the atoll were analyzed to be strongly affected by the wind. This area is lagoon area where it is difficult for deep-sea waves to reach, and the lagoon has a distance of 17 km which makes harder for deep-sea waves affecting the shoreline without having wind waves. Wind speed during November 16$^{th}$ to December 5$^{th}$ is observed and analyzed in Figure 2.3 and wave characteristics are observed and analyzed in Figure 2.4.

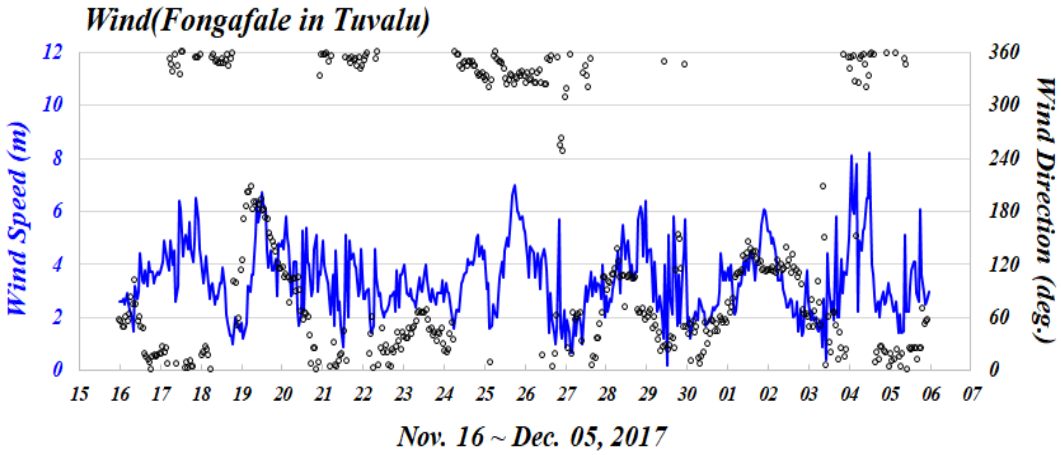


Figure 2.3: Wind data during the observation

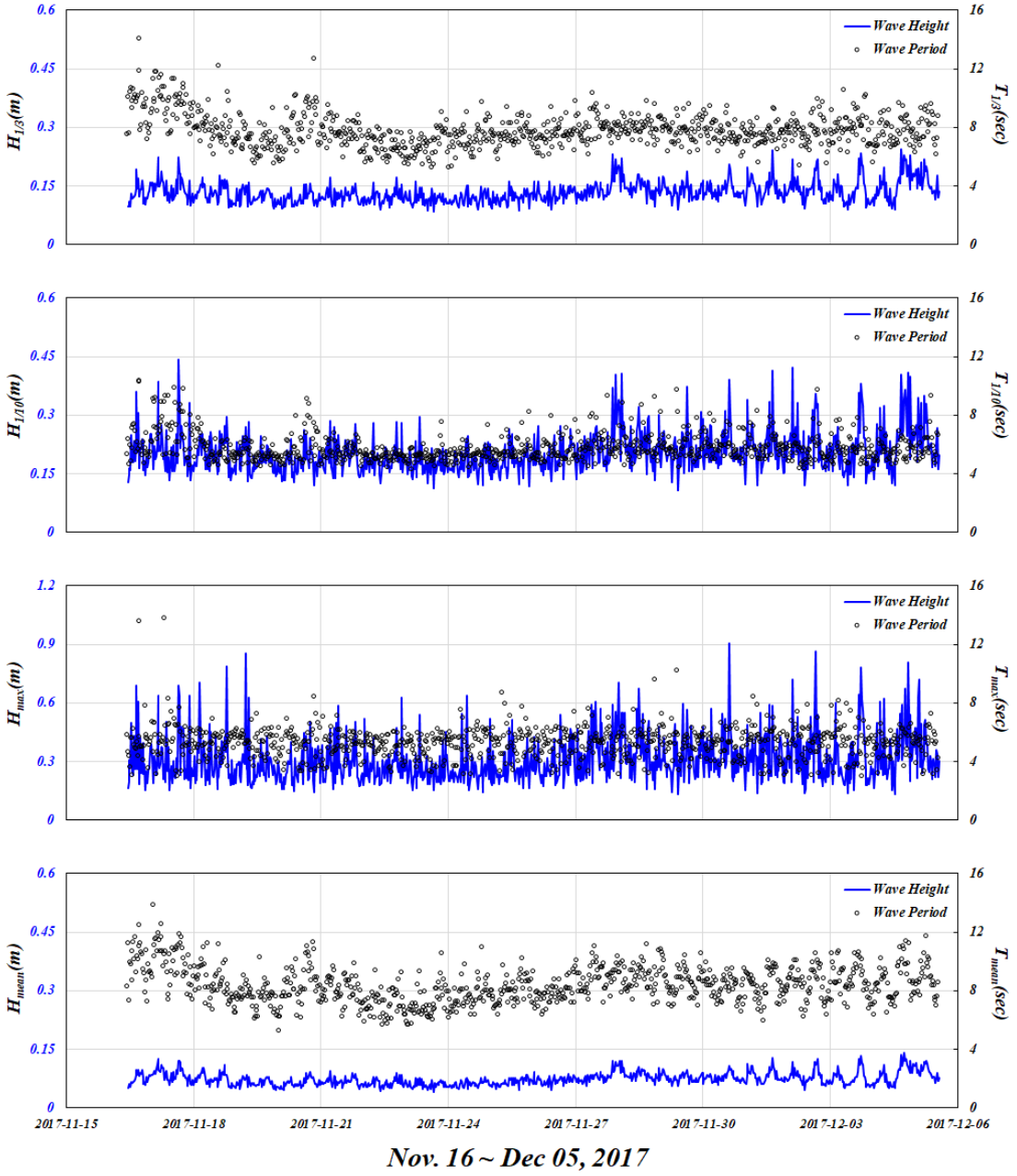


Figure 2.4: Time series of wave height and period

As a result of analyzing wind data observed for 24 years by the Australian Bureau of Meteorology from 1993 to 2017 at the Funafuti, Tuvalu (Figure 2.5), Tuvalu's lowest annual average wind speed was 2.8m/sec, and the highest annual average wind speed was 4.3m/sec. The yearly average wind speed during the observation period was 3.3 m/sec, and the annual average wind speed was increased by 2.8 cm/sec every year and was increased by 60 cm/sec for 24 years.

Tropical cyclones do not occur much in equatorial regions within 5 degrees of latitude; however, Tuvalu is located in 8-degree latitude that the number of invasions of a cyclone which is directly affected is less than once per year. Due to Tuvalu’s low and narrow topographical characteristics, it is very vulnerable to storm wave and has a great deal of damage. Recent cyclones (shown in Table 2.4) affected Tuvaluan coast which caused beach erosion and flooding problems. Because of having wind dominant wave conditions, these storms cause tremendous damages to the Tuvaluan coast.

Table 2.4: Recent cyclones impacted Tuvalu

| Cyclone | Category | Dates | Affected area |
|---|---|---|---|
| Winston | Category 5 Severe Tropical Cyclone | Feb 7, 2016~ March 3, 2016 | Fiji, Vanuatu, Tonga, Queensland |
| Pam | Category 5 Hurricane | Mar 7, 2015~ Mar 20, 2015 | New Zealand, Fiji, Papua New Guinea, New Caledonia, Vanuatu, Tuvalu, Kiribati, Solomon Island |
| Ula | Category 4 Severe Tropical Cyclone | Feb 26, 2015~ Jan 16, 2016 | Tonga, Tuvalu, American Samoa |
| Gitta | Category 5 Severe Tropical Cyclone | Feb 3, 2018~ Feb 22, 2018 | New Zealand, Fiji, Samoa, Tonga, Vanuatu, Queensland, American Samoa |

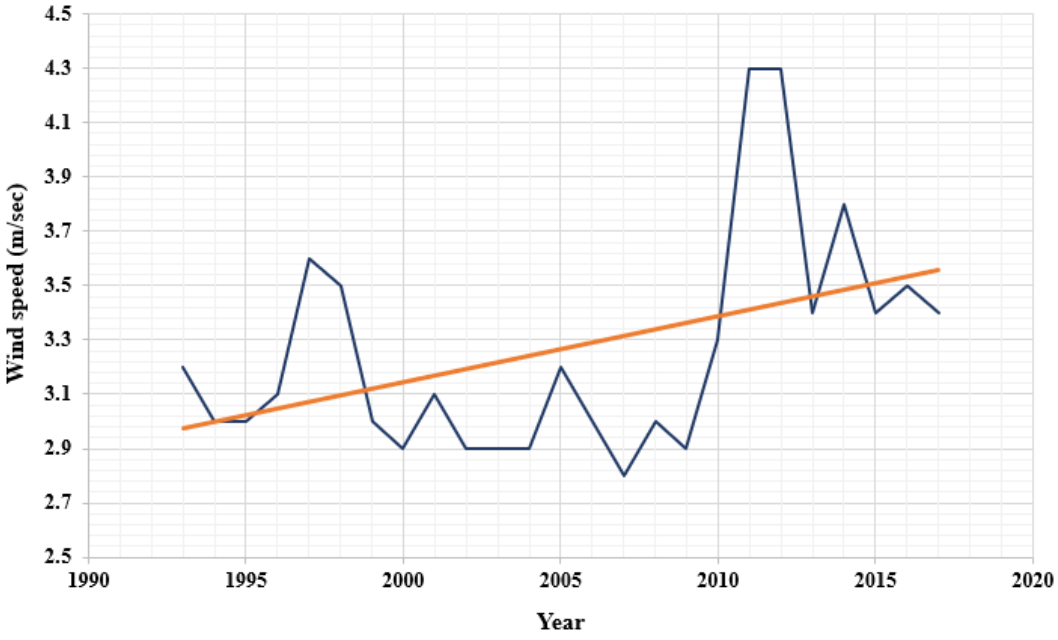


Figure 2.5: Average annual wind speed in Tuvalu (1993~2017)

To compare the observed tide data with obtained tide data from the Australian Bureau of Meteorology, tide observation was conducted from November 16th to December 5th, 2017, with the same period of wave observation. Observed tide data shows a minimum of -0.92 m and a maximum of +1.21 m with the tide difference of 0.29 m. For the same duration, the Australian Bureau of Meteorology data shows a minimum of -0.96 m and a maximum of +1.12 m and difference of 0.26 m as shown in Figure 2.6 with the tide elevation time series. By comparing the two data, it was considered that the existing tide observation data could be applied in the numerical simulations since the difference was minimal.

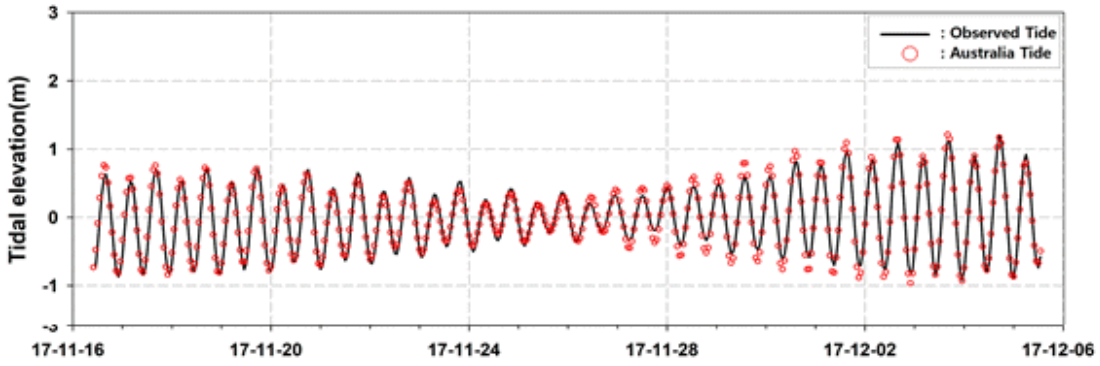


Figure 2.6: Observed tide comparison with that of the Australian Bureau of Meteorology

Again, from the observed data, Fongafale shore, surrounded by atoll, has less impact on deep-sea water waves and mostly affected by the wind wave. That being said, the Tuvaluan coast is considered as a low-wave energy coast that the beaches would be vulnerable to the storm sized wind wave.

## 2.3 Topographic Survey

A topographic survey was performed by a 3D station using Total Station, GPS instrument RTK (GNSS), and used to survey geographical features, boundary exposed in the area to observe the coordinate information, and produce it in the form of numerical data. RTK survey used a combination measurement of station's GPS receiver, and two mobile station's GPS receiver with one controller. Coordinates and heights were determined using control points directly provided by the Tuvalu Government's PMU project manager, and the drawing elements could be edited freely. Drawing display functions enable marking of geographical features, and prevents overlapping of the current line and contour lines.

Total Station and RTK(GNSS) were used for the topographic survey, and terrain composition was created. A drone measurement was carried out outside the task area and marked on the drawings to identify the surrounding topography. All the conducted survey areas were larger than a task area to improve the survey performances. The maximum elevation of the topographic survey result was (+) 8.72m, measured from the east side of Fongafale to the north side of runway near the Mainaga Fou Church, where the runway was composed with the dunes. Moreover, the lagoon side zone has (+) 4.53m elevation near the community church, and the ocean side zone has (+)5.17m elevation near the harbor container.

UAV survey and comparison with past satellite images have been conducted in this section. DJI Phantom 4 Pro was used for the UAV survey, and Pix 4D Mapper pro (Rossi et al., 2017) was used for data processing. A topographic survey using UAV was performed, and the GCP (Ground control point) survey results were used to correct the

distorted images. The result of the UAV image was compared with past satellite images to examine the erosion analysis.

Uniform results were derived using unified values for each step configuration, including initial processing, point cloud, mesh generation, ortho-image, and DSM extraction. Form a grouping of points (Point Cloud) with the Pix 4D program and model it in exact contact with the location of ground control points taken on each photo and identified the QC errors recorded on the verification reports' results.

UAV survey for the GCP survey at the Fongafale was conducted by installing a reference station based on existing control points (FUN42, FUN43, FUN48), as shown in Figure 2.7 with the coordinates on table 2.5. UAV survey can be used to view the entire area of the Fongafale at a glance. Also, it was confirmed that the error value is within the range compared to the land survey and confirmed the error value by comparing the location and altitude information of the GCP point generated by UAV and survey results conducted by RTK GPS. Using UAV surveys, it was possible to compare and analyze with Google images and continuously monitor the erosion of nourished areas.

Table 2.5: Coordinates of control points

| No. | WGS4 ellipsoid (UTM coordinates) | | H (DL) | note |
|---|---|---|---|---|
| | X (Norhting) | Y(Easting) | | |
| FUN 43 | 9057957.56 | 742099.76 | 4.472 | unit : m |
| FUN 42 | 9057816.17 | 742062.06 | 4.821 | |
| FUN 48 | 9056444.91 | 741181.28 | 3.715 | |

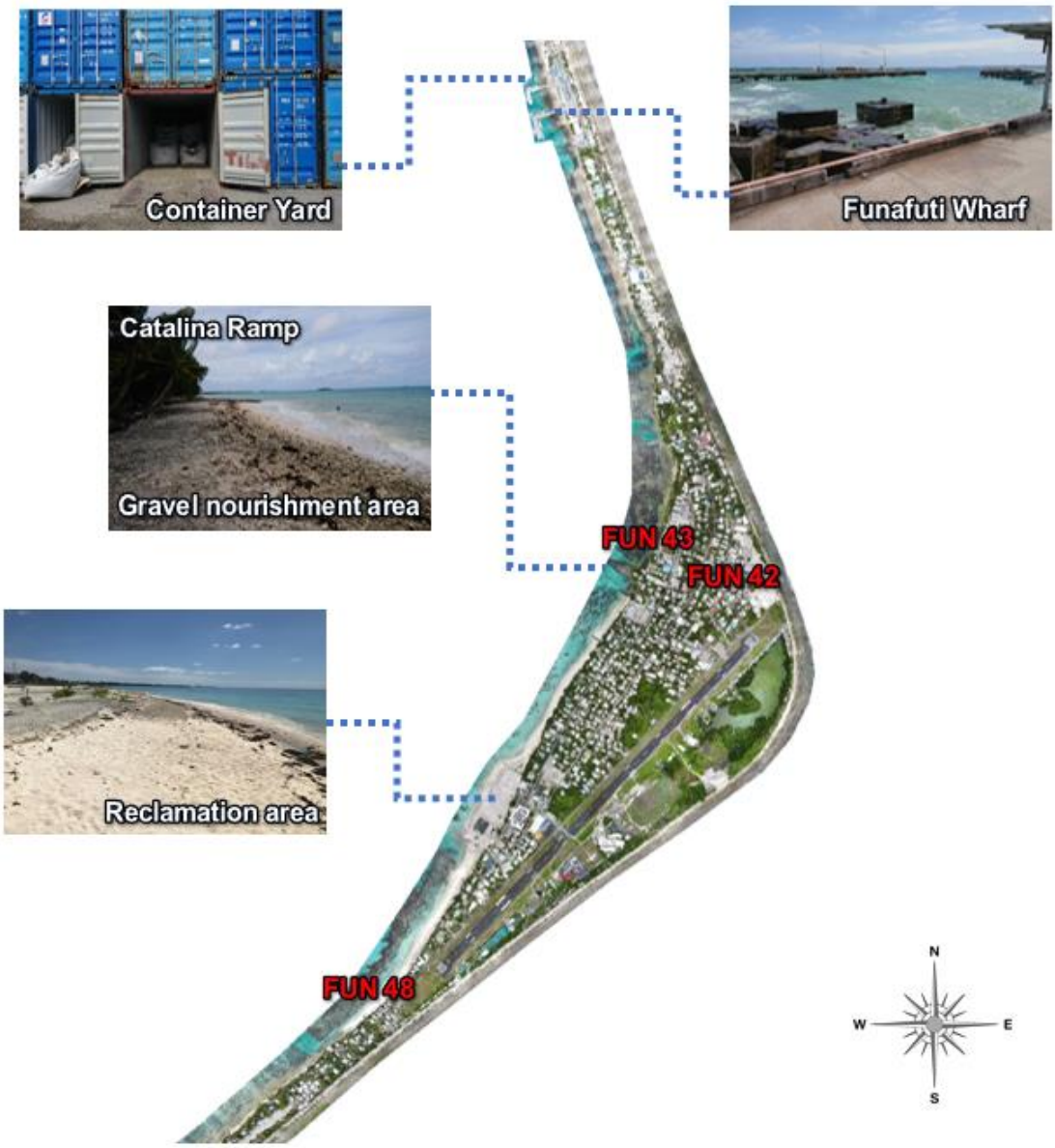


Figure 2.7: Fongafale GCP points with some of measured locations

The accuracy verification of UAV survey performance can be confirmed by the performance of the Ground control Point (GCP), which is used for the positioning and altitude calibration and the DSM (Figure 2.8). The accuracy of data generated by the program can be verified by checking the error values of each ground control point recorded in the QC report are formed within the tolerances.

Fongafale has a narrow and long shape, about 20m to 70m wide, and has major facilities such as airports, hotels, government buildings, hospitals, and schools. As a result of creating a topographical survey (Figure 2.9, and Figure 2.10), the ocean side datum level was higher with DL.(+) 4.5m to 5m, than the lagoon side datum level with DL.(+) 4m to 4.5m.

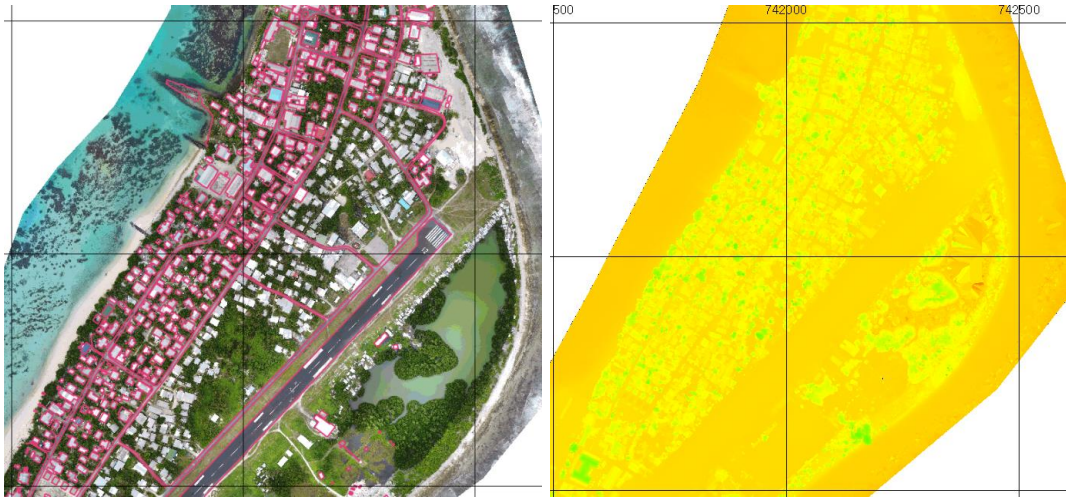


Figure 2.8: Combining UAV survey result and field survey data (left: visual inspection result, right: DSM result)

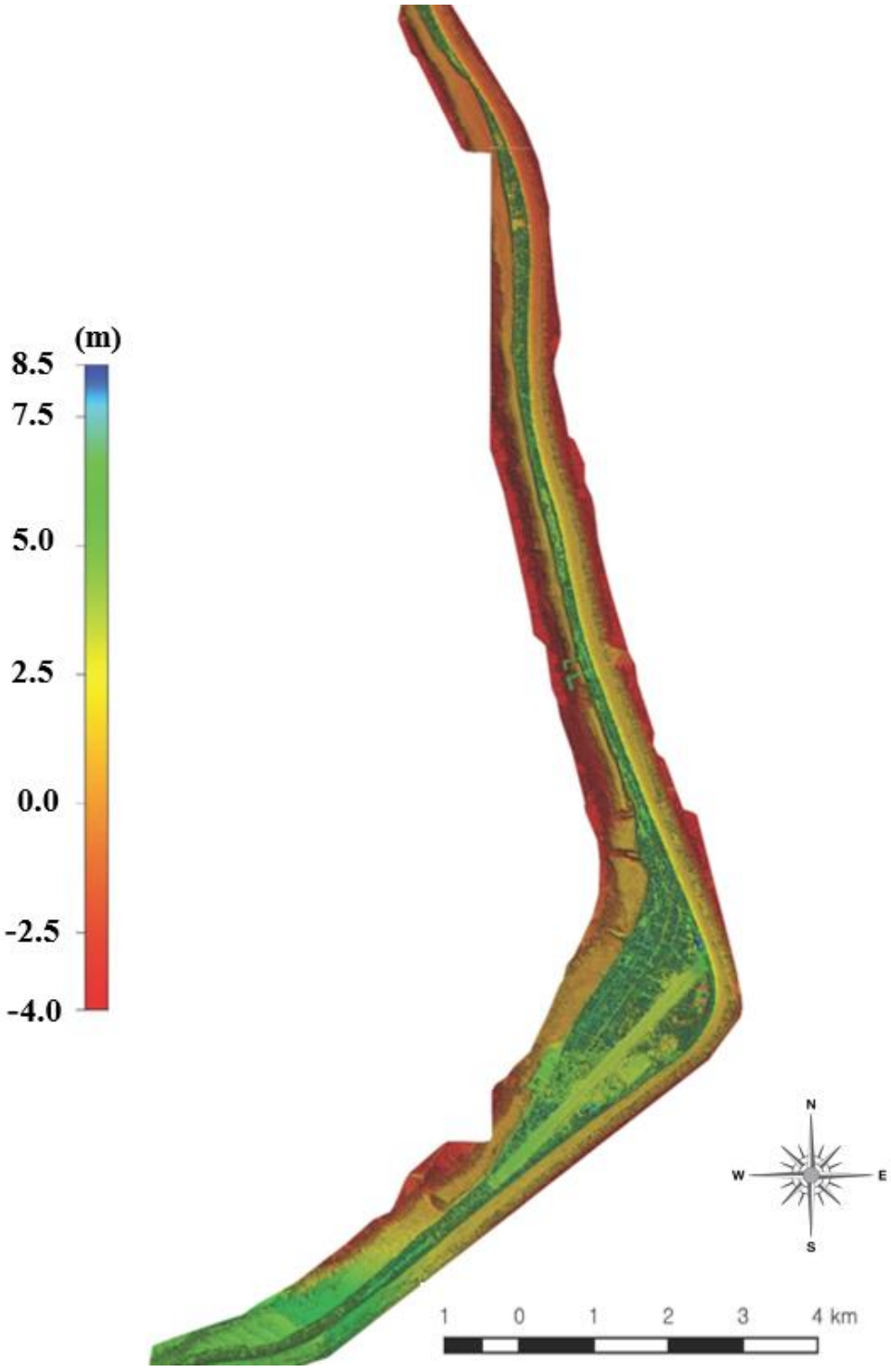


Figure 2.9: Cross-section of Fongafale Atoll in Tuvalu

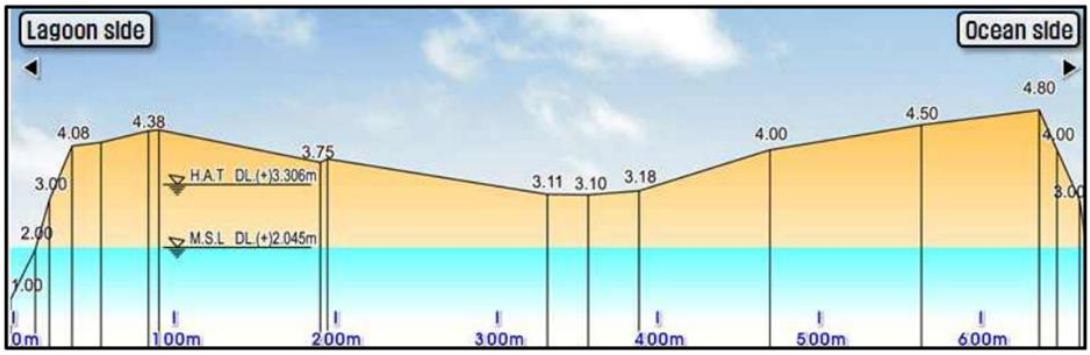


Figure 2.10: Cross-section of Fongafale Atoll in Tuvalu

Past satellite images from 1941 to 1984 were collected from the SOPAC report (SOPAC, 2006), and satellite images from Google Earth (2003, 2005, 2007, 2012, and 2016) have been used as the past satellite images to compare with the present UAV survey result (Figure 2.12). Using past and present satellite images, the approximate beach area has been compared, as shown in Figure 2.12 and Table. 2.6.

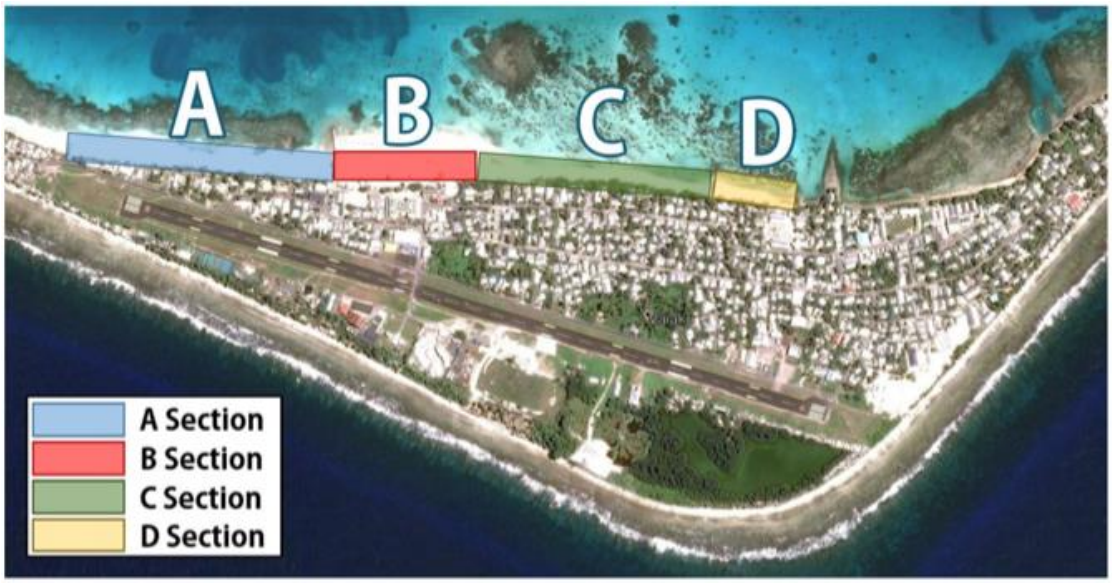


Figure 2.11: Sections of nourishment conducted in Fongafale

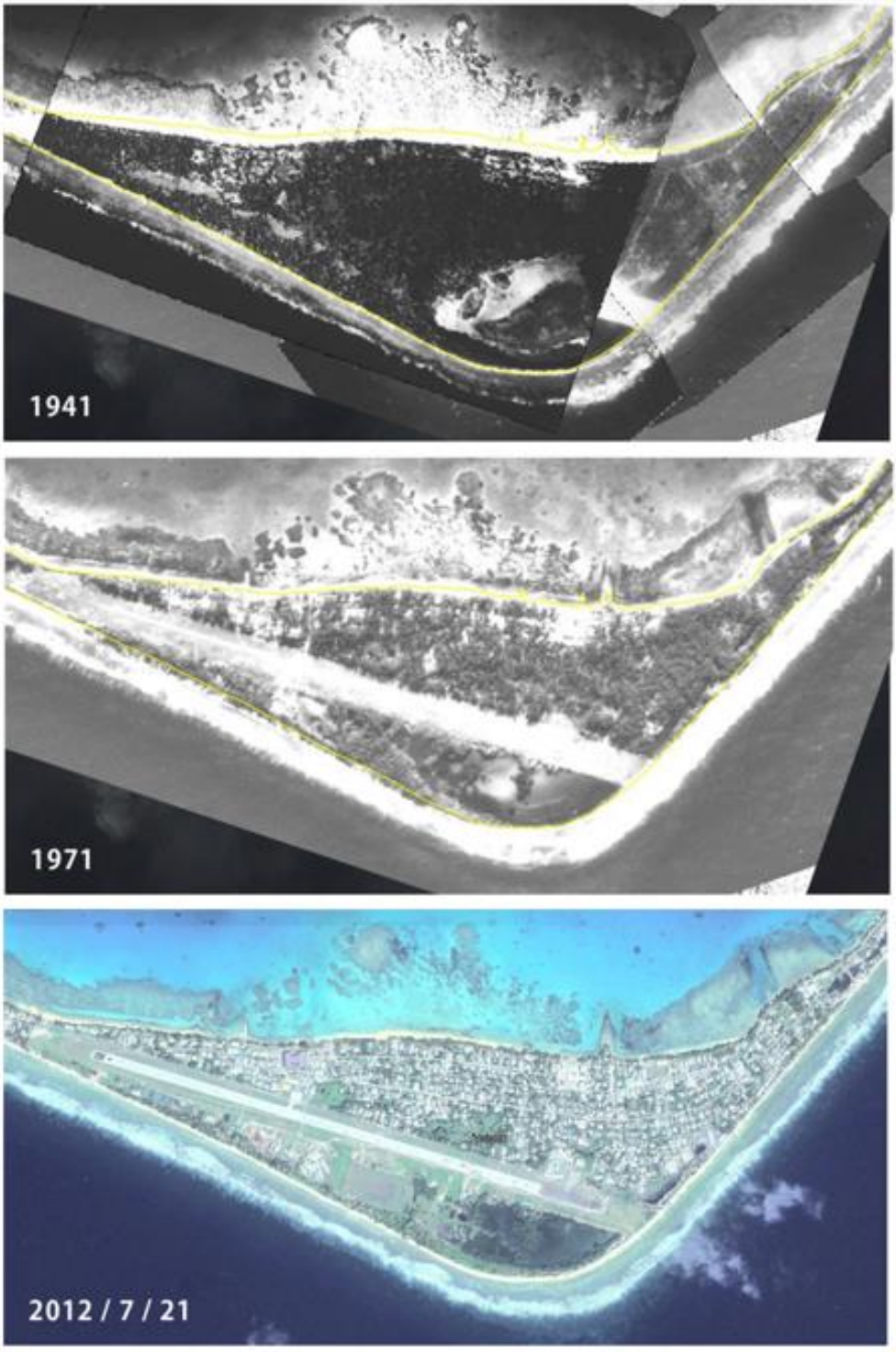


Figure 2.12: Some of satellite images from 1941 to present survey (SOPAC 1941-1984; Google Earth 2003-2016; Present UAV Survey 2017)


Figure 2.12: Some of satellite images from 1941 to present survey (SOPAC 1941-1984; Google Earth 2003-2016; Present UAV Survey 2017) continuous

Table 2.6: Sectional beach area

| Year | Area of each section ($m^2$) | | | |
|---|---|---|---|---|
| | A section | B section | C section | D section |
| 1941 | 18,210.50 | 9,718.69 | 11,018.00 | 3,816.03 |
| 1943 | 14,368.90 | 8,702.61 | 9,967.17 | 3,769.30 |
| 1971 | 9,685.50 | 8,366.54 | 9,188.93 | 2,624.07 |
| 1984 | 8,555.62 | 7,966.31 | 8,971.56 | 1,407.48 |
| 2003 | 7,963.07 | 4,034.89 | 6,582.45 | 1,182.35 |
| 2005 | 3,990.00 | 2,068.04 | 3,343.30 | 988.07 |
| 2007 | 3,989.02 | 1,376.52 | 2,852.29 | 926.58 |
| 2012 | 3,865.80 | 1,306.47 | 2,679.84 | 924.98 |
| 2016 | 24,285.83 | 32,381.05 | 14,263.40 | 4,470.68 |
| 2017 | 18,403.72 | 26,100.43 | 11,053.92 | 3,818.85 |

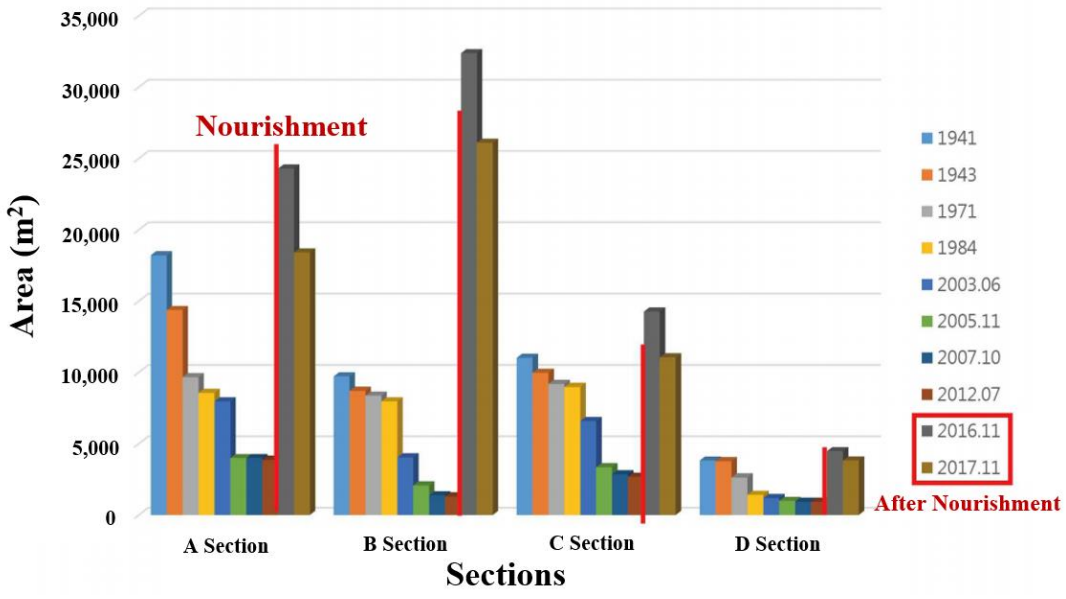


Figure 2.13: Changes of beach area by sections

By comprehending the long-term changes in the coastal area and by analyzing the causes of coastal erosion through the examination of satellite images of the Fongafale, satellite image analysis was used as a basic data for the planning of erosion prevention measures. Satellite images from 1941 to 2017 were collected, and unmanned aerial surveys (UAV) were conducted (Fig. 2.9), the results of which were added to analyze the sedimentation patterns of the study area. Analysis of the cause of erosion was made by dividing the project site into four different sections (A, B, C, and D), as shown in Figure 2.11, in consideration of existing facilities and the configuration of the beach. Tidal increases – which directly affect the shoreline's retreat and increases in wind velocity – a predominant factor in local wave characteristics, were analyzed through weather forecast data. On 2015, there was nourishment and reclamation on the Tuvaluan coast. After the nourishment in 2015, there was a significant decrease in the beach area, which was caused by a damage from the cyclones. From 2015, several cyclones hit the Fongafale area. Cyclone Pam occurred in mid-March of 2015; Cyclone Ula occurred from late December of 2015 to early 2016, and Cyclone Winston occurred in mid-February of 2016. Cyclone Pam showed the strongest wind speed at 14.4m/s on March 11, 2015; Cyclone Ula showed the strongest wind speed at 17 m/s on December 28, 2015. Thus, it was found that around 25% of area were divested between 2016 and 2017 except the section D where decrease was only 15%. This is because the D section is the location with the gravel nourishment designed by JICA. The detailed physical test will be discussed in the next chapter.

## 2.4 Bathymetric Survey

Processing of the data was carried out using HypackTM, validated by the International Hydrographic Organization (IHO), to increase the quality and compatibility of the data. Location data can vary significantly from the original depth value and the location data due to mechanical errors in the acoustic sounder with GPS, and from the atmospheric instability. These errors considerably reduce the accuracy of the final depth values. Thus, the error data is removed by thoroughly performing the measured and position error with SBAS. Bathymetric data is obtained from the sonic velocity corresponding water depth and calibrated with sound wave velocity value (1,531 m/sec).

The distribution of water depth in this study area is gently distributed from DL (+) 1.0m ~ DL (-) 12.0 m near Catalina ramp, DL (-) 10.0 m ~ DL (-) 18.0 m steeply near the rock area. DL (+) 1.0 m ~ DL (-) 15.0 m distribution is shown in the survey area. As shown in Figure 2.14, the route section shows a gentle appearance with DL (-) 32.0 m ~ DL (-) 41.0 m. The bathymetric survey of this task provides high water depth data (Koo, 2018) based on precise depth information obtained by comprehensive bathymetric and topographic survey throughout the survey area.

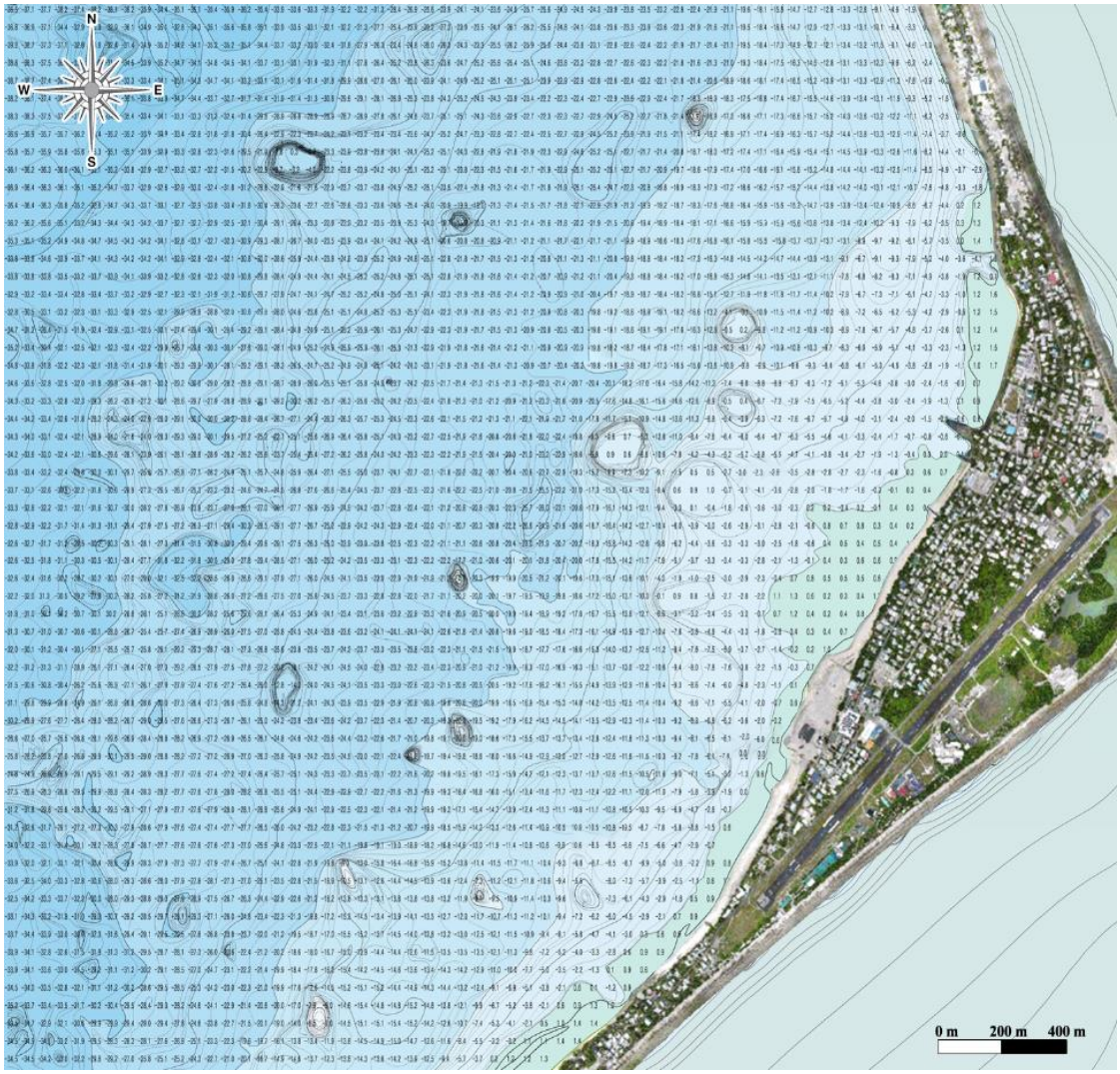


Figure 2.14: Bathymetric survey result of Fongafale shore

## 2.5 Grain Size Composition

Since most of the population is located in the Fongafale area where the most protections are needed, gravels from the other area have sufficient to be used in gravel nourishment. JICA has conducted gravel nourishment on 2015 before cyclone Ula attacks. The survey was conducted after the cyclone's impact on the beach. From the measurement of the D section of the Fongafale shore, unlike the typical beach, gravel was dominant in onshore of the beach. The analysis of the grain size was conducted on this beach, as shown in Figure 2.16. The gravel covering the surface at the beach had a particle diameter of 8-15 cm, and bottom of these thick gravel, there was gravel smaller than the surface around 2-6 cm.

Nonetheless, not all the beach was formed with gravel unlike ordinary pebble or gravel beach. By the time measurement was conducted, the beach was more like a composite gravel-sand beach where gravel and sand were mixed and formed on the beach. This seems to be the reason for the Cyclone Ula's impact since the slope of the beach was very steep, as shown in the right photo of Figure 2.15.

Figure 2.15: Gravel beach on the Catalina Ramp (D section)

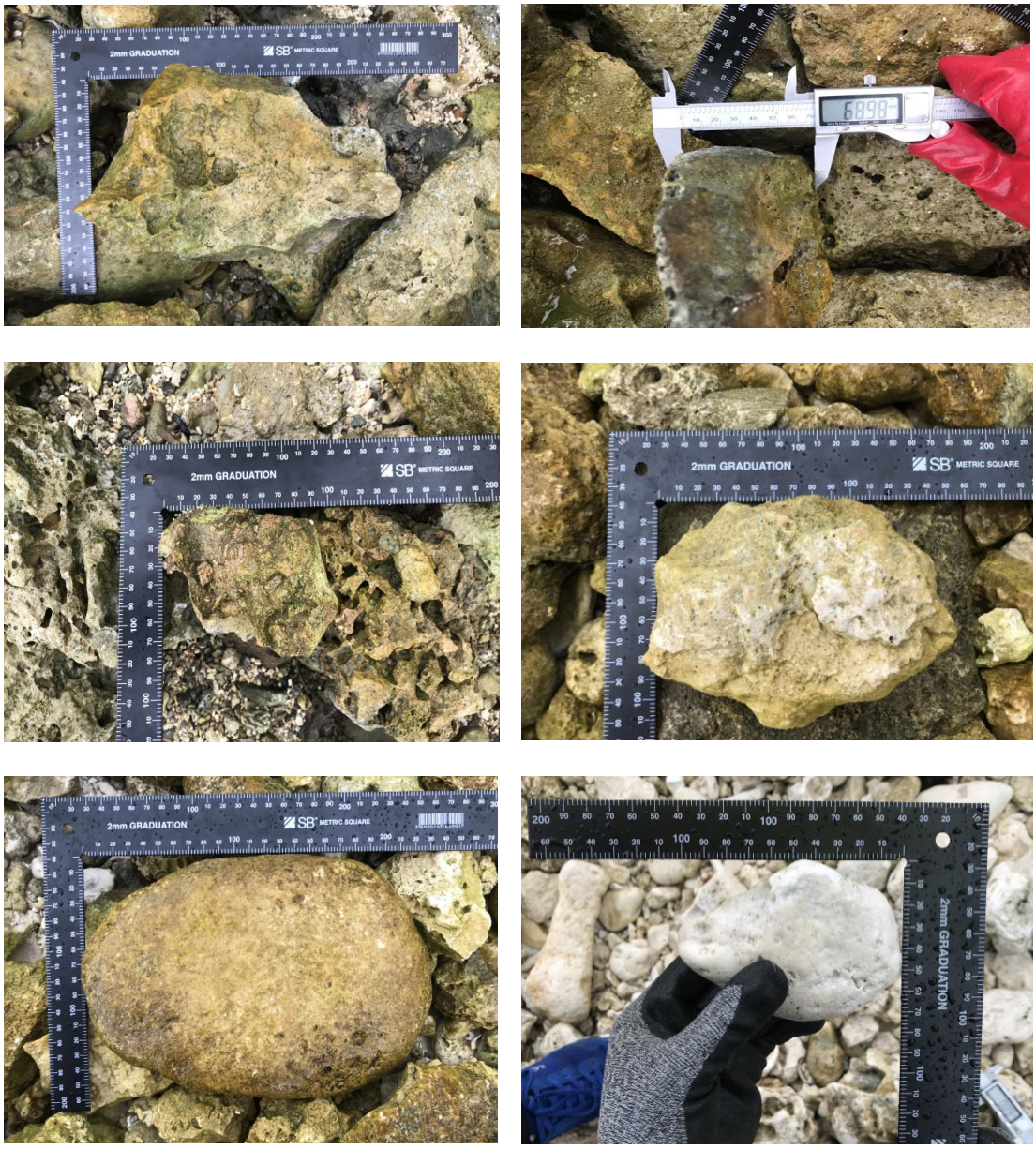


Figure 2.16: Grave size measurement at the gravel nourished beach

## 2.6 Simple wind wave test

Using the obtained data, a simple wave deformation test using SWAN (Simulating Waves Nearshore) model has been conducted to determine the wave condition when the cyclone Ula impacted. SWAN is a third-generation wave action model that uses typical formulations for wave growth by wind, wave dissipation by white capping, and four nonlinear wave interactions. It also includes physical processes associated with intermediate-depth and shallow water. The governing equation of SWAN action balance equations to calculates the random, short-crested wind-generated waves in coastal regions and inland waters (Settlelmaier, et al., 2011). 24 years (1993-2016) of the Tuvalu observation data of the Pacific sea level monitoring provided by the Australian Bureau of Meteorology were used as input and verified with the observed wave data conducted during the survey. For the model verification, the same time wind data from Tuvalu observation and the present wave observation (November 15$^{th}$, 2017 – December 6$^{th}$) were used as input to the model in real time and the output of real time wave was obtained to verify at the observation point. Result of the verification on Figure 2.17 found to be reasonable.

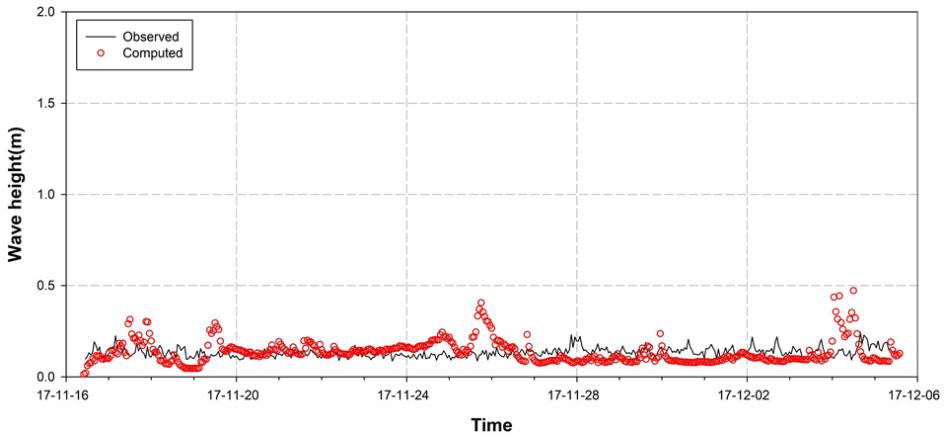


Figure 2.17: Model verification result

Numerical simulations were carried out for nine wave directions (S, SSW, SW, WSW, W, WNW, NW, NNW, N) in large (grid size ds = 50 m) and detailed (grid size ds = 20 m) scales (shown in Figure 2.18) which affect the study site in abnormal and normal wind conditions. Non-excess probability of 97.5% was considered as normal wind and wave conditions, and that of 99.9% was considered as abnormal wind and wave conditions (Ministry of Maritime Affairs and Fisheries, 2005). Table 2.7 and 2.8 show the test results with maximum wind speed in normal and abnormal conditions, and wave height analysis results on nine wave directions.

As a result of the wind-induced wave test, the WNW wave direction was the highest in the study site's vicinity, and the maximum wave heights were 1.76 m and 1.08 m, respectively. As from the Figure 2.20, when abnormal wind condition on the Fongafale coast, sections A, B, C, and D have similar wave heights which confirms the gravel nourishment area (section D) protected cyclone damage well compared to the other sections.

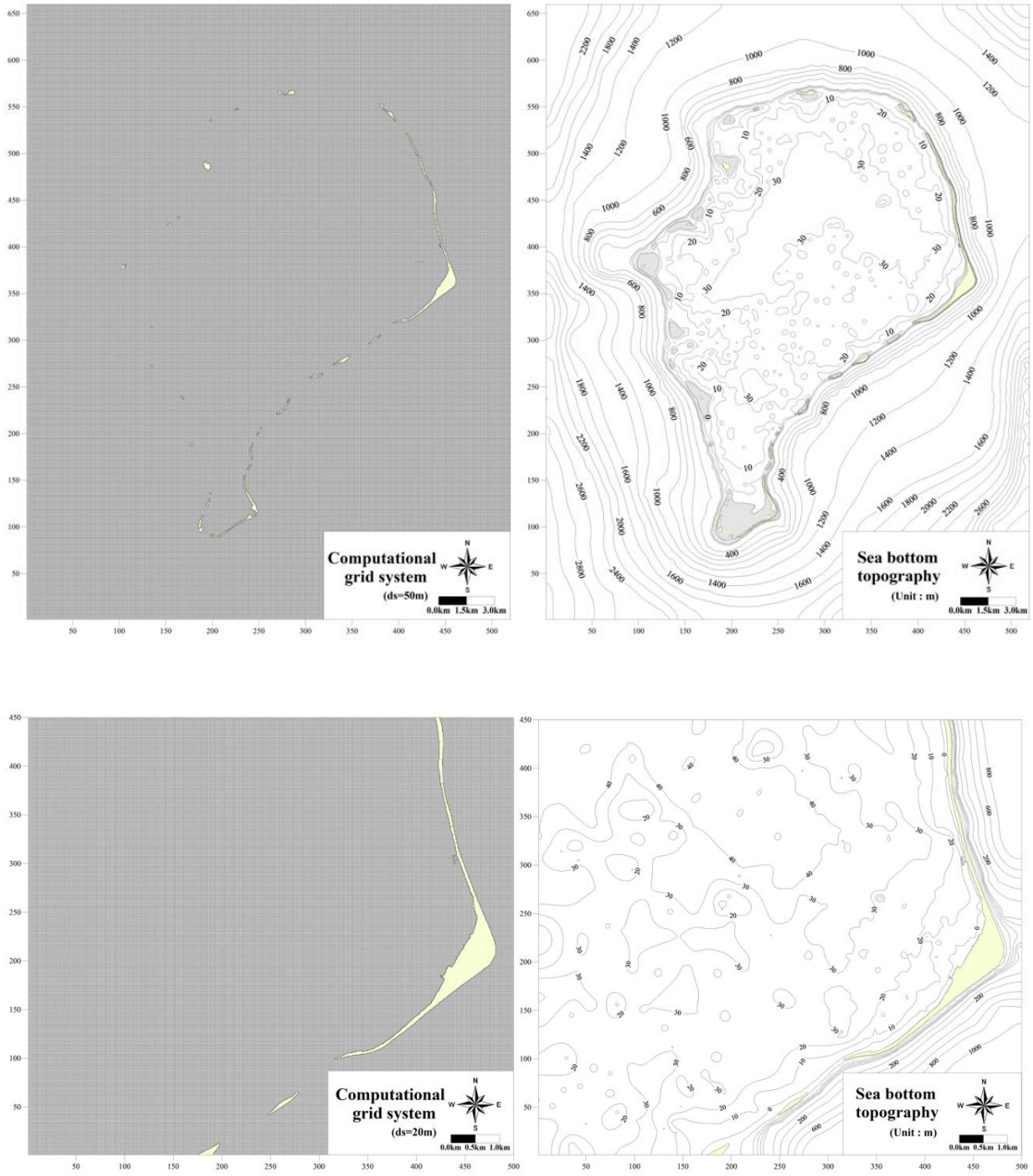


Figure 2.18: Large and detailed scales of wave deformation test grids and contour plots

Table 2.7: Maximum wind speed in normal and abnormal by wind direction

| Wind Speed (m/sec) | S | SSW | SW | WSW | W | WNW | NW | NNW | N |
|---|---|---|---|---|---|---|---|---|---|
| **Normal Condition (97.5%)** | 7.32 | 7.66 | 9.02 | 10.55 | 11.34 | 12.09 | 11.77 | 9.71 | 7.32 |
| **Abnormal Condition (99.9%)** | 11.67 | 11.54 | 13.56 | 15.45 | 15.22 | 17.05 | 16.21 | 13.87 | 10.95 |

Table 2.8: Wave height analysis result

| Wave height (m) | S | SSW | SW | WSW | W | WNW | NW | NNW | N |
|---|---|---|---|---|---|---|---|---|---|
| **Normal Condition (97.5%)** | 0.27 | 0.40 | 0.60 | 0.80 | 0.98 | 1.08 | 0.99 | 0.71 | 0.39 |
| **Abnormal Condition (99.9%)** | 0.52 | 0.72 | 1.05 | 1.35 | 1.52 | 1.73 | 1.56 | 1.15 | 0.71 |

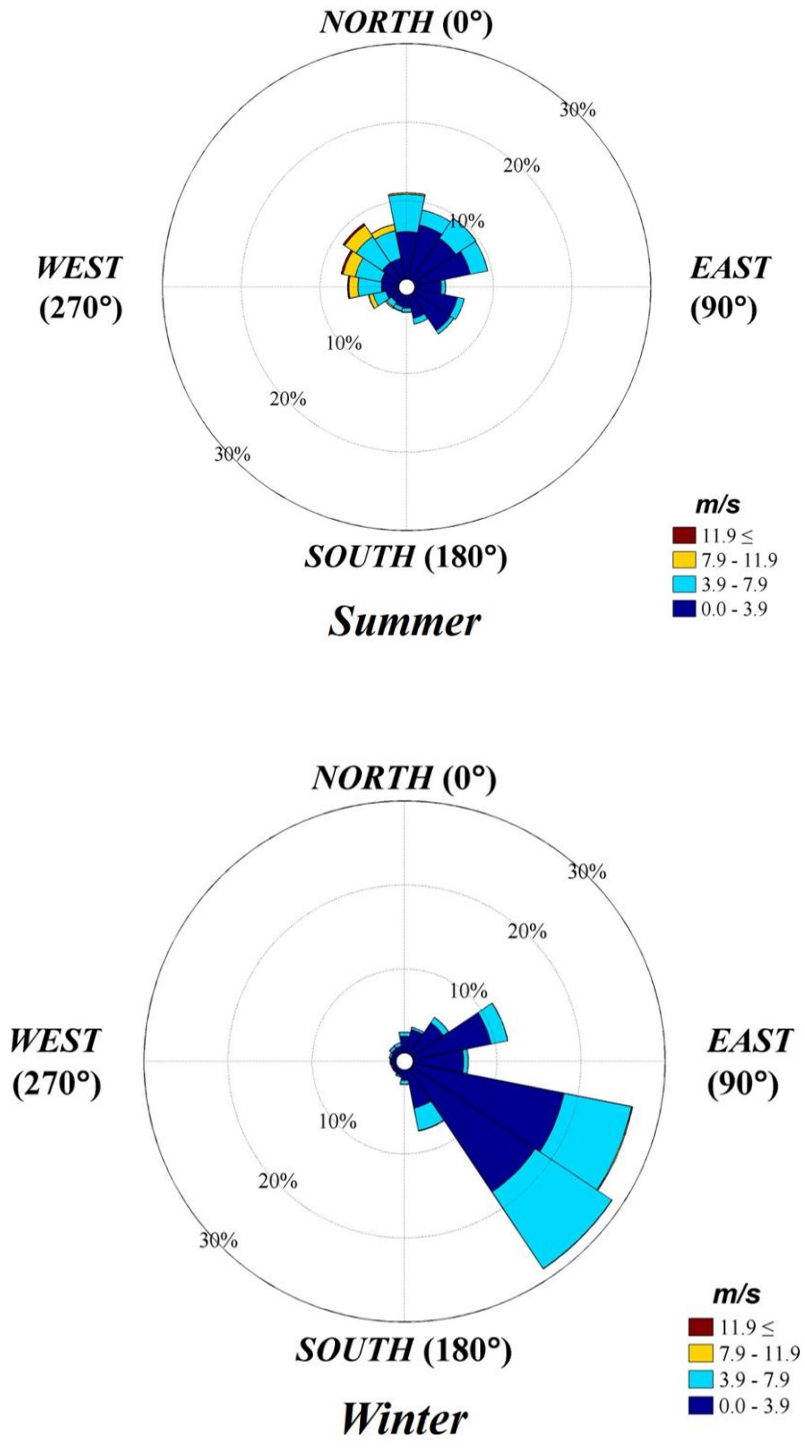


Figure 2.19: Summer and winter wind rose diagram

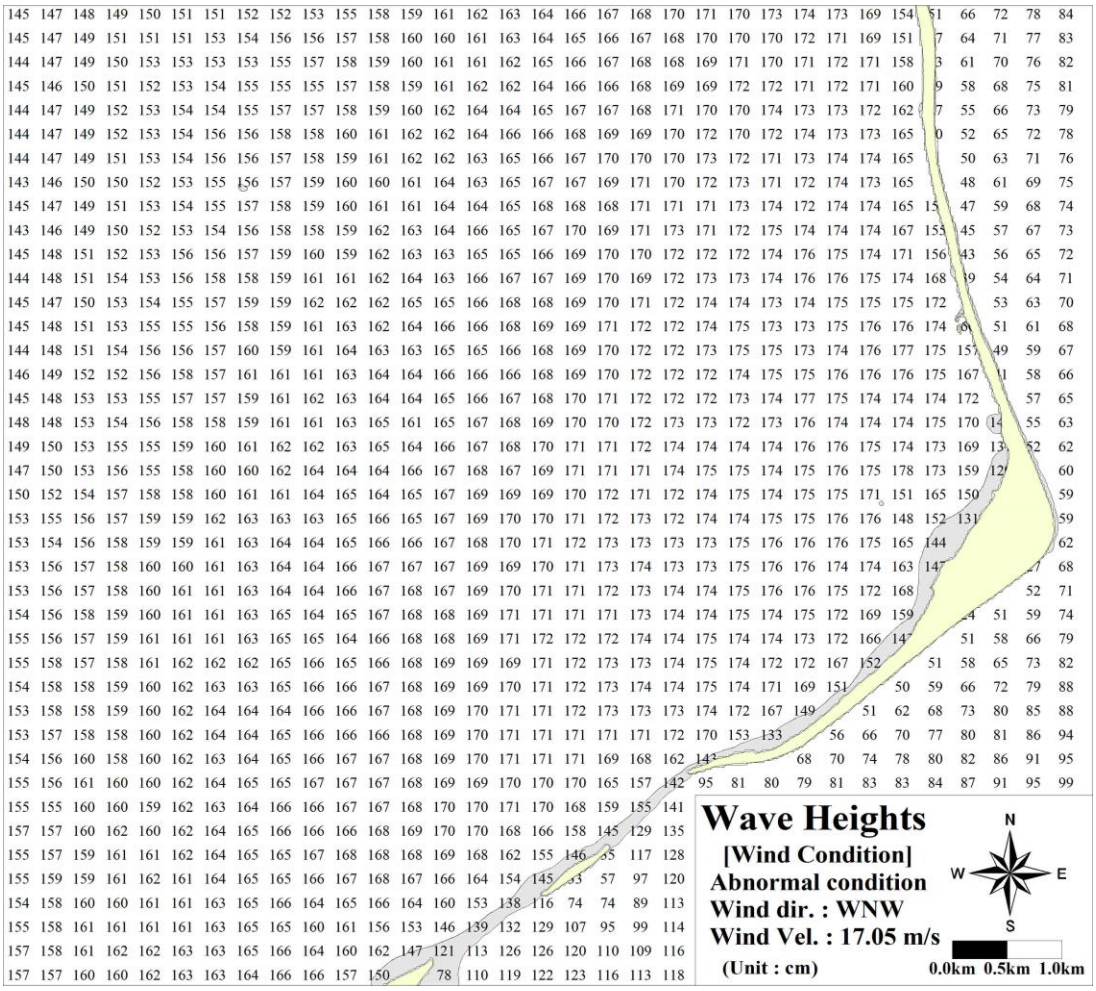


Figure 2.20: Wave height test result for WNW wind direction in abnormal wind condition

## 2.7 Conclusions

General topographic, UAV, bathymetric survey, and wave observation have been conducted at the Tuvalu, Funafuti Fongafale area for the basic measurement and an understanding of the study area. This area is a lagoon with a distance of around 17 km, where it is difficult for deep-sea waves to reach. Even with low-wave energy shore conditions, Tuvalu was suffering from beach erosion. This was found to be the problem of the cyclone damage, which occurs once or twice regularly every year. Thus, it was considered that this study area has low-wave energy conditions with a dominant wind. A recent cyclone impacted this area was found to be the Cyclone Ula. Ula had a maximum wind speed of around 17 m/sec during the period of the cyclone. This cyclone's damage was analyzed by UAV and past satellite image comparisons and was observed that on the section with gravel nourishment (section D), cyclone damage was less than the other nourishment sections. That being said, on the section with gravel nourishment, grain size composition was measured. Using all the data obtained through survey, simple wind-wave simulation using the SWAN model was conducted to see if the wave height varies by the sections. With the highest wind direction of WNW, all the sections (A, B, C, and D) had similar wave height affected at both normal and abnormal wind conditions.

# Chapter 3

# HYDRAULIC MODEL EXPERIMENT

## 3.1 Introduction

This chapter provides an overview of the hydraulic model experiment conducted in the wave flume located in the Waterfront and Coastal Research Center. This chapter also provides an overview of the experiment setup, beach profiles, and characteristics of gravel. The details of this experimental setup were given by Kim et al. (2019). Gravel nourishment with different placements were used in the experiment.

## 3.2 Experiment Setup

A hydraulic model experiment using a 2-dimensional wave flume was conducted to observe the sediment transport and profile evolution of the different nourishment types. The wave flume used in this experiment was 30 m long, 1 m in width, and 1.8 m in height (see Figure 3.1). The wavemaker can generate both random and regular waves. Furthermore, the wavemaker has a wave height gauge attached to the front of the wave paddle to enable reflected wave absorbing control based on the data read by the indicator. Also, a wave damper consisting of rubbles, Styrofoam, aluminum pieces, and an absorption filter was installed to minimize the generation of reflected waves (Kim et al., 2019).

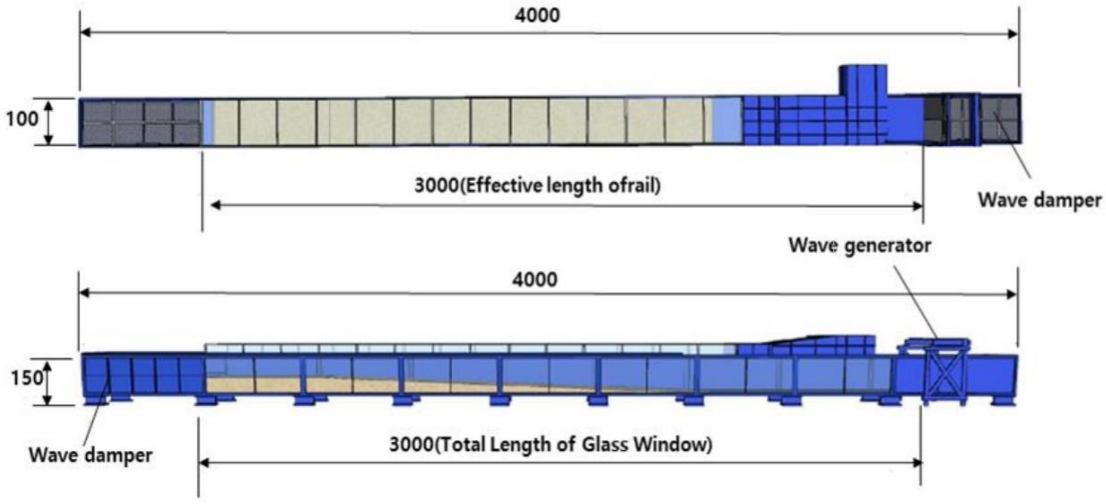


Figure 3.1: Wave flume used in the hydraulic model experiment

JICA conducted a gravel nourishment project at the Tuvaluan beach (see Figure 3.2). This cross-section of the gravel nourished Tuvaluan coast in the Fongafale was used as an initial profile for the hydraulic model experiment, and the geometric scale 1/25 was used in the experiment (Figure 3.3). The initial profile had a berm slope of 1:3.5 and a beach slope of 1:11. Two different still water levels (6 and 8 cm above the MSL, i.e., HHWL (+1.42 m from MSL) and ground-level (+1.92 m from MSL)) were used throughout the experiment. Beach nourishment can help mitigate the erosion process; however, single nourishment is not a long-term solution; the erosion process will continue to erode the nourished sand until renourishment is required. Accordingly, the aim was to see the erosion tendency when using different grain sizes with varying placement methods.

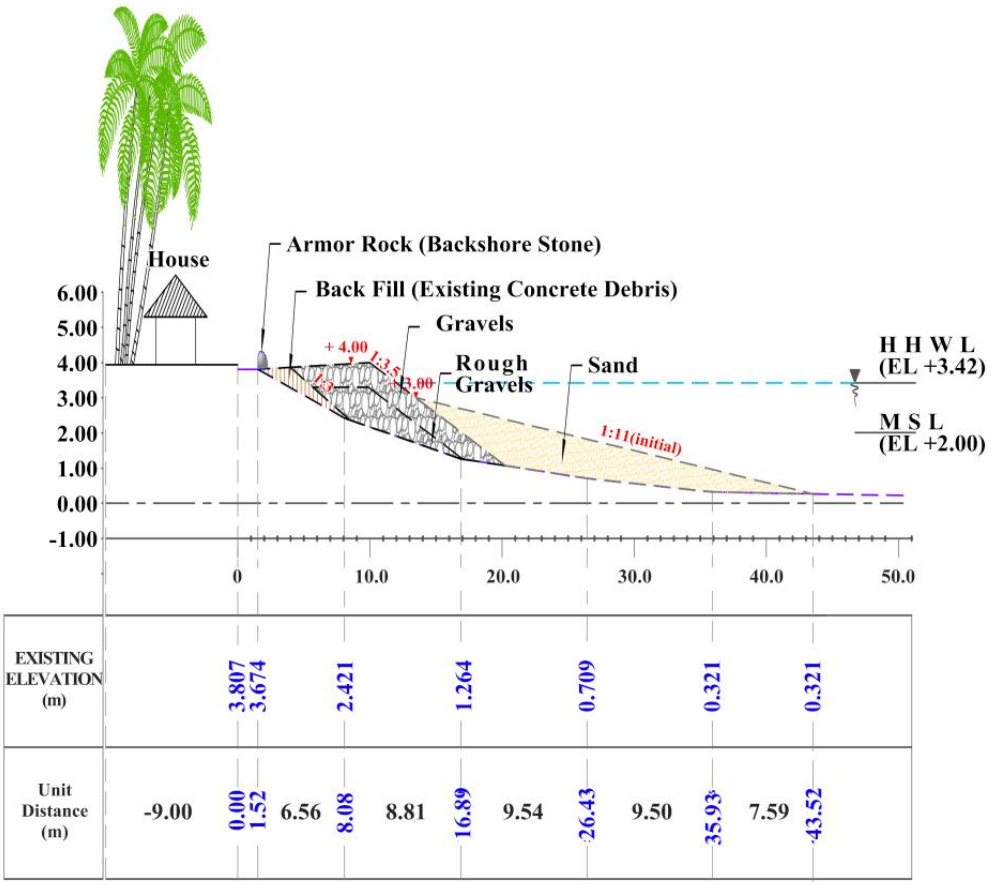


Figure 3.2: Gravel nourishment typical cross section on the Fongafale shore

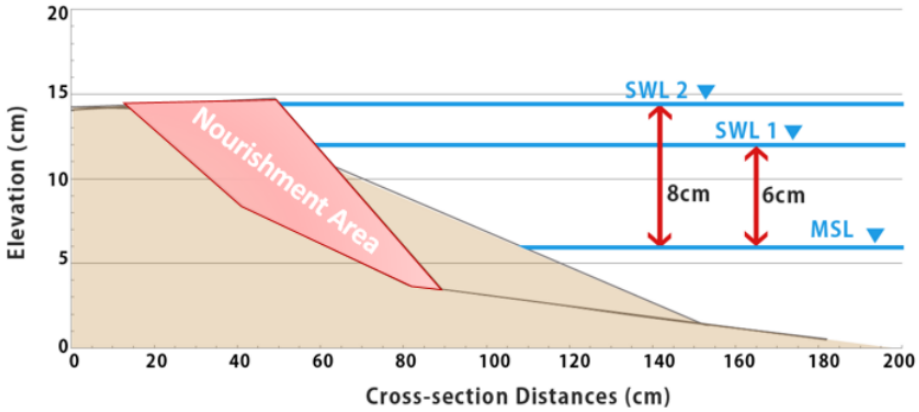


Figure 3.3: Experimental cross-sectional beach profile

Most parameters of experiments were considered based on the actual conditions of the Fongfale shore, Tuvalu. From the field survey, it was observed that the Tuvaluan coast is a low -wave energy coast where erosion was accelerated by storm waves. Since this experiment was small-scale, reproducing the actual damage was not the main focus. Instead, the aim was to see how the gravel nourishment would react to a large external force like Cyclone Ula, which impacted the beach, causing severe damage to the Tuvaluan coast in 2016, and which morphological changes would occur in these situations. Various placement methods were also considered to find economical methods by prolonging the period of renourishment without disturbing the aesthetic view. From the satellite image comparisons in Chapter 2, Cyclone Ula severely impacted the nourished beach; therefore, incident wave characteristics of Cyclone Ula were selected as wave characteristics used in the experiment. The wave parameters in test cases used prototype significant wave height and the period of 5.2 cm and 1.1 sec (actual $H_s$ =1.33m, shown in Figure 3.4) for 2 hours. To scale down the sand grain size without scale effect is usually difficult that the grain size ($D_{50}$) used in the experiment for sand and gravel was 0.16 mm and 5.0 mm, respectively.

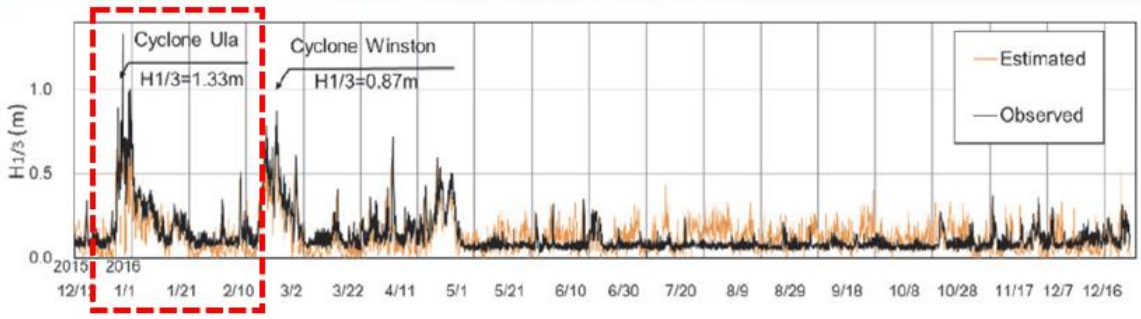


Figure 3.4: Wave height at the lagoon side during the monitoring period (Onaka et al., 2017)

A total of four test cases with using two still water levels (SWL) in each case in the wave flume—one with HHWL (SWL 1, 6 cm above the MSL) and one with ground level (SWL 2, 8 cm above the MSL)—were used to examine the damage of each test (see Table 3.1). Sand and gravel with different placements were selected as design options and used to plan an effective nourishment strategy. A larger grain sized nourishment is more resistant to erosion; however, to achieve similitude, mean diameters similar to those of local, prototype gravels were chosen. Therefore, four types of nourishments with different mean diameters – namely, $D_{50}$ of 0.16 mm of sand and $D_{50}$ of 5.00 mm of coral gravel – were used for the experiments (see Figure 3.5).

The initial profiles for each of the four test cases are shown in Figure 3.6. The experiments were performed for four test cases with the same wave conditions with irregular waves. The spectrum of the irregular wave used in the experiment was Modified Bretschneider-Mitsuyasu (Eq. (3.1)) proposed by Goda (1985) for the frequency spectrum of wind waves. For each test case, the profile was measured every 30 minutes and stopped at 120 minutes. Total irregular wave energy $E_I$ was computed using Eq. (3.2), where $H_s$ and $T_s$ represent the significant wave height and period, respectively.

$$S(f) = 0.205\, H_s^2 T_s^{-4} f^{-5} \exp\left(-\frac{0.75}{(T_s f)^4}\right) \tag{3.1}$$

$$E_I = \rho g \int_0^{+\infty} 0.205\, H_s^2 x^{-5} e^{-0.75x^{-4}} dx = 0.068 \rho g H_s^2 \tag{3.2}$$

Four test cases with two sea levels for each test cases were conducted and each test case consisted 120 minutes and profile were measured in every 30 minutes.

Table 3.1: Four test cases with different sea level

| Test case | Condition | Sea Level |
|---|---|---|
| **Case 1-1** | Sand Only | EL +3.42 m |
| **Case 1-2** | | EL +3.92 m |
| **Case 2-1** | Gravel Only | EL +3.42 m |
| **Case 2-2** | | EL +3.92 m |
| **Case 3-1** | Sand (Top) + Gravel (Bottom) | EL +3.42 m |
| **Case 3-2** | | EL +3.92 m |
| **Case 4-1** | Sand (Left) + Gravel (Right) | EL +3.42 m |
| **Case 4-2** | | EL +3.92 m |


Figure 3.5: Sand and gravel used in the experiment

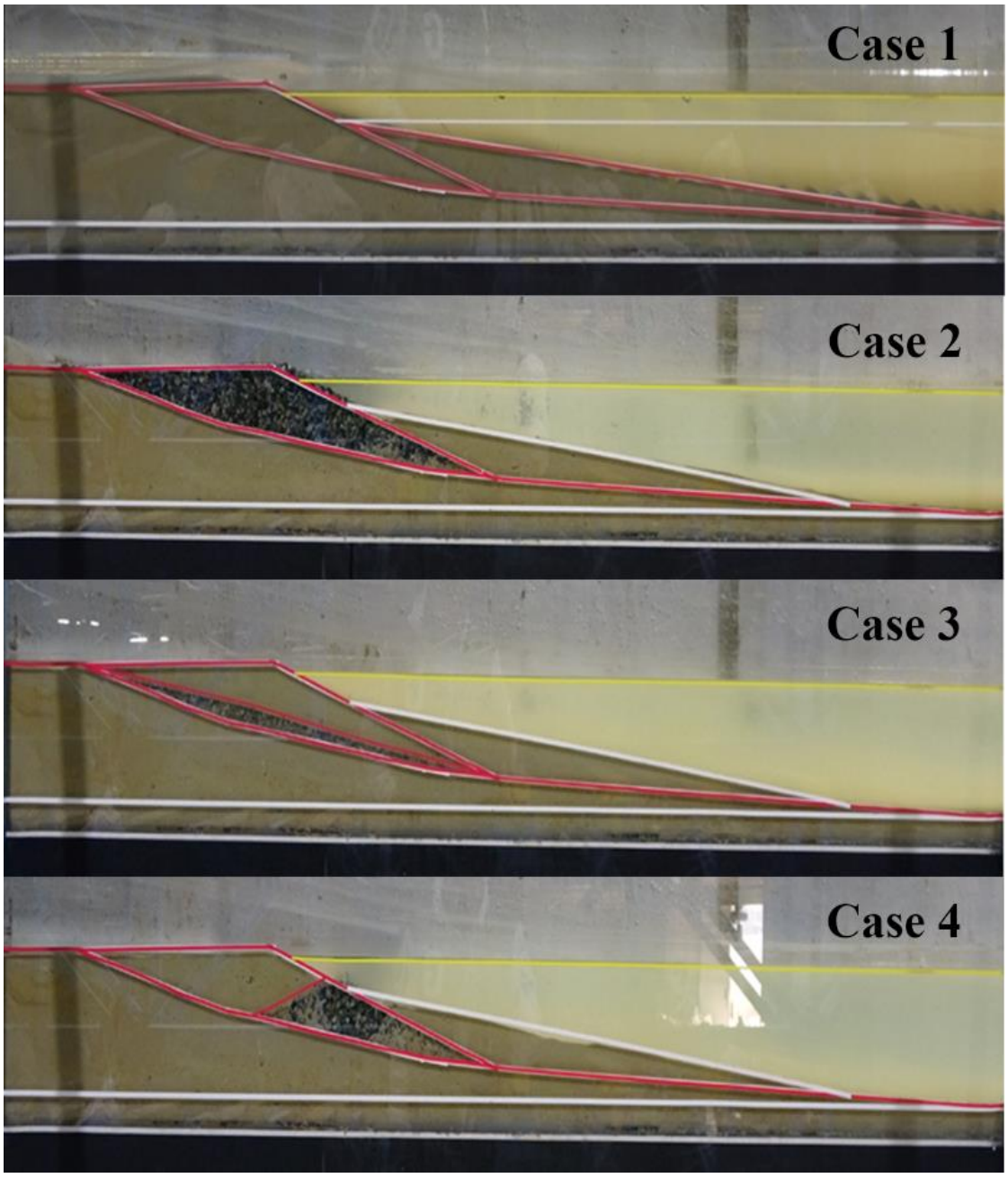


Figure 3.6: Four test cases with two SWL tested with 120 minutes runs each

### 3.3 Hydraulic model test cases

The first test case with a berm slope of 1:11 and a foreshore slope of 1:3.5 corresponded to the sand berm and sand beach, SBB test case, without gravel on a berm (see Figure 3.7) was tested. The berm was exposed to 120 minutes runs using 5.2 cm significant wave heights with 1.1 sec significant wave period using irregular waves. The SBB test case with each SWL was tested for 120 minutes, and the same initial profile was rebuilt after SWL 1 test. The SBB test case was conducted to see how the other test cases would differ from SBB, where only sand was used. Under breaking waves, most of the sand on the foreshore was moved onshore as bed loads, and offshore as suspended loads.

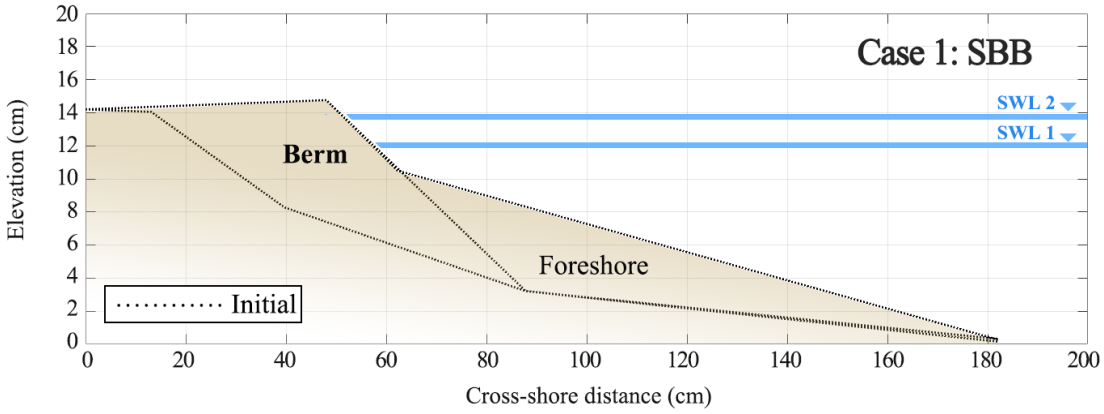


Figure 3.7: Test Case 1 – Sand Berm and Beach (SBB) initial profile

For the test case GBS, gravel berm and sand beach, the initial berm profile was rebuilt on the initial profile for case SBB and a berm was replaced with the gravel (see Figure 3.8). $D_{50}$ of 5 mm of the gravel used in the test was replaced on the sand berm from SBB. This profile was the same as the profile JICA built on the Tuvaluan coast gravel nourishment section. The idea of this profile was to compare with the SBB and see how to decrease or protect the erosion from storm waves effectively. As in the SBB test case, the gravel berm was exposed to 120 minutes runs using 5.2 cm significant wave heights with 1.1 sec significant wave period for irregular waves. The GBS test case with each SWL was tested for 120 minutes, and the same initial profile was rebuilt after SWL 1 test.

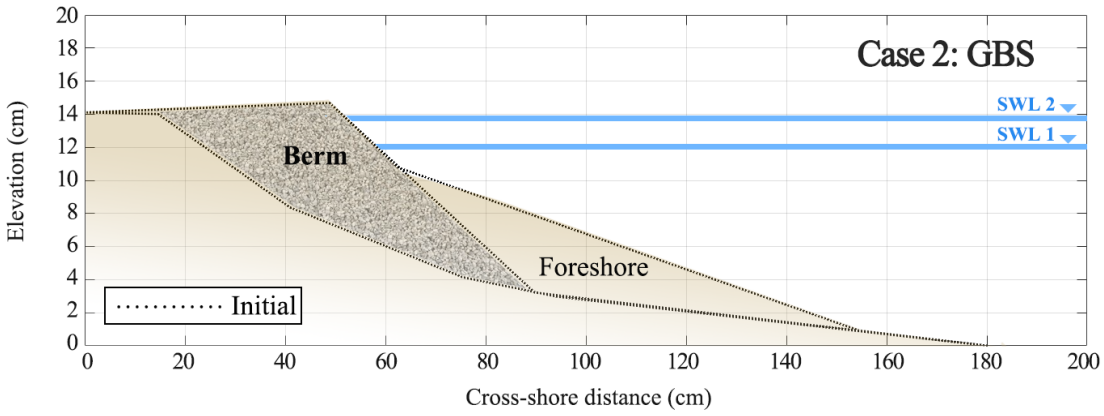


Figure 3.8: Test Case 2- Gravel Berm and Sand Beach (GBS) initial profile

Gravel nourishment can disfigure the aesthetic view and adversely affect the natural beach. Therefore, using only half amount of the gravel used in GBS, the buried gravel layer, was applied to reduce the extent of berm erosion without spoiling the shore aesthetics. As shown in Figure 3.9, gravel layer was first placed on the berm, and sand was covered on top of the layer. Similarly, to the other two test cases, the BGL test case with each SWL was tested for 120 minutes, and the same initial profile was rebuilt after SWL 1 test using 5.2 cm significant wave heights with 1.1 sec significant wave period for irregular waves.

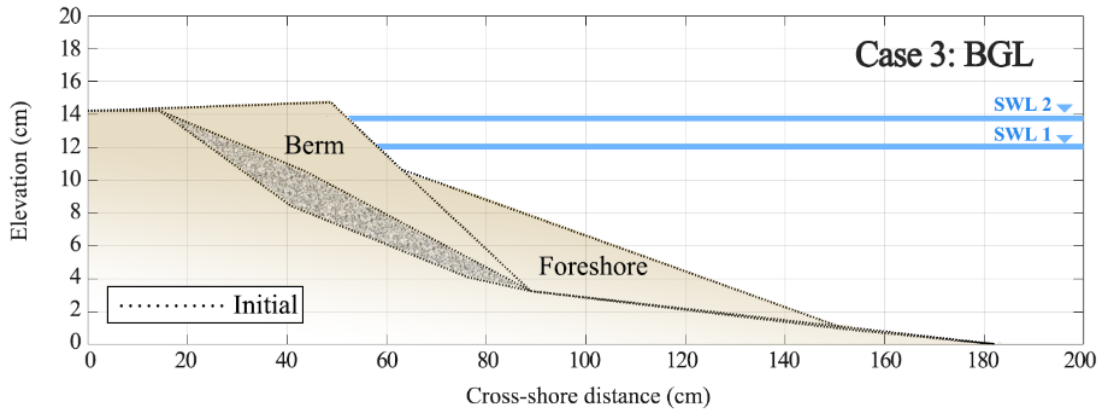


Figure 3.9: Test Case 3- Buried Gravel Layer (BGL) initial profile

The buried gravel sill (BGS) test case had a concept of using the same amount of gravel on the test case 3-BGL, but build sill type of gravel on the berm covered with sand to look like sand berm but gravel buried inside (see Figure 3.10). After rebuilding the berm sill, a mixture of sand and water was poured into the gravel sill to cover the gravel and fill its voids. The BGS test case with each SWL was tested for 120 minutes, and the same initial profile was rebuilt after SWL 1 test using 5.2 cm significant wave heights with 1.1 sec significant wave period for irregular waves.

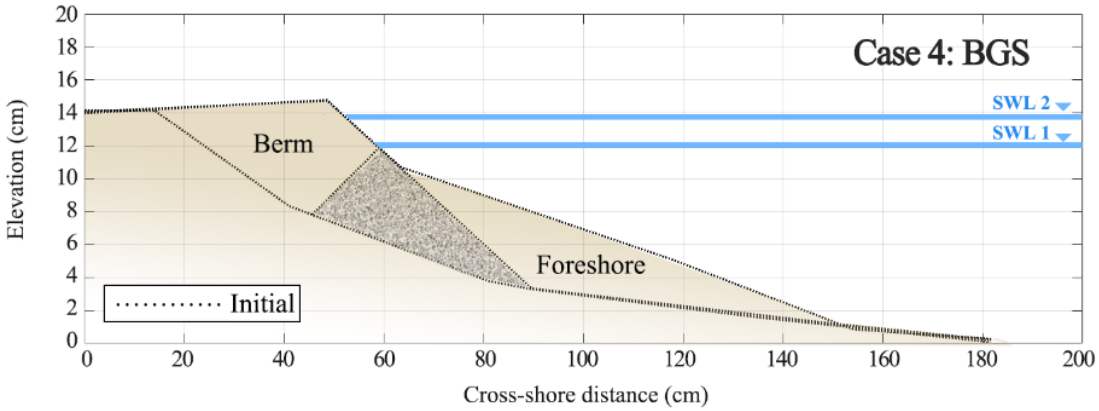


Figure 3.10: Test Case 4- Buried Gravel Sill (BGS) initial profile

## 3.4 Beach Profile Evolution

Figures 3.11-3.13 and 3.15-3.20 show the measured profiles of test cases 1,2,3 and 4 at t= 0, 30, 60, 90, and 120 min for all four test cases with the elevation SWL 1 and 2. For brevity, in Figures 3.11- 3.20, $t_1$= 30 min, $t_2$=60 min, $t_3$=90 min, and $t_4$=120 min. The profiles were measured along x= 0-200 cm.

As can be seen in Figure 3.11 with SBB test case with SWL 1, there was a sand dune formation right after $t_1$. Continuous erosion accelerated on the sand berm and after $t_3$, deposited sand dune on the backshore disappeared.

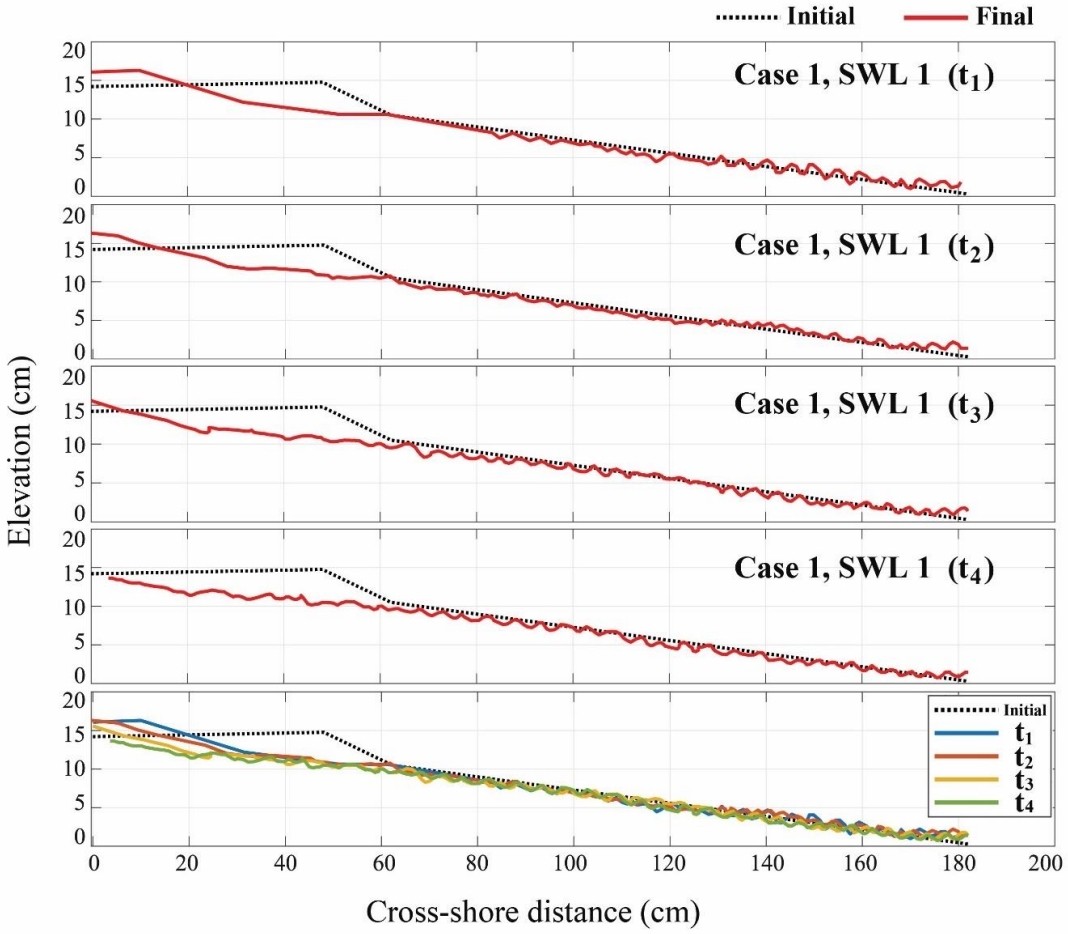


Figure 3.11: Case 1, SBB with SWL 1 profile evolution of $t_1$, $t_2$, $t_3$, and $t_4$

The SBB test case with SWL 2 caused the trend of foreshore erosion and berm erosion during $t_1$ and $t_2$. The pattern of forming the sand dune on the backshore was similar to the SBB test case with SWL 1; however, the erosion persisted and created deposited sand dune which disappeared quicker with a higher SWL. By comparing two profiles in Figured 3.11 and 3.12, it was observed that when using only sand as nourishment, the beaches were less sensitive to SWL, and the final profiles for SWL 1 and SWL 2 seemed similar.

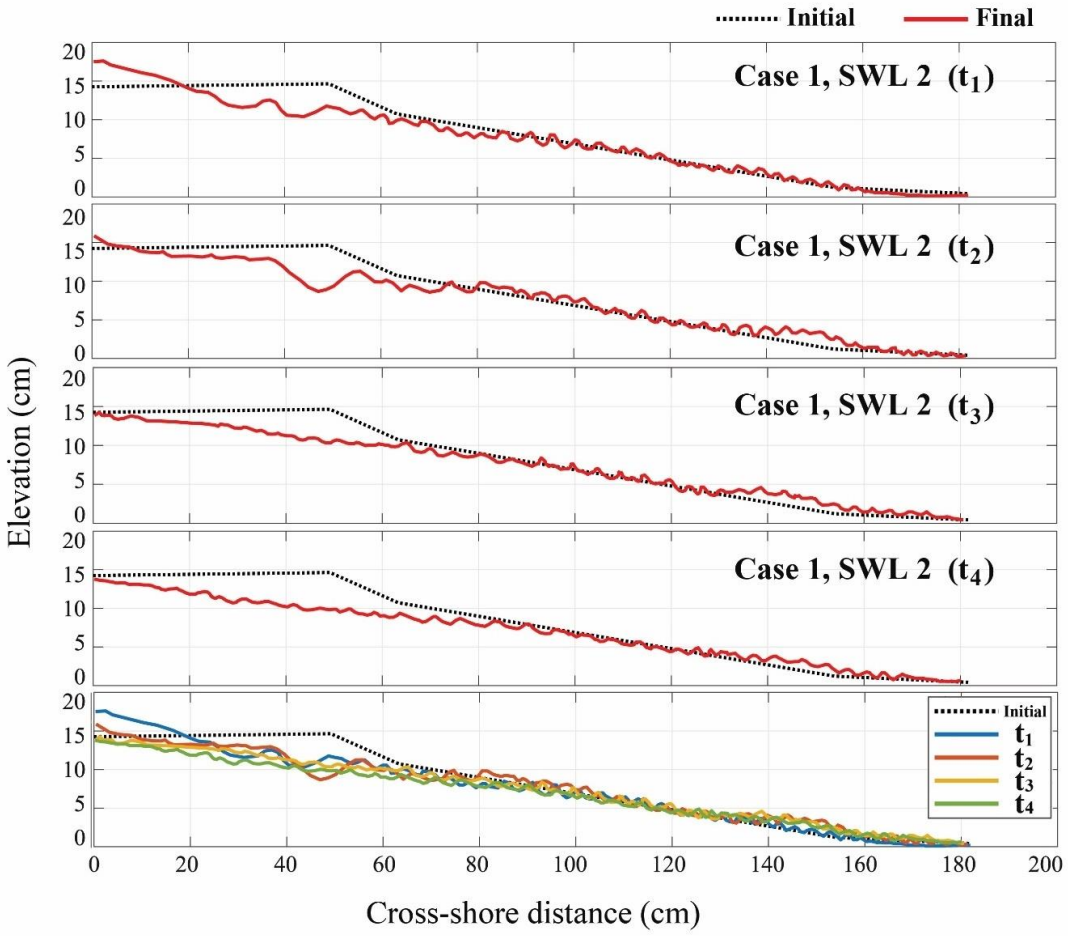


Figure 3.12: Case 1, SBB with SWL 2 profile evolution of $t_1$, $t_2$, $t_3$, and $t_4$

For the gravel berm and sand beach test case GBS, Figure 3.13 shows the profile evolution of measured profile at $t_1$=30 min, $t_2$=60 min, $t_3$=90 min, and $t_4$=120 min. During $t_1$-$t_2$, a gravel dune was formed on top of the berm. This gravel dune protected minor waves from overtopping. Gravel dune was formed on the backshore; however, since the gravel did not easily move onshore, scouring occurred on the foreshore. As time passes, the gravel dune migrated backshore, and the size of the dune increased. Scour trench was created landward of the berm and the seaward slope, and the crest of the berm was eroded. In the case of SWL 2 (Figure 3.15), berm became saturated with an increase in the water level. Accordingly, the results confirmed that a large amount of erosion occurred within a short time. Compared to the results of SWL 1 in Figure 3.11, the erosion pattern showed a marked difference.

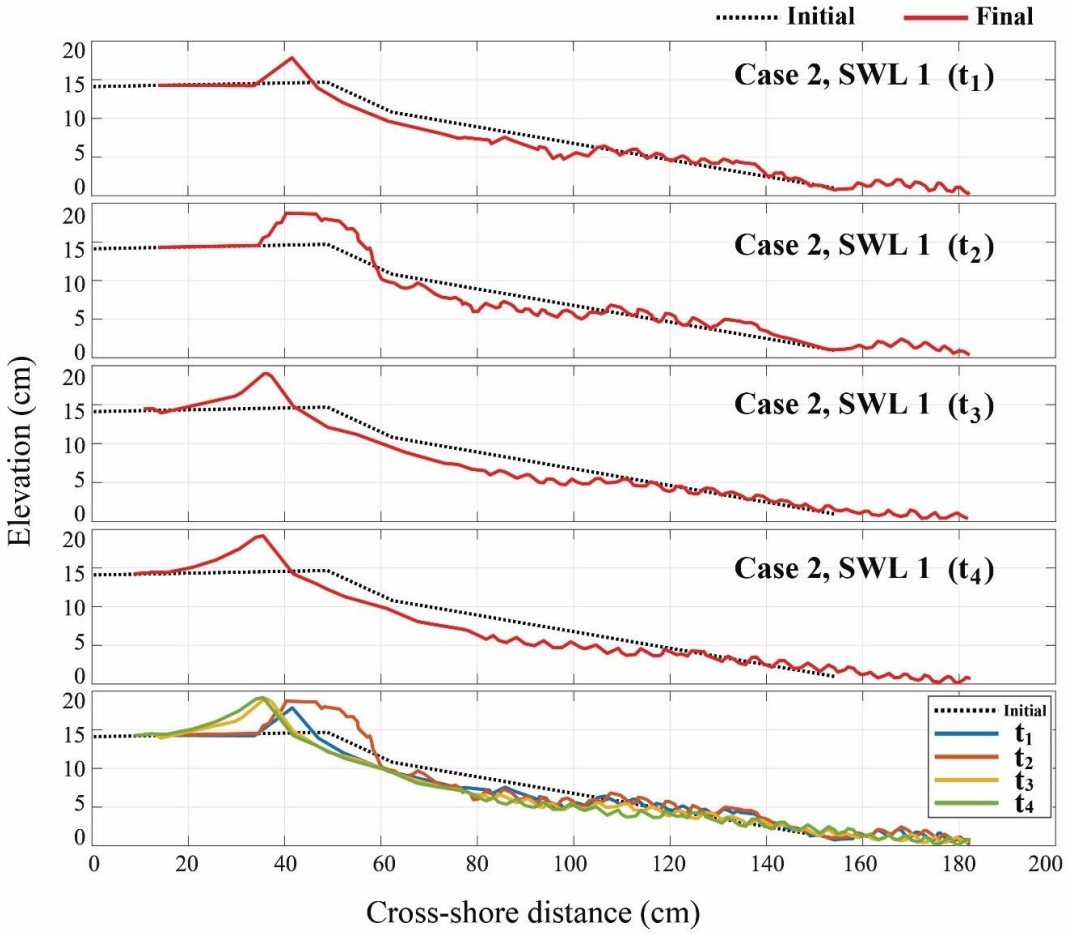


Figure 3.13: Case 2, GBS with SWL 1 profile evolution of $t_1$, $t_2$, $t_3$, and $t_4$

Figure 3.14: Southern part of Catalina Ramp with gravel nourishment

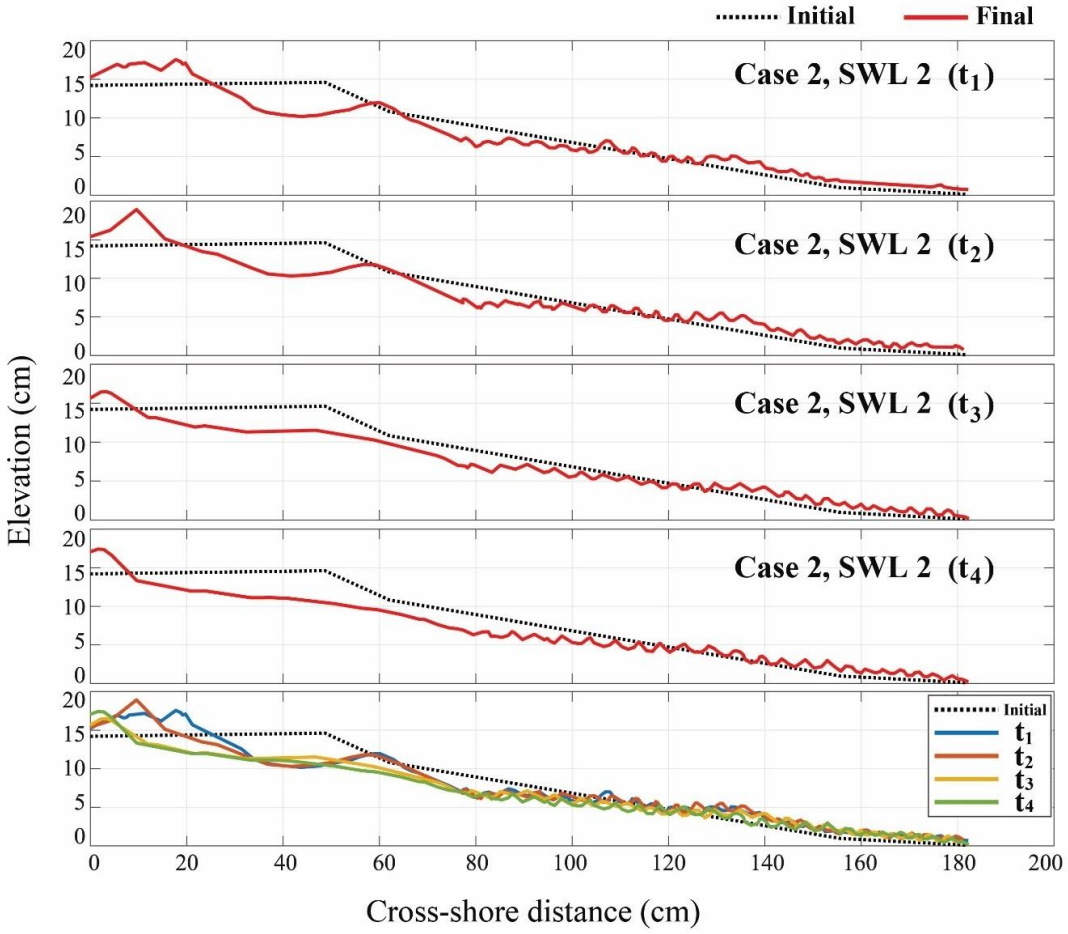


Figure 3.15: Case 2, GBS with SWL 2 profile evolution of $t_1$, $t_2$, $t_3$, and $t_4$

In the case of the GBS, for the SWL 1, the deposition of the berm appeared over the time and the deposited gravel-sand tends to retreat. This test case was found to have a good result as a countermeasure against erosion.

From the photo taken before and after the cyclone Ula at the southern part of Catalina Ramp where the gravel nourishment was conducted (Figure 3.14), one on the left was taken after the gravel nourishment and before the damage of cyclone Ula. The photo on the right was taken in December 2017 after the cyclone Ula invasion, where a

large amount of the gravel dune with steep slope was formed, similarly to the experimental results. According to Shim et al. (2019) and Muhajjir et al. (2019), the gravel on the beach tended to create a gravel dune after the induced high waves. Figure 3.16 shows the results reported by Shim et al. (2019). These results cannot be quantitatively compared to those of the present study due to the differences in the experimental conditions such as incident waves, beach profile, range of beach nourishment and generation of the wind (*U*). However, the experimental results for a similar particle size can be compared qualitatively. Erosion occurred at the beginning of the experiment, but a large-scale accretion occurred on the rear side of the shoreline after a certain period. Overall, comparing the tendencies of profile evolutions, it was observed that the results were similar to those of the GBS study case by forming the gravel dune and foreshore erosion.

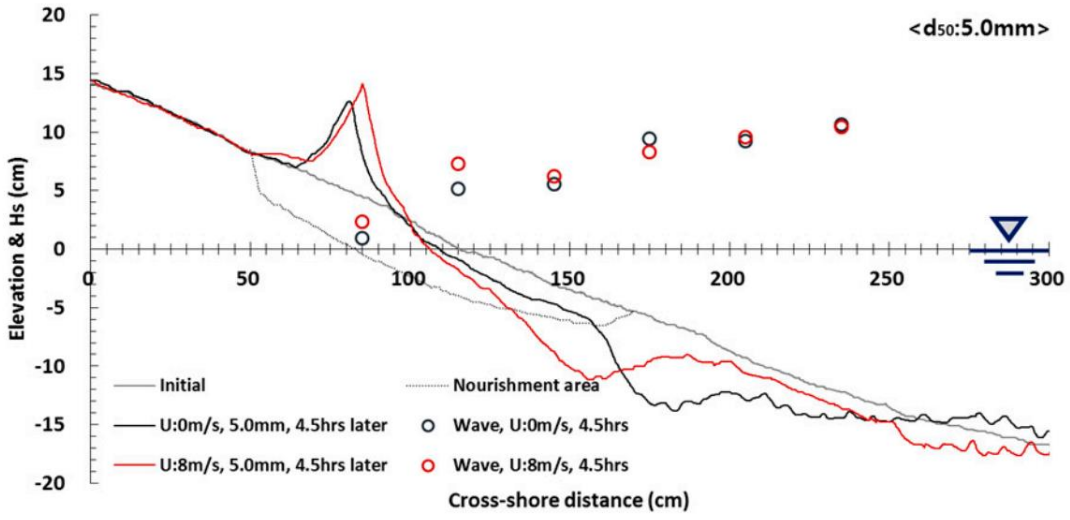


Figure 3.16: Experiment of gravel nourished beach (Shim et al., 2019)

Nonetheless, unlike the SWL 1, SWL 2 showed the erosion of the berm caused by the sea level rise in the case of GBS. The erosion problem was more pronounced in the saturated and unsaturated state than in the sand or gravel problem. Erosion pattern was almost the same for both sand berm from SBB and gravel berm from GBS, and only the pattern of deposition behind the berm was different.

With an increase of the still water level to SWL 2, gravel dune formed in different locations (Figure 3.15), and the formation of gravel dune was located more on the far backshore. Scour continued and created the sand dune between the berm and foreshore at $t_2$. These gravel dunes seemed to protect from the wave overtopping as well as wave overwash. Unlike in the SBB test case, gravel deposition and landward migration were sensitive to SWL, as wave run-up on gravel is sensitive to SWL. The results of this test case with SWL 2 suggest that the gravel nourishment perform at the Tuvaluan coast with a higher cyclone surge more than in the case of Cyclone Ula.

The profile evolution in the case of buried gravel layer, BGL, is shown in Figure 3.17. As demonstrated by the initial profile with a bird's eye view, gravel was hidden so that the initial profile looked the same as the test case of SBB; however, the gravel layer was placed underneath of the berm. Only half the amount of the gravel from GBS was applied in this test case. By the end of the $t_1$, a similar tendency with SBB was observed; however, once the gravel layer was exposed, gravel protected the erosion and created a gravel composite sand dune on the backshore. As time passes, the beach became equilibrium; however, it was found that the composite gravel sand protected the beach from slowing down the erosion. After $t_3$, beach profile evolution became similar to the SBB test cases.

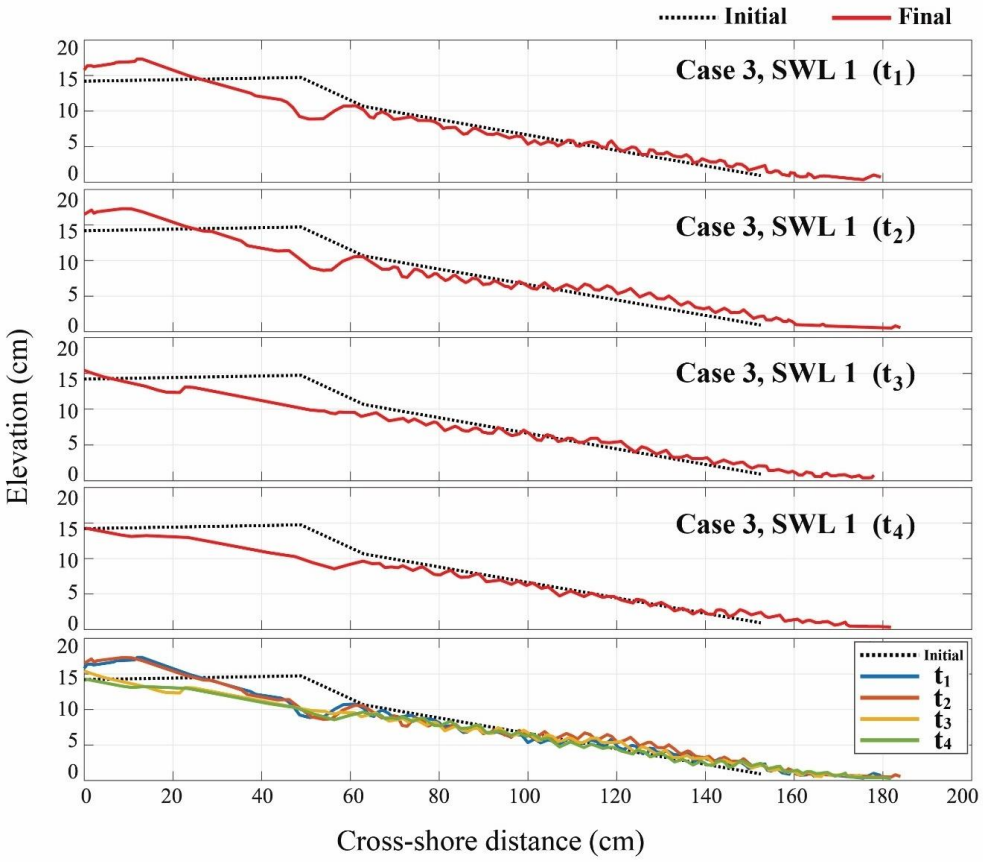


Figure 3.17: Case 3, BGL with SWL 1 profile evolution of $t_1$, $t_2$, $t_3$, and $t_4$

BGL is a type where gravel exists inside the berm to form a permeable layer. The gravel layer inside the sand berm acts as a water-permeable filter, and, unlike SBB in the case of only a sand berm, it has the effect of slowing the erosion rate in the area behind the gravel. This can be seen that it acts as a filter for the permeable layer of gravel and keeps the sand inside the rear section unsaturated for a certain period of time.

For the SWL 2 (Figure 3.18), erosion accelerated; however, as compared to the test case 1 with SWL 2, the gravel layer protected from the scour. In the overall comparison with SWL 1, the landward edge of the gravel layer was eroded after the berm erosion progressed landward, and the thin layer of gravel provided some protection for the sand below the gravel layer.

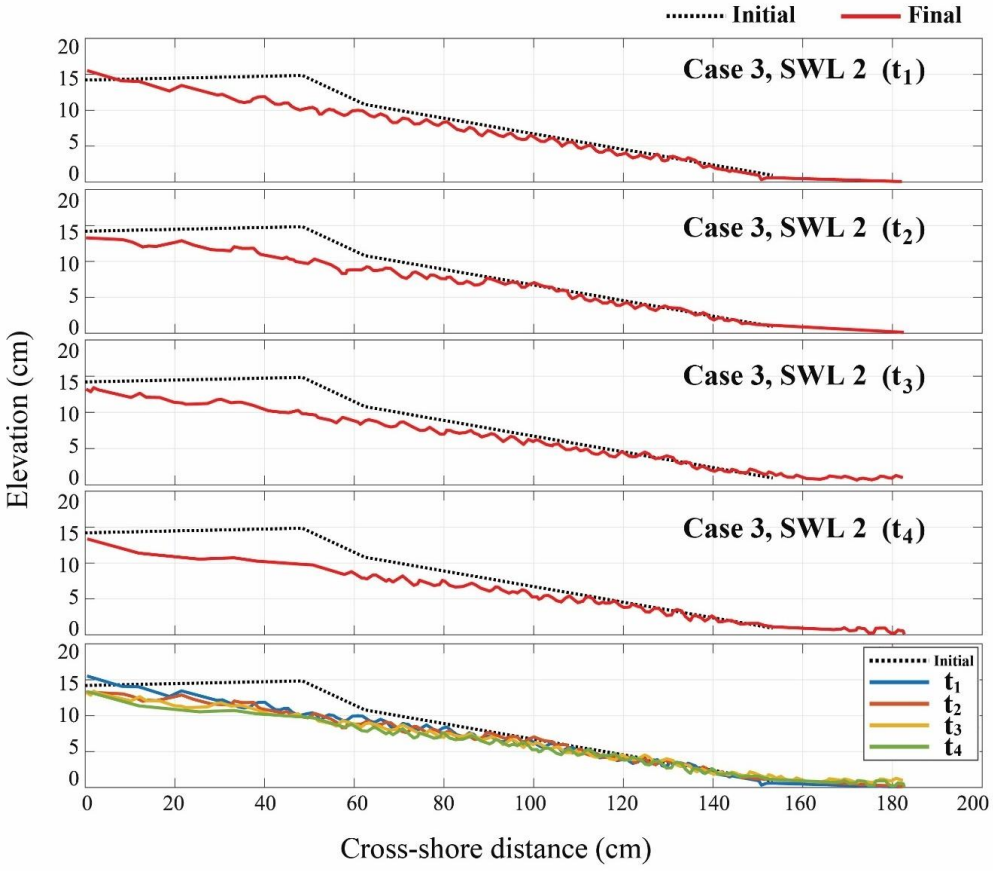


Figure 3.18: Case 3, BGL with SWL 2 profile evolution of $t_1$, $t_2$, $t_3$, and $t_4$

The profile evolution of buried gravel sill, BGS, is shown in Figure 3.19. Similarly, to the BGL test case, gravel was hidden underneath the sand berm with sill shape. The same amount of the gravel was used as test case 3, BGL. Due to the gravel sill, when gravel was exposed, scour occurred on the sand berm. The sill's effect became noticeable only after the sill's crest was exposed, but wave breaking over the exposed crest created a scour hole landward of the sill. Even in the case of BGS, the results confirmed that the role of the gravel filter permeable layer shown in SLW 1 was not exerted at the water level of SWL 2.

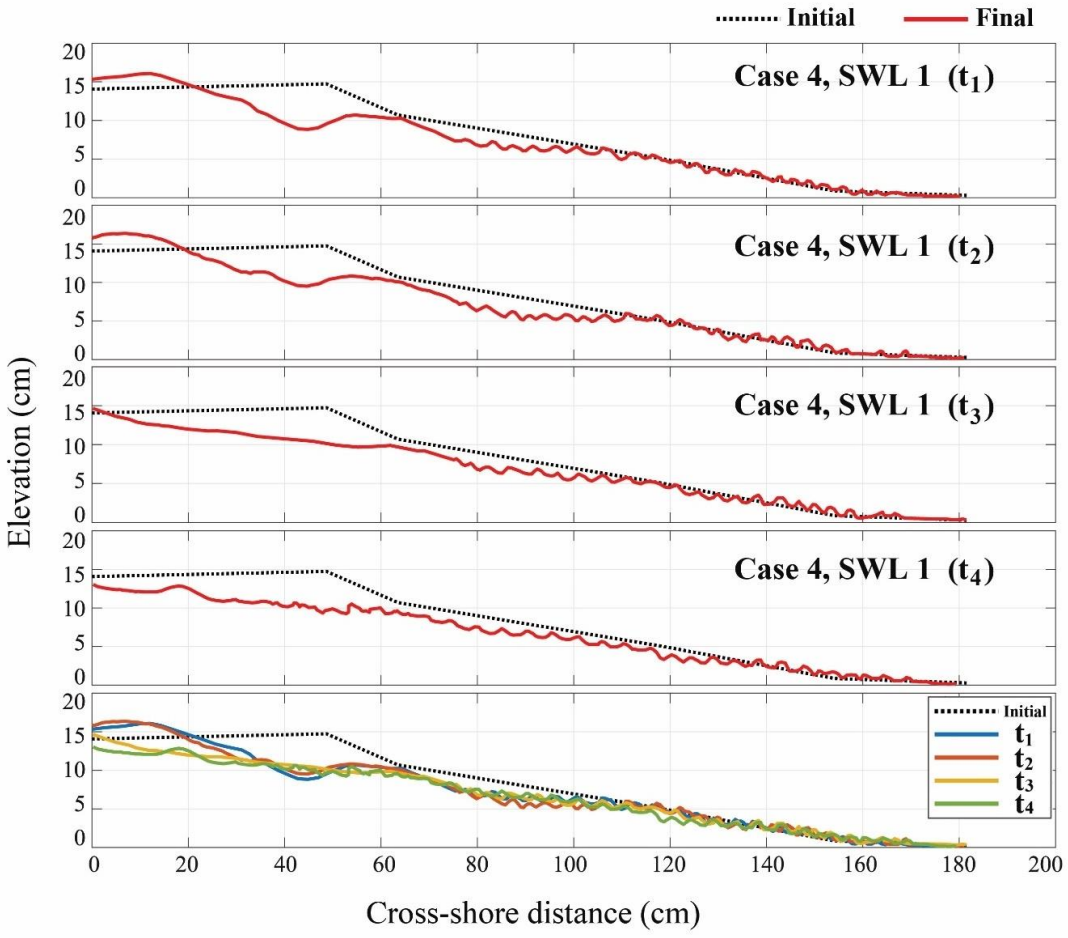


Figure 3.19: Case 4, BGS with SWL 1 profile evolution of $t_1$, $t_2$, $t_3$, and $t_4$

In the case of buried gravel sill with SWL 2 (Figure 3.20), the scour hole occurred after $t_1$, as wave breaking accelerated the erosion on the sand. Therefore, a dune was not formed on the landward, and the scour hole became larger on the berm; however, the scour hole on the berm recovered with the sand after $t_2$.

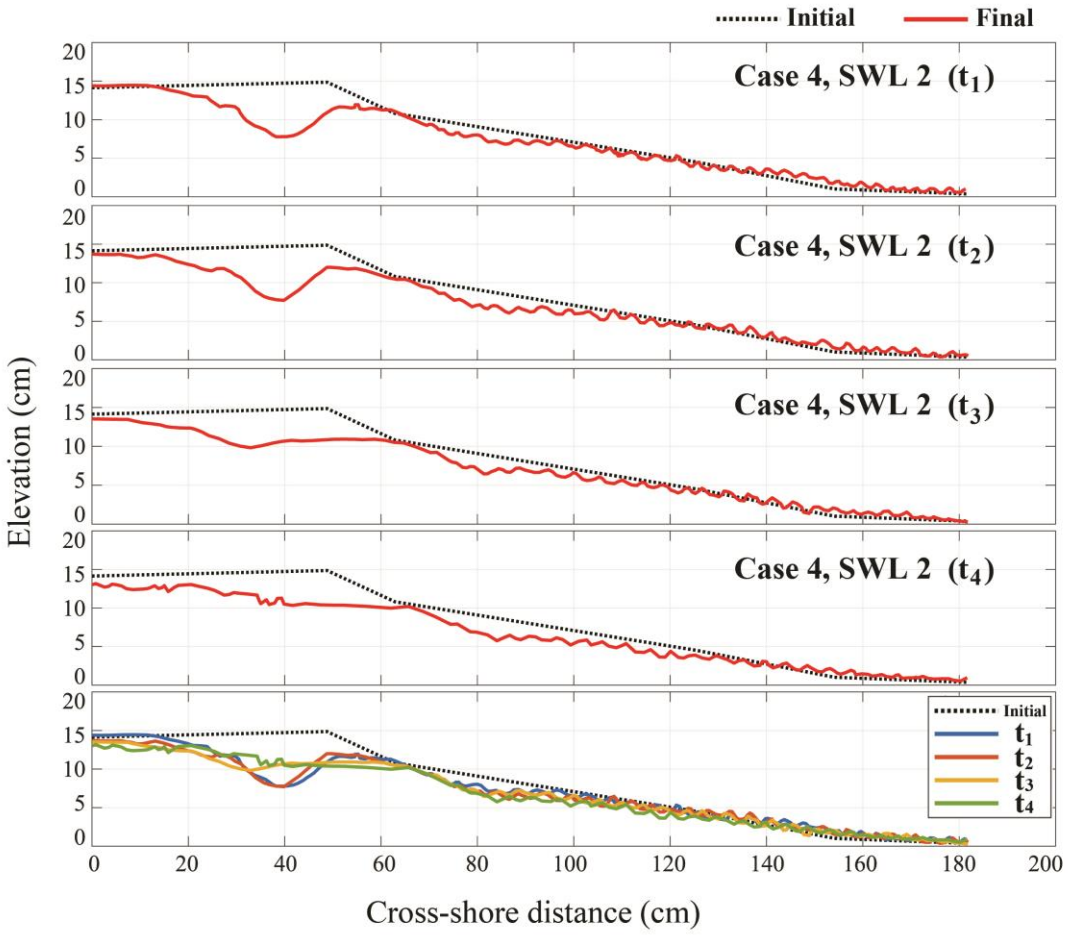


Figure 3.20: Case 4, BGS with SWL 2 profile evolution of $t_1$, $t_2$, $t_3$, and $t_4$

## 3.5 Extra test case using gravel bag

Although Case 3 with gravel layer can initially cover the gravel, and the layer provided some protection to slow down the erosion, the results showed that, when gravel was used in nourishment, there was a problem of gravel moving onshore and, therefore, gravel nourishment can impact on the aesthetic view of the sand beach (see Figure 3.21), as gravel will move onshore.

Therefore, there emerges a question of how to prevent the gravel's moving onshore without changes in the gravel's performance used as nourishment. Accordingly, a gravel filled bag was applied to see whether the usage of the gravel-filled bags could measure the problem. In test case 5, the gravel bag layer (GBL) used the gravel-filled net made of synthetic fiber to substitute the gravel layer from the BGL test case. Usually, such gravel bags are used to protect the foundations of large bridges and are applied in civil engineering for rivers and coastal works.

Gravel-filled bags are a type of fill-containing geosystems (bags, mattresses, geotubes) where the units are filled with sand, gravel, or mortar. Examples of these systems include bags, mattresses, tubes, containers, and open bags filled with gravel, stones, or asphalt. These systems have been extensively used various coastal engineering applications (Havelin, 2012). One of the first applications was in the scope of the Delta Works in the Netherlands in the 1960s and 1970s. However, more rapid developments all over the world took place in the 1980s (Pilarczyk, 2012).

Among various types of sand or gravel-filled bags used for the coastal protection, a gravel bag can be used as a berm and placed along a level contour where sheet flow may be detained and ponded, promoting sedimentation. This gravel bag filters may be used to trap sedimentation or reduce velocity. They have also been used in places where flows are moderately concentrated, such as ditches, swales, and storm drain inlets to

divert and detain currents. A gravel berm consists of a single row of gravel bags installed end to end to form a barrier across a slope to intercept runoff, reduce runoff velocity, release runoff as sheet flow, and provide some sediment removal. Another example is a Grout-filled bag. A major advantage of this bag is that the units hold their shape after the fabric deteriorates or is torn. Sand-filled bag breakwaters are constructed of stacked bags in a staggered pattern. The integrity of the structure depends on the individual bags remaining in place and intact. Among many types of gravel bags, in the experiment, the filter unit, manufactured by Kyowa (Sumitomo Corp., 2017) shown in Figure 3.22 was applied using the same initial profile and the same amount of gravel used in the BGL test case. (see Figure 3.23 -3.24).


Figure 3.21: End of the test case 3 test

Figure 3.22: Kyowa's Filter Unit (Gravel-filled bag)

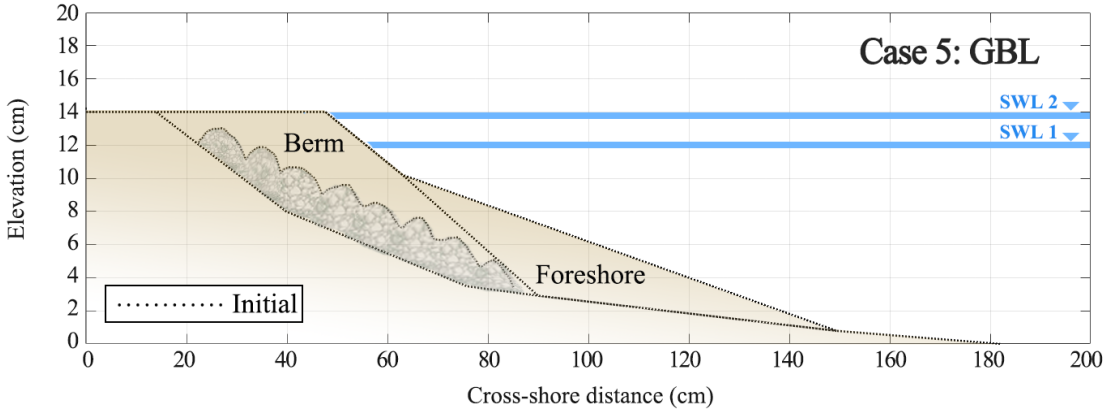


Figure 3.23: Test Case 5 Gravel Bag Layer (GBL) initial profile

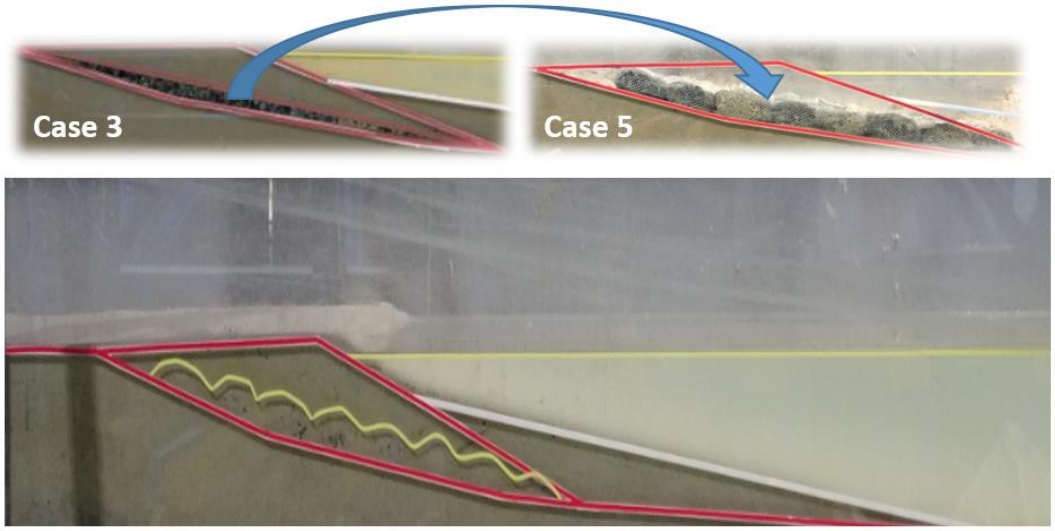


Figure 3.24: Hydraulic model experiment using gravel bags

Due to the interaction among gravel bags using the hydraulic model experiment conducted using SWL 1, no considerable difference was observed compared to the buried gravel layer, test case 3, except for the mixture of composite gravel sand moving onshore was not observed in this test case (Figure 3.25). This was so because gravel tied in a synthetic fiber mesh, and no movement of the filter unit was detected throughout the experiment.

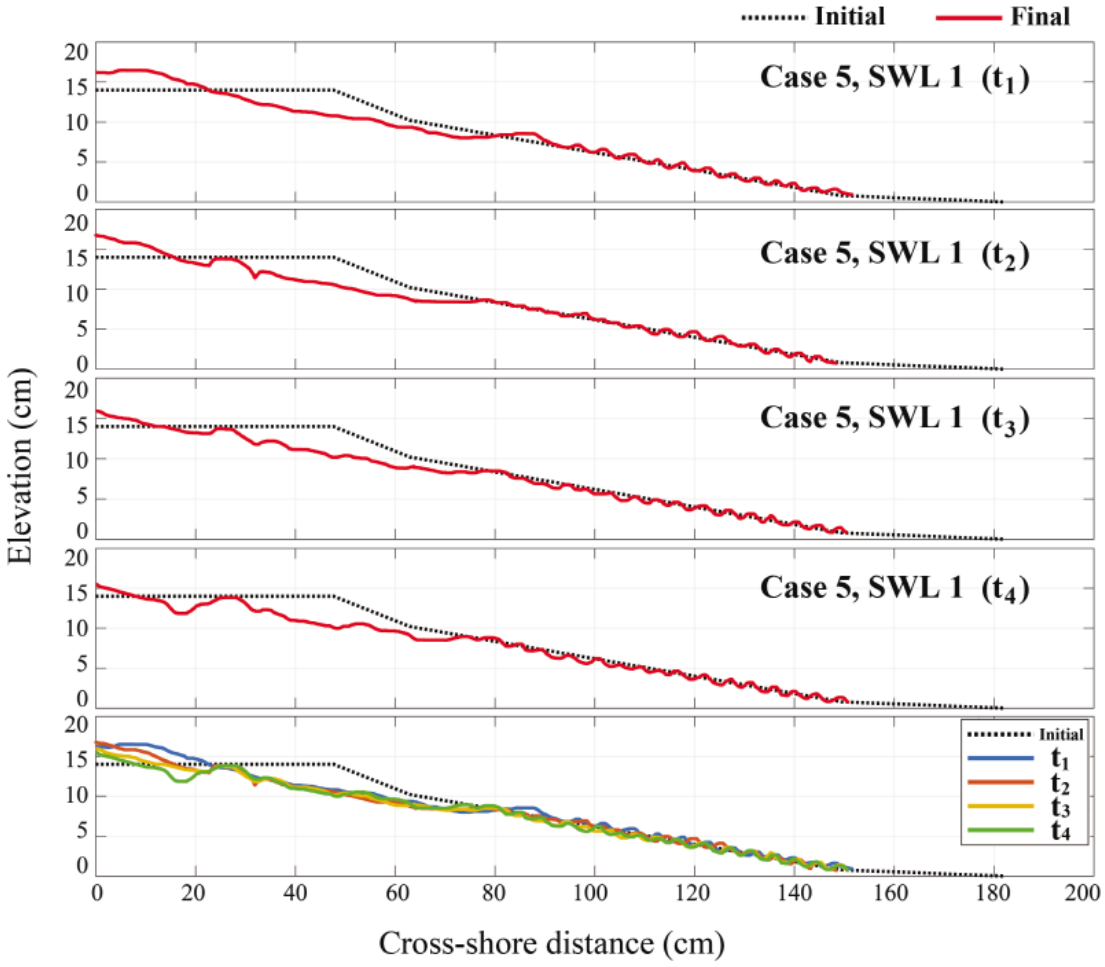


Figure 3.25: Case 5, GBL with SWL 1 profile evolution of $t_1$, $t_2$, $t_3$, and $t_4$

For the GBL with SWL2, as time passed, the erosion persisted; however, the filter unit did not move; therefore, there was no movement of gravel (see Figure 3.26).

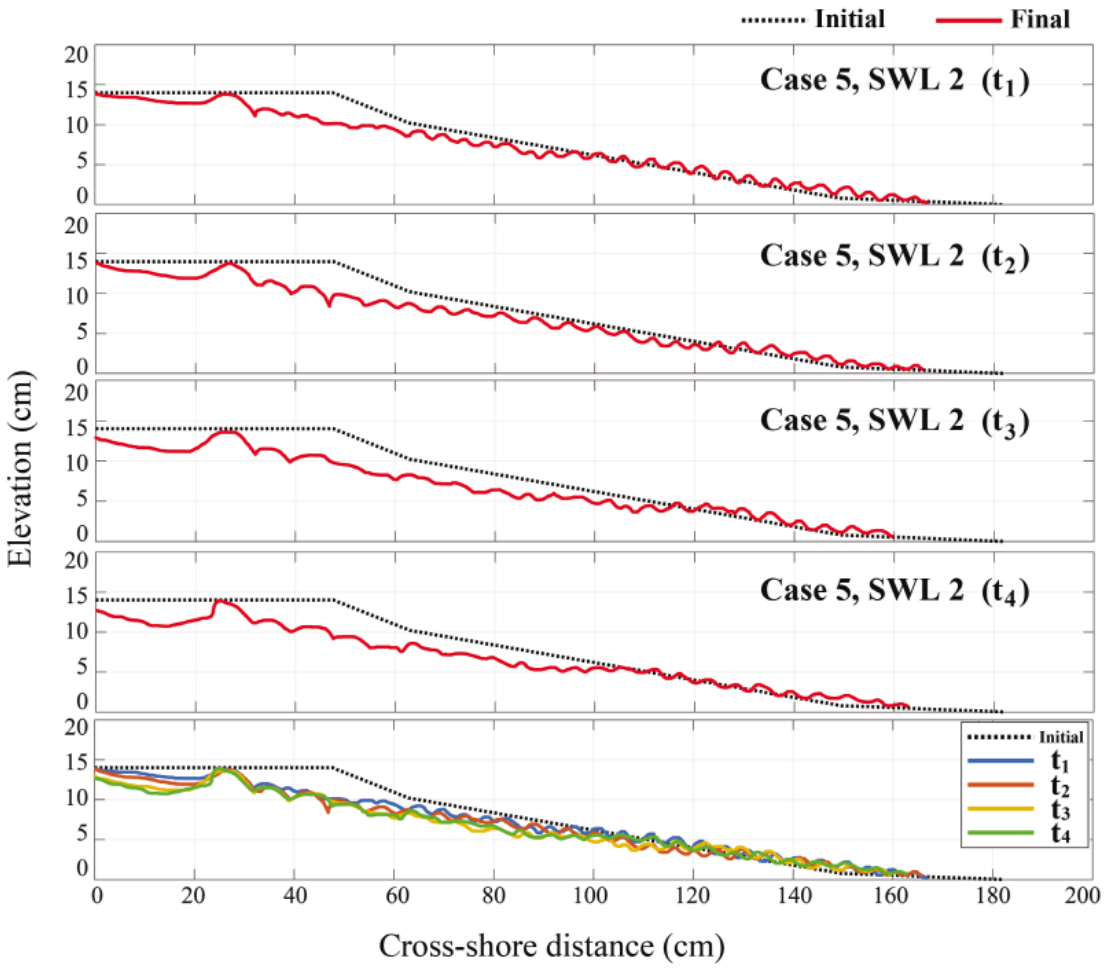


Figure 3.26: Case 5, GBL with SWL 2 profile evolution of $t_1$, $t_2$, $t_3$, and $t_4$

The overall tendency was similar; however, while BGL created a berm at the initial landward, it also created scouring at the gravel layer and caused gravel moving onshore. Unlike in the case of BGL, the GBL test case was more stable and created no gravel movement.

The results of comparison of the erosion tendencies for case 3 and case 5 at the water level of SWL 1 showed that, when the gravel of GBL was replaced with the gravel bag, there was no significant difference in the profile between them. As shown in Figure 3.27, the rear of the berm showed different sedimentation patterns in the time condition of $t_2$, where in case 5, the gravel bag could not be installed to the ground, which caused erosion faster than in case 3.

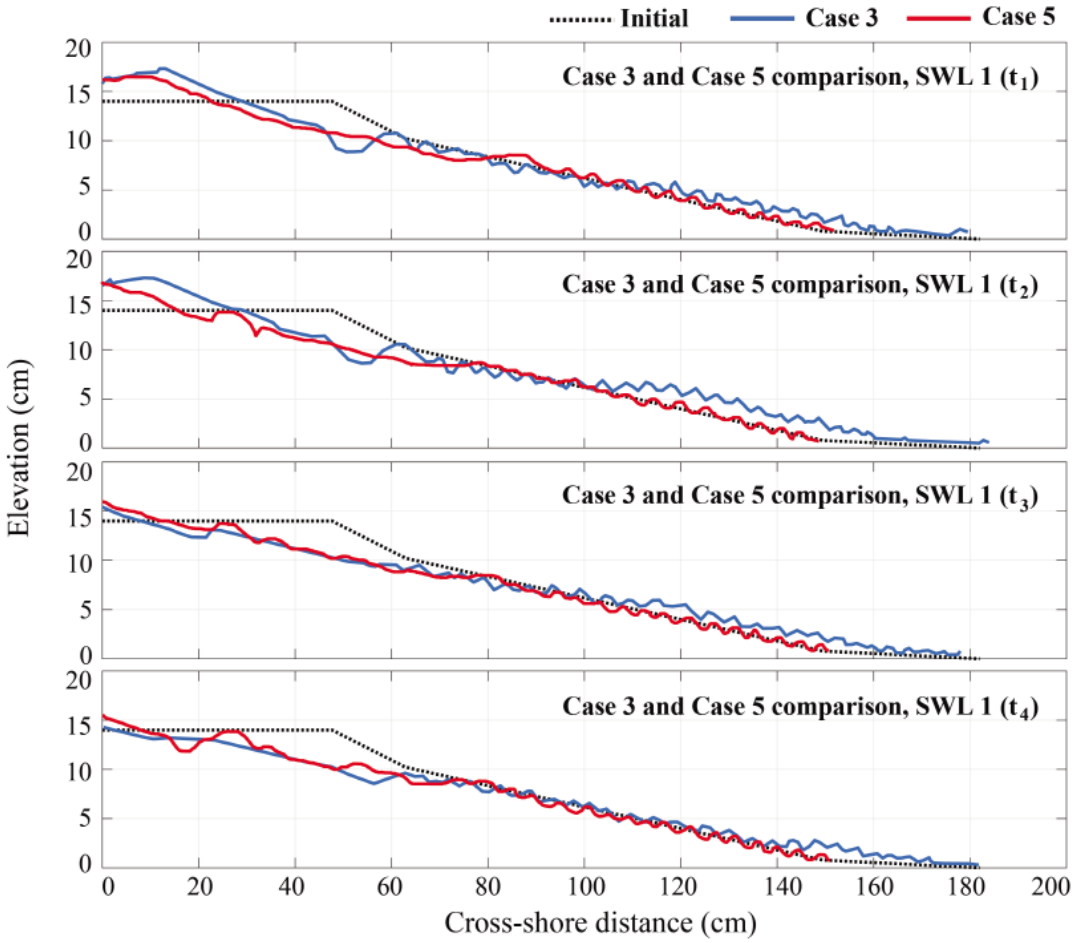


Figure 3.27: Case 3 and 5 SWL 1 comparison of $t_1$, $t_2$, $t_3$, and $t_4$

In SWL 1, overall erosion and deposition patterns of case 3 and case 5 were similar; however, in SWL 2, case 5 was found to have superior erosion control ability as compared to case 3. This was so because, in the case of test case 3, as time passed, the role of the gravel permeable layer was reduced by the scattering of some moving gravel into the surface layer. On the other hand, the results confirmed that the gravel bag of case 5 demonstrated the ability to control erosion for a long time by sufficiently exerting the permeable layer's role despite the passage of time.

When SWL increased, the difference was considerable. Since the gravel bag protected the berm from forming the scour hole, erosion persisted. By the end of $t_1$, unlike in test case 3, a large amount of sand dune formed on the backshore. When test case 3 has eroded dune on the backshore, in test case 5, a sand dune formed even higher. This dune slowly eroded after $t_2$; however, not much erosion was observed on the backshore as compared to the other test case. Erosion on the berm on top of the gravel and the gravel bag layer appeared similar; however, after $t_3$, in test case 5, the formation of the scour hole was prevented. This method is effective in the event of high waves such as hurricanes, and the results confirmed that sedimentation was trapped by gravel bags to prevent erosion. Besides, due to their low cost, simple processing, and the possibility of being tailor-made, gravel bags are considered as a great countermeasure to be used with nourishment.

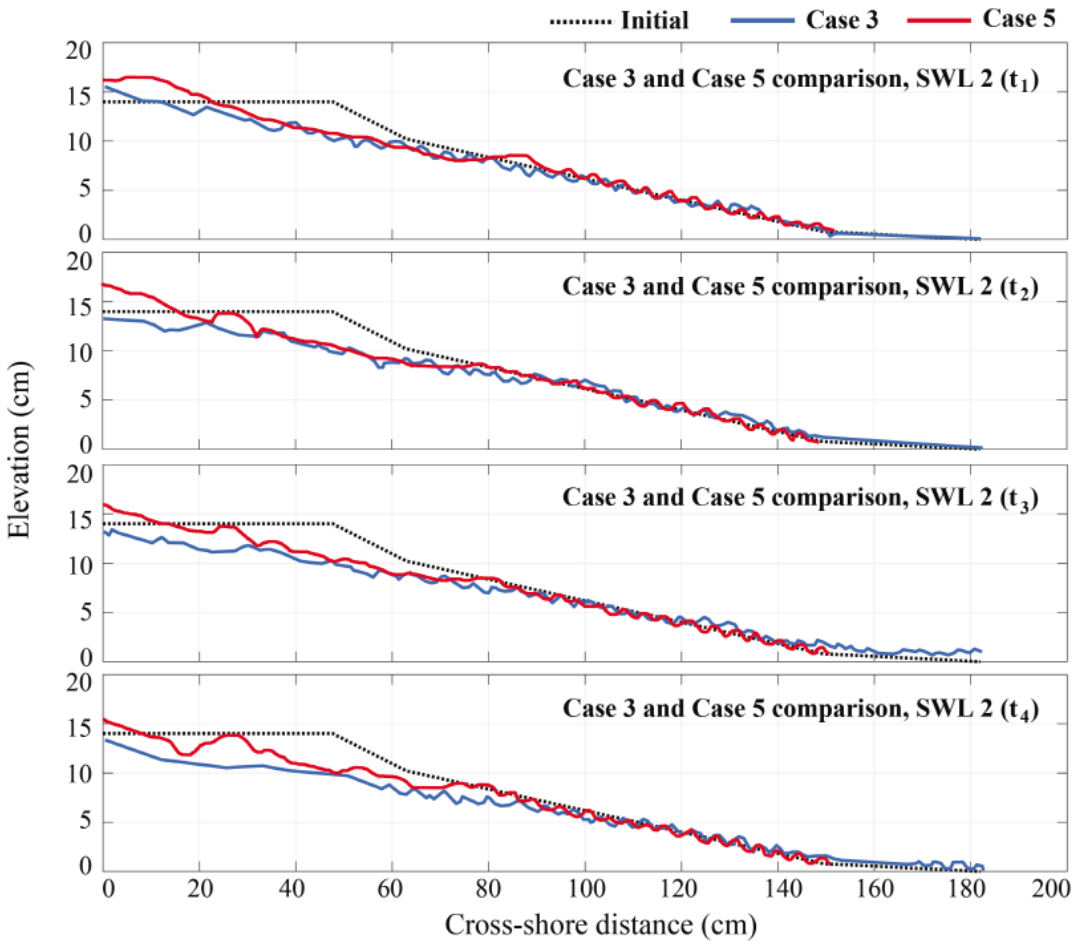


Figure 3.28: Case 3 and 5 SWL 2 comparison of $t_1$, $t_2$, $t_3$, and $t_4$

Thus, by looking at the Figure 3.29, A comparison of the outcomes of test cases 3 and 5 showed that, in the latter case, due to gravel's being tied in synthetic fiber mesh, no movement of filter unit was detected throughout the experiment (see Figure 3.29).


Figure 3.29: Top view of the end of test cases 5 and 3.

## 3.6 Conclusions

In this chapter, beach profile evolution and sediment transport were experimentally investigated using gravel to reinforce a nourished sand beach for low wave energy shores with limited sediment availability. Porous gravel berm interacted with wave action in the swash zone and reduced wave overtopping and berm erosion. Sand particles moved as bedload and suspended load, whereas gravel particles moved as bed load only. When gravel bags substituted the gravel layer, gravel particles did not move, and only sand particles moved as bedload and suspended load. Therefore, it can be concluded that, for the purposes of both aesthetic value and effectiveness in low wave energy shores, gravel nourishment can be replaced by gravel bags.

# Chapter 4

# NUMERICAL SIMULATIONS AND ARTIFICIAL INTELLIGENCE

This chapter explains the numerical simulation models to compute beach profile evolution and sediment transport of four different test cases conducted through hydraulic model experiments. Since the current numerical simulation models cannot simultaneously reproduce the gravel and sand, artificial intelligence that uses the neural networks was applied as a new way to cluster and classify sediment transport. The efficiency of application back-propagation neural network with three hidden layers to emitter identification was examined. This chapter reports the results obtained through ANN model.

## 4.1 Introduction

Most shorelines worldwide are experiencing some form of erosion, and this trend can aggravate if the mean sea level rise accelerates due to the greenhouse effect (Nicholas and Cazenave, 2010). The recent increase of coastal storm damage necessitates the development of numerical models to predict the damage progression and breaching of beaches, coastal stone structures, and earthen leaves during extreme storms. In this context, in order to quantitatively understand the beach morphology and damage progression, robust and straightforward models to reproduce the phenomenon are necessary. Unfortunately, current models cannot calculate the damage while simultaneously using different grain sizes.

Current models are based on the combinations of many physical equations (e.g., the wave energy equation) and are calibrated and verified using small-scale hydraulic model experiments. Throughout the experiment, test case 1 was the only sediment of sand with $D_{50}$ 0.16 mm used, compared with various 2D numerical simulations.

Numerical models CSHORE, SBEACH, and XBEACH were tested and compared with the results of the hydraulic model experiment. Moreover, the results of the artificial model were compared with the results of numerical simulations.

Other than test case 1, hydraulic model experiments of test case 2,3, and 4 with different SWL were compared with the AI model prediction. In this chapter, the aim is to explore the possibility of reproducing the AI convergence and application on sediment transport. Since only the data obtained from the current hydraulic model experiment were used in the AI prediction, the results may not be entirely reliable; however, they can show the application's possibility.

## 4.2 Numerical Simulations

This chapter aims to validate the ability of three cross-shore numerical models (CSHORE, SBEACH, and XBEACH-G), and artificial neural network model developed in this study to overcome the shortcomings of other numerical simulations.

Due to dramatic advances in the capabilities of personal computers, the usage of numerical model tests for coastal regions has become increasingly popular. Combining numerical and hydraulic model plays a vital role in quantifying the natural processes, such as beach profile performance or sediment transport behavior. Such a relationship produces the potential capacity to replicate complex features that cannot be obtained in the field. Moreover, soft techniques such as beach nourishment should be tested before actual nourishment; furthermore, to be nourished in the best placement, numerical simulation can be simply and quickly applied.

With regard to the sediment transport profile behavior, in the literature, numerous numerical models for the littoral zone have been proposed (Yuan, 2017). For instance, in a pioneering study on the beaches along the Danish North Sea coast and the California coast, Bruun (1954) developed a predictive equation for the equilibrium beach profile. Furthermore, using the wave energy approach and differentiation between bedload and suspended load, Bagnold (1966) developed formulas to calculate sediment transport rates, including cross-shore transport. Several subsequent studies, including Bailard (1982), and Stive and De Vriend (1987) refined Bagnold's (1966) work. Using a combination of theory and field observation, Larson (1996) proposed the SEBACH model to predict profile changes due to storms; similarly, the CSHORE model was used to predict such changes in response to the interactions between waves and currents. Finally, the XBEACH-G model was proposed that uses non-linear shallow water equations, such as a non-hydrostatic pressure term and a source term for the exchange

with groundwater. However, a limitation of all aforementioned models is that all of them reply to the equilibrium profile assumption to estimated profile and sediment transport.

The initial version of the CSHORE model, developed by Kobayashi and his colleagues at the University of Delaware, was based on irregular nonlinear wave theory which uses the time-averaged continuity, momentum, and wave energy equation together with a non-Gaussian probability distribution of the free surface elevation (Kobayashi and Kim, 2017; Kim et al., 2016). However, due to complex natural environments and the limitations of empirical formulas, this model has several limitations. Therefore, in the present study, for the case of alongshore uniformity, the model was developed based on the equilibrium profile and linear wave theory combined with the current. The sediment transport rate was computed based on a combination of cross-shore and longshore suspended load and bedload in the surf zone. The calculation of the wave and current model was based on the time-averaged continuity equation, the cross-shore and longshore momentum equation, and the wave action equation in the surf zone. Given that the CSHORE is a time-averaged probabilistic model, the sediment transport model formulation involved predicting both suspended load and bedload transport rate. For the CSHORE sediment transport, the time-averaged bedload transport rate $q_{bx}$ was estimated using Eq. (4.1), and time-averaged cross-shore suspended sediment transport rate $q_{sx}$ was computed based on Eq. (4.2).

$$q_{bx} = \frac{bP_b\sigma_U^3}{g(s-1)} G_s(S_{bx}) \tag{4.1}$$

$$q_{sx} = a\bar{U}V_s \; ; \;\; a_x = [a + (S_{bx}/\tan\,\emptyset)^{0.5}] \geq a \tag{4.2}$$

where $b$ is the empirical bed load parameter with the value in the range of 0.001-0.004, $S_{bx}$ is the cross-shore slope, and $G_s$ is the bottom slope function where $G_s = \left(1 - \frac{S_{bx}}{tan\phi}\right)$, $tan\phi$ is the avalanching angle, $s$ is the sediment specific gravity, $a = (0.2 + \sqrt{S_{bx}/0.63})$ is the suspended load parameter of the order of 0.2 under the action of waves and wave-induced currents for upward slopes, $P_b$ is the sediment movement probability, $U_0$ is the onshore current due to the wave overtopping rate $q_0$, $\overline{U}$ is given in Eq. (4.3), $C_e$ is an empirical coefficient, $V_s$ is the suspended sediment volume per unit horizontal area in Eq. (4.4), $V_{Bf}$ is the potential suspended sediment volume on a horizontal bottom (see Eq. (4.5)). Overbar indicates time-averaged values.

$$\overline{U} = -\frac{g\bar{h}}{{C_e}^2}\sigma_U\sigma * \left(1 + \frac{C_e q_r}{g\sigma_\eta^2}\right) + \frac{Q_x}{\bar{h}} \tag{4.3}$$

$$V_s = P_s V_{Bf}(1 + S_{bx}^2)^{0.5}(1 + S_{by}^2)^{0.5}\ ;\ S_{bx} = \frac{\partial z_b}{\partial x};\ S_{by} = \frac{\partial z_b}{\partial y} \tag{4.4}$$

$$V_{Bf} = \frac{e_B D_r + e_f D_f}{\rho g(S-1)ws} \tag{4.5}$$

where $e_b$ = 0.005, $e_f$ = 0.01, and $w_s$ is the sediment fall velocity. $P_{s,}$ the probability of sediment suspension, was included in Eq. (4.4). The sediment transport direction was assessed by both suspended $q_{sx}$ and bed load transport rate $q_{bx}$. The following cross-shore equilibrium profile concept proposed by Dean (1991) was used: $q_{sx} + q_{bx} = 0$. When $q_{sx}$ was negative, the transport direction was offshore, as the return current $\overline{U}$ was negative (offshore). Alternatively, when $q_{bx}$ was positive, the transport direction was onshore for $S_{bx} < (tan\phi)/2$, and when $q_{bx}$ was negative, transport was offshore for $S_{bx} > (tan\phi)/2$ (Kobayashi, 2016). Although equations used in the CSHORE model pertain to various sectors, only the sediment transport part was reviewed.

The SBEACH model, originally developed by the US Army Corps of Engineers, is a numerical model for simulating cross-shore storm-induced beach transport that can simulate long-term recession processes with empirical coefficients derived from process-based models (Roelvink et al., 2009). The SBEACH model simulates beach profile changes, such as the formation and movements of significant morphologic features (e.g., berms and bars) for various parameters of storm waves and water levels. Breaking waves and changes in the sea level are the major parameters accounted for by the SBEACH model. This model is based on the equation of mass conservation that requires the mathematical expression for the cross-shore transport rate. The transport direction and the rate of transport equations are developed separately for monochromatic waves and irregular waves. The model enables determining the direction of net cross-shore transport based on the deep-water wave steepness ($H_o/L_o$) and sediment fall velocity ($w_s$). Eq. (4.6) is the transport direction equation for monochromatic wave types.

$$\frac{H_o}{L_o} = M\left(\frac{H_o}{wsT}\right)^3,\ M = 0.00070 \tag{4.6}$$

where $\frac{H_o}{L_o} > M\left(\frac{H_o}{L_o}\right)^3$ is accretion, while $\frac{H_o}{L_o} < M\left(\frac{H_o}{L_o}\right)^3$ is erosion. $H_o$ is deep water wave height, $T$ is the wave period, and $L_o$ is the deep water wave length. The monochromatic wave transport equation under broken waves is shown in Eq. (4.4), where $q$ is the net cross-shore transport rate, $\frac{m^3}{sec*m}$, $\epsilon$ is the slope related transport rate coefficient $\frac{m^2}{sec}$, $K$ is the sand transport rate coefficient $\frac{m^4}{N}$, and $h$ is the still water level in m. x is the cross-shore coordinate directed positive offshore in m, D is the wave energy dissipation per unit water volume $\left(\frac{Nm}{m^3 sec}\right)$, and $D_{eq}$ is the equilibrium wave energy dissipation per unit water volume $\left(\frac{Nm}{m^3 sec}\right)$. $\in$ is slope related transport rate coefficient.

$$q = \begin{pmatrix} K\left[D - \left(D_{eq} - \frac{\in}{K}\frac{dh}{dx}\right)\right] & D > D_{eq} - \frac{\in}{K}\frac{dh}{dx} \\ 0 & D \leq D_{eq} - \frac{\in}{K}\frac{dh}{dx} \end{pmatrix} \quad (4.7)$$

where $D = \frac{1}{h}\frac{df}{dx}$, $D_{eq} = \frac{5}{24}\rho g^{3/2}\gamma^2 A^{3/2}$, and the energy flux = $\frac{1}{8}\rho g H^2\sqrt{gh}$ ($A$ is dean's scaling parameter, and $\gamma$ is a wave breaker index).

For irregular wave types, the transport direction is determined as follows (see Eq. (4.8)):

$$\xi = 2\frac{e^{-\frac{1}{M}\frac{H_{rmso}}{L_o}\left(\frac{wsT}{H_{rmso}}\right)^3}}{e^{-\left(\frac{H_{bo}}{H_{rmso}}\right)^2}} - 1, \quad -1 \leq \xi \leq 1 \quad (4.8)$$

In Eq. (4.3), $\xi$ represents the net transport direction, $H_{rmso}$ is the deep-water root mean square (rms) wave height and $H_{bo}$ is the wave height at incipient breaking transformed seaward to deep water, $M$=0.0007. Net erosion occurs when $\xi$ is positive, whereas net accretion is predicted when $\xi$ is negative.

The transport rate equation for random wave types is shown in Eq. (4.9).

$$q = K\xi\left[D - \alpha\left(D_{eq} - \frac{\epsilon}{K}\frac{dh}{dx}\right)\right] \quad (4.9)$$

where D is the average energy dissipation per unit water volume, K is the sand transport rate coefficient $\xi$ that weights the influence of erosion versus accretion waves on the transport rate and determines the net direction of transport. In Eq. (4.9), $\alpha\left(D_{eq} - \frac{\epsilon}{K}\frac{dh}{dx}\right)$ part must be in positive in order to make the transport to occur; otherwise, the transport is set to zero (Wise et al., 1996). Furthermore, transport rate is set to zero when the

sections where $\frac{dh}{dx} < 0$ as the computations progress up the foreshore (Larson, 1996). Therefore, SBEACH is unable to model the accretion process under irregular waves.

XBEACH—a model used to model the nearshore processes, such as wave breaking, surf and swash zone processes—was originally proposed by Reolvink et al. (2007). A powerful tool to reproduce the erosion for sediment transport, the XBEACH model includes long wave transformation, short wave transformation (refraction, shoaling, and breaking), time-varying depth-averaged currents, wave-induced setup and run-up, wave-current interaction, roller momentum exchange, over-wash, as well as inundation and hard structures. . A limitation of this model is that it requires extensive modelling input and running time. Reviewing the significant sediment transport formula, the sediment transport is modelled with a depth-averaged advection-diffusion equation (see Eq. (4.10); Galappatii and Vreugdenhil, 1985).

$$\frac{\partial hC}{\partial t} + \frac{\partial hCu^E}{\partial x} + \frac{\partial hCv^E}{\partial y} + \frac{\partial}{\partial x}\left[D_h h \frac{\partial C}{\partial x}\right] + \frac{\partial}{\partial y}\left[D_h h \frac{\partial C}{\partial y}\right] = \frac{hC_{eq} - hC}{T_s} \qquad (4.10)$$

where $C$, which varies on the wave group time scale, is the depth-averaged sediment concentration, $C_{eq}$ is the equilibrium concentration computed as shown in Eq. (4.11), and $D_h$ is the sediment diffusion coefficient. Furthermore, $T_s$ is an adaptation time based on the local water depth h and sediment fall velocity $w_s$, representing the entrainment of the sediment. The continuity equation, which indicates bed-updating, is shown in Eq. (4.12).

$$C_{eq} = \frac{A_{sb} + A_{ss}}{h}\left(\left(|u^E|^2 + 0.018\frac{u_{rms}^2}{C_d}\right) - u_{cr}\right)^{2.4}(1 - \alpha_b m) \qquad (4.11)$$

$$\frac{\partial z_b}{\partial t} + \frac{f_{mor}}{1-p}\left(\frac{\partial q_x}{\partial x} + \frac{\partial q_y}{\partial y}\right) = 0 \tag{4.12}$$

where $A_{sb}$ is a bed load coefficient, $A_{ss}$ is a suspended sediment coefficient, $u_{cr}$ is critical velocity for sediment to move, and $C_d$ is drag coefficient. To account for bed-slope effects on the equilibrium sediment concentration a bed-slope correction factor is introduced, where the bed slope is denoted by $m$ and $\alpha_b$ represents a calibration factor. $f_{mor}$ is a morphological acceleration factor of order (1-10), $p$ is the porosity, while $q_x$ and $q_y$ are the sediment transport rates in x and y direction, respectively (see Eq. (4.13)-(4.14)).

$$q_x(x,y,t) = \left[\frac{\partial hCu^E}{\partial x}\right] + \left[\frac{\partial}{\partial x}\left[D_h h \frac{\partial C}{\partial x}\right]\right] \tag{4.13}$$

$$q_y(x,y,t) = \left[\frac{\partial hCu^E}{\partial y}\right] + \left[\frac{\partial}{\partial y}\left[D_h h \frac{\partial C}{\partial y}\right]\right] \tag{4.14}$$

The formulation in XBEACH uses the Soulsby-Van Rijin transport concept (Roelvink et al., 2009) and the avalanching approach to update the morphology. XBEACH-G, which was used in this study is based on the XBEACH model for sandy coasts, which has previously been modified to solve intra-wave flow and surface elevation variations for waves in intermediate and shallow water depths by means of a one-layer, depth-averaged, non-hydrostatic flow model (McCall, et al., 2015).

## 4.3 Numerical Simulation Results

Sandy beaches without any protection are vulnerable to storm waves and cause a large amount of erosion. Similarly, to the results of test case 1, when only sand was used in the nourishment, beach acquired equilibrium soon after the storm wave attacks. As current numerical models cannot reproduce test case 2, 3, and 4 with gravel nourishment, only test case 1 was compared among other numerical models.

The aim of this section is not to compare and see which model is the best, but to see whether AI model can reproduce the reasonable prediction like the other numerical simulations as will be discussed in section 4.7. For all three numerical models used 0.16 mm for the $D_{50}$ and used irregular waves with same wave heights and wave period used in hydraulic model experiment. Since SBEACH and XBEACH-G models are made with GUI, all the input factors were easily set as same as the hydraulic model experiments. All the models used number of calculation cells or grid sizes smallest as possible. For the different parameters each model requires, 30 degrees were used for maximum slope prior to avalanching in SBEACH, and 30 degrees were used for angle of repose in XBEACH-G. For the sediment friction factor, default value of 0.025, and for the hydraulic conductivity, *K*, 0.1 m/s was used. For the CSHORE, version developed in 2017 (Kobayashi and Kim, 2017) was used throughout the test; however, among many parameters, only parameters calculate sediment transport were selected and used as same as the hydraulic model experiments. SBEACH and CSHORE computational running time was short, unlike XBEACH requires extensive computational running time.

Again, the focus of this section is to see numerical simulations can reasonably generate equilibrium beach profile like hydraulic model experiment did and later compare it with AI model results to see whether AI model is comparable with these numerical models. Therefore, after runtime of 120 minutes, beach profile was compared

as shown in Figure 4.1 and Figure 4.2. Using SWL 1 with the same wave conditions, it was found that the results of CSHORE showed the most similar profile evolution as compared to that of the measured profile. XBEACH created the dune on the backshore; however, a relatively good agreement was observed. On the other hand, the results of SBEACH showed too much deposition on the foreshore. Overall, all the numerical simulations could reproduce the equilibrium beach profile with SWL 1.

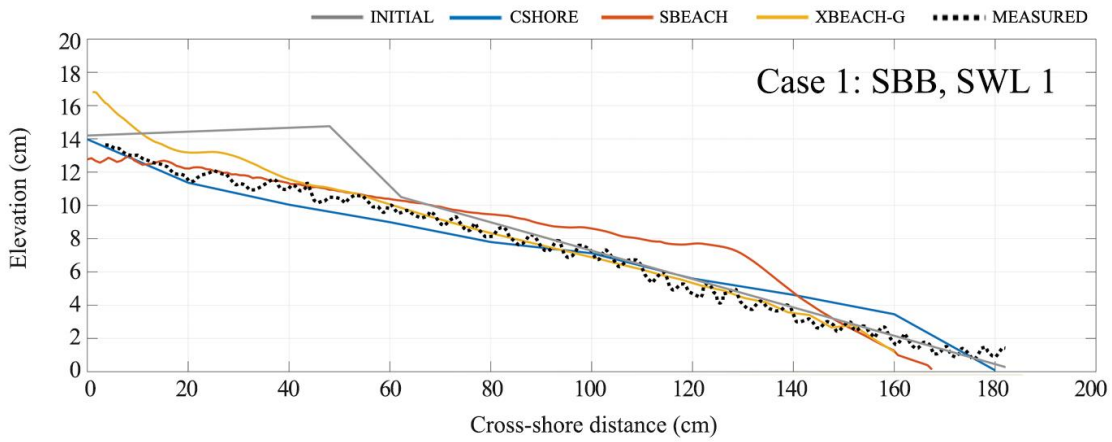


Figure 4.1: Case 1 SBB, SWL1 numerical simulations and measured comparison

When SWL was increased to SWL 2, the results varied. Soon after the SWL increased, the final profile of SBEACH, which is sensitive to water level changes, became parallel to the ground. SBEACH is sensitive to both wave climate and water level changes, which is an advantage of the model; however, in this case, when SWL increased to almost the same as the ground level, an accurate calculation could not be performed. On the other hand, the final profile of CSHORE showed extensive erosion on the backshore; however, the general profile looked most similar to that of the measured profile. XBEACH showed extensive erosion both on the berm and foreshore.

By examining each model's formulations, it can be seen that the empirical models with equilibrium profile concepts were more economical; however, this computation is not always accurate compared to energetic models, especially with high seawater level (see Figure 4.2). Energetic models have an advantage in accuracy and theory of formulation, but are time-consuming and not suitable for the long-term simulation.

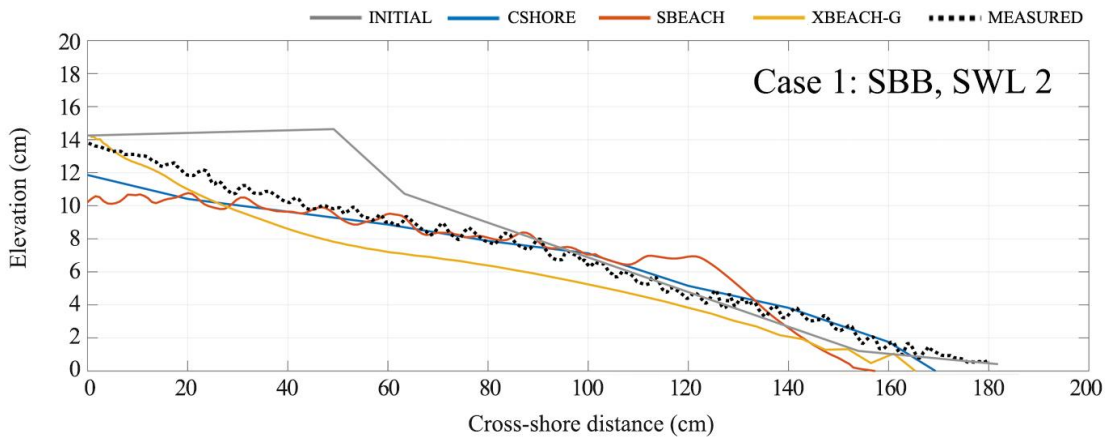


Figure 4.2: Case 1 SBB, SWL2 numerical simulations and measured comparison

## 4.4 Artificial Neural Networks (ANN)

Artificial neural networks (ANN), a major tool in deep learning computing, are widely used across all coastal and ocean engineering disciplines, including offshore, deep-ocean, and marine engineering. ANN are being used in the areas of prediction and classification, areas where regression and other related statistical techniques have traditionally been used (Abambres et al., 2017; Banihabib et al., 2020). ANN, in general, have provided either substitutive or complementary options to traditional computational schemes of statistical regression, time series analysis, pattern recognition, and numerical methods (Chaudhuri et al., 2016; Konate, 2019; Tealab, 2018). Due to the limitations of numerical simulation reproducing the gravel nourishment, in this chapter, ANN were used to try to predict the future profile evolution of test cases 1, 2, 3 and 4 using the hydraulic model experiment data as a training dataset. Recently, ANN have been studied as an alternative to the non-linear model-driven approaches. ANN rely on a data-driven approach where the analysis depends on the available data, with little *a priori* rationalization about the relationships between variables and about the models. The process of constructing the relationship between the input and output variables is addressed by a certain general-purpose learning algorithm.

In the present study, the ANN were inspired by information processing and communication nodes in biological systems (Salahudeen et al., 2018). ANN follow the cognition process of the biological neurons of a brain and develop the intelligence from communications between different artificial neurons. An ANN are basically composed of a set of interconnected artificial neurons, nodes or a group of processing units that process and transmit information through activation functions.

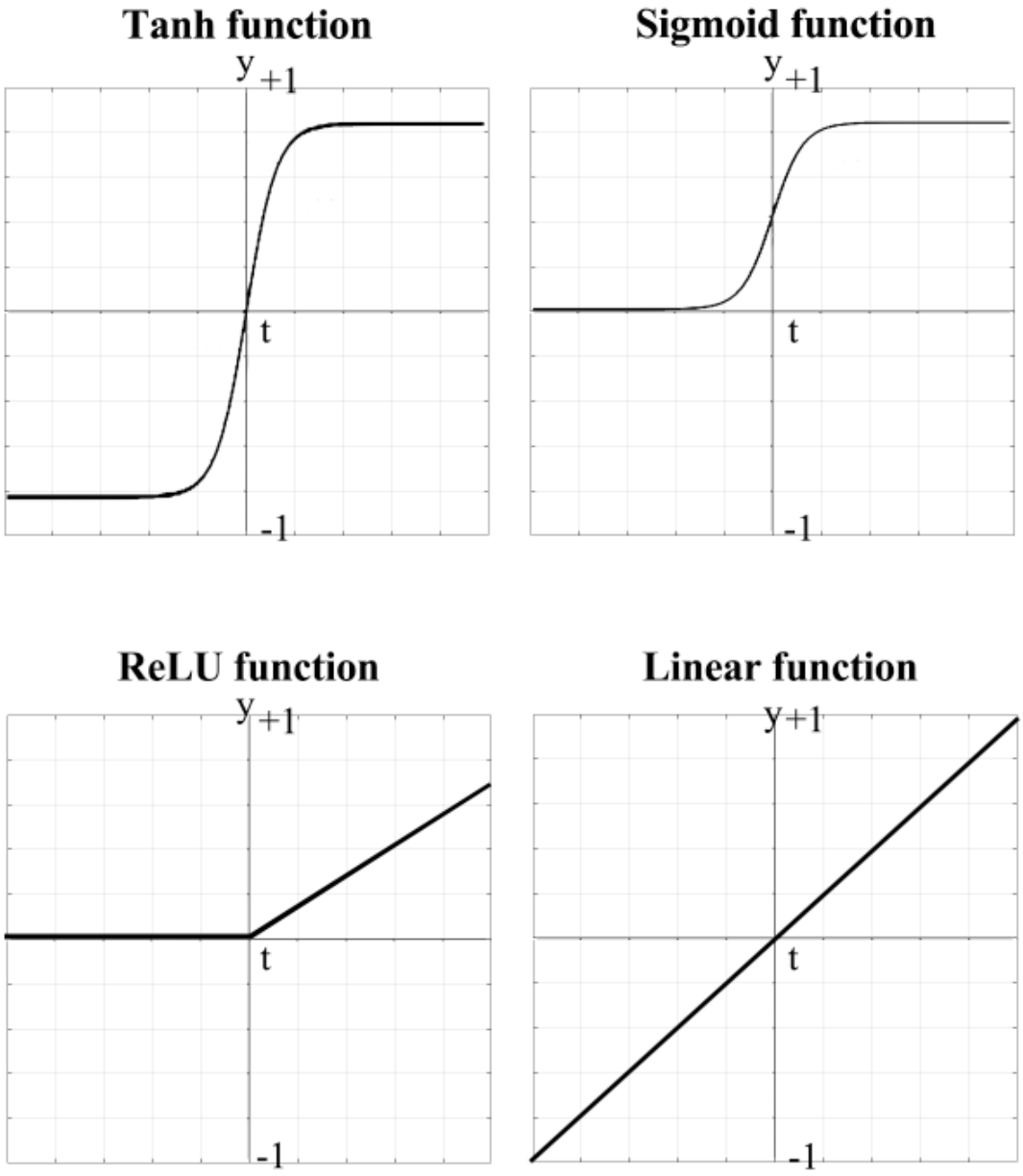


Figure 4.3: Activation functions tanh, sigmoid, ReLU, and linear functions

The most frequently used activation functions are the linear and non-linear functions- the logistic, ReLU, hyperbolic tangent functions, and others, all of which define the output of that node given an input or set of inputs.

$$f(x) = \tanh(x) = \frac{(e^{x} - e^{-x})}{(e^{x} + e^{-x})} \ (tanh\ function) \tag{4.15}$$

$$f(x) = \sigma(x) = \frac{1}{1 + e^{-x}} \ (sigmoid\ function) \tag{4.16}$$

$$f(x) = \begin{cases} 0\ for\ x \leq 0 \\ x\ for\ x > 0 \end{cases} \ (ReLU\ function) \tag{4.17}$$

In recent years, the Rectified Linear Unit (LeLU) has become very popular. It outputs the function *f*(x)=max(0,x). In other words, the activation is simply thresholds at zero. Comparing with tanh or sigmoid neurons that involve exponentials, the ReLU can be implemented by simply thresholding a matrix of activations at zero. The neurons of a network are structured in a single or multi-layer. The most frequently used perception for deep learning is the multi-layer perceptron or MLP (Matuszewski et al., 2017). The nodes of one layer are connected to the next layer's nodes to which they can send information. More precisely, ANN consist of neurons that have learnable weights and biases. Each neuron receives inputs, performs a dot product, and optionally follows it with non-linearity. ANN receive the input and transform it through a series of hidden layers. As shown in Figure 4.4, the last connected layer is called the output layer.

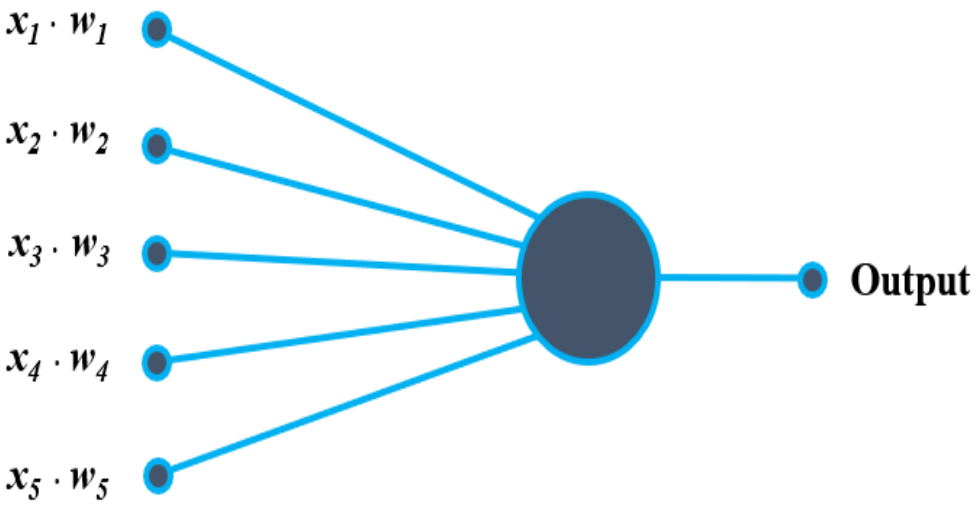


Figure 4.4: Structure of neurons of network

Here, ANN with $O = f\left(\sum_{i=0}^{d} w_i x_i + b\right)$ where $x_0, x_2, x_3, \ldots, x_d$ and output is $O$. Every activation function takes a single number and performs a certain fixed mathematical operation on it.

The advantage of a multi-layer perceptron is that both input and output data can be processed in a continuous or discrete format. It has good predictability in general or is always compared to other algorithms. It is powerful and useful when the relationship between attributes or features is more complex. However, it is difficult to describe the structure and relatively difficult to derive the optimal model, since it is composed of a model close to the black box.

Predictive analytics deals with information retrieval to predict an unknown event of interest, typically a future event. In the present study, sediment transport and profile evolution were intended for the prediction. Using technology that learns from data to predict these unknown events could drive better decisions. Usually, these predictive analytics include readily available data like age, income, marital status, or other open-text types. Using various data, predictive models can uncover patterns and relationships, which allow organizations to anticipate outcomes based on more concrete information than an assumption. The advantage of the ANN is the feedforward networking and back propagation of error (Fine, 1999; Matuszewski et al., 2017), by which the network can be trained to minimize the error up to an acceptable accuracy. The training procedure of the network can select to fit the purpose of supervised and unsupervised training types. In the present study, the back-propagation algorithm with supervised learning was used.

## 4.5 Dataset and Architecture

Each hidden layer consists of a set of neurons. Each neuron is fully connected to all neurons in the previous layer, and where neurons in a single layer function entirely independently and do not share any connections. The last fully-connected layer is called the output layer. The architecture of this research is based on a three-layer perceptron (see Figure 4.5). Seven nodes with the input layer and three hidden layers with 254 nodes were used. These nodes from the hidden layer can be made up infinitely. Here, after using more than 254 nodes, results changed minimal that 254 nodes were used.

The intention was to obtain the final predicted profile; therefore, the node of the output layer was set to one. The aim was to predict the future profile and to compare it with the measured data obtained from the hydraulic model experiments. Thus, beach profile evolution with $t_1$, $t_2$, and $t_3$ was used for the training, and $t_4$ was tested with the output from the prediction.

As the architecture of the ANN model in Table 4.1, seven input parameters were used for both training and testing. Profiles of Case 1, 2, 3, and 4 with SWL 1 and 2 for time $t_1$, $t_2$, $t_3$ were trained. Seven input parameters include cross-shore distance, initial profile, time, height, period, case, and seawater levels with the output (profile evolution) were used in training. For the testing ($t_4$ of each test case), the same input parameters were used to get a final profile evolution as an output. Later, tested outputs were compared with the measured profiles, and the differences were analyzed to see the performances of ANN model in Table 4.2-4.4.

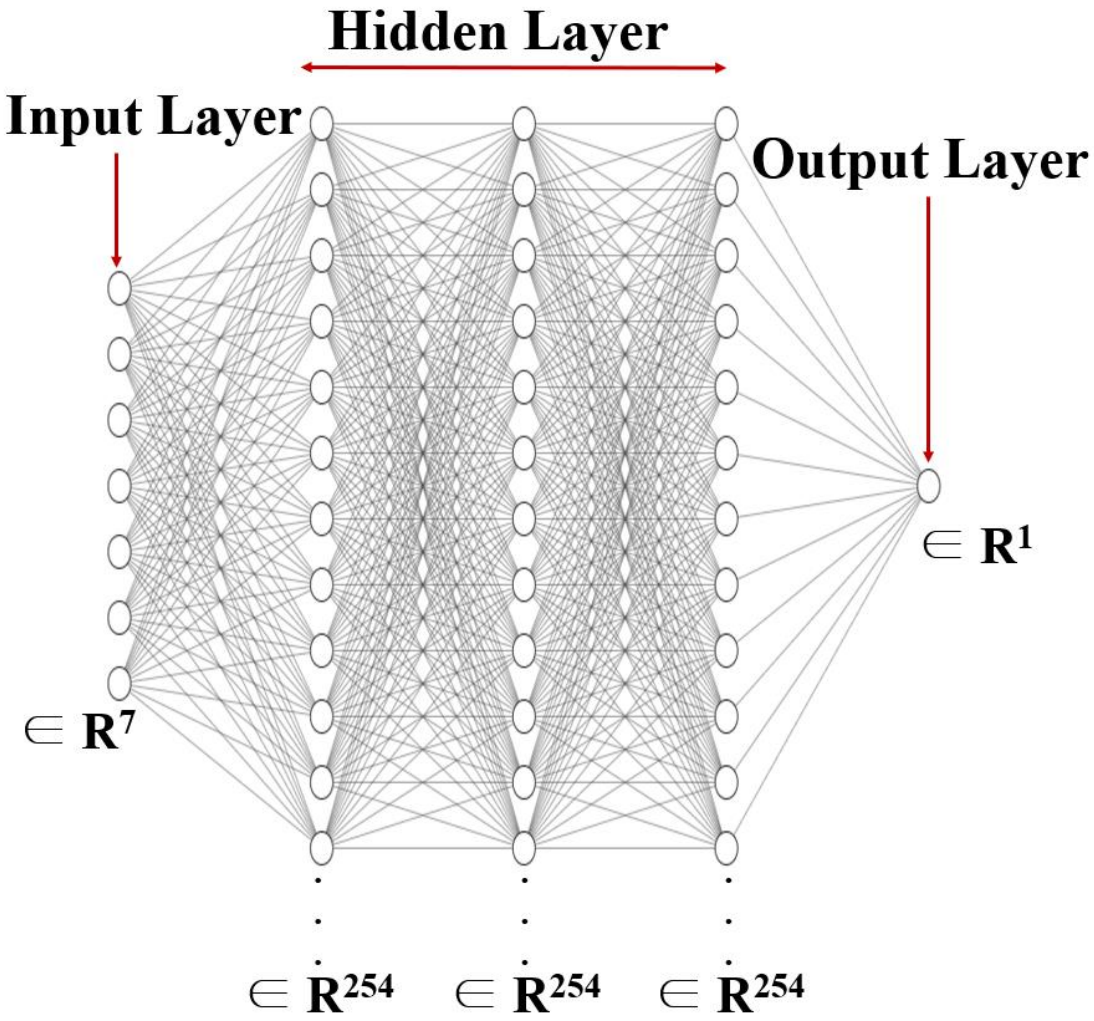


Figure 4.5: Neural network architecture used in the present study

Table 4.1: Architecture of the present study

| **Parameter** | LAF case | RAF case | SAF case |
|---|---|---|---|
| **Model** | Deep Neural Network | | |
| **Input parameter** | Cross-shore distance | | |
| | Initial profile | | |
| | Time | | |
| | Height | | |
| | Period | | |
| | Case | | |
| | Sea Water Level | | |
| **Activation function** | Linear | ReLU | sigmoid |
| **Hidden layer** | 3 | | |
| **Hidden layer's node** | 254 | | |
| **Output node** | 1 | | |
| **Target** | Changed Profile (Profile evolution) | | |

For the parameter of each activation function, Linear activation function (LAF), ReLU activation function (RAF), and sigmoid activation function (SAF) cases were compared. The developed ANN model's performance was evaluated to ensure that the model was able to perform within the pre-defined limits set by the data used for training generally. The conventional approach was used to evaluate the model performance on an independent validation set of data not used in the training process. Root mean square error (*RMSE*), mean absolute error (*MAE*), and mean squared error (*MSE*) were used as evaluation metrics to gauge the prediction accuracy. The *RMSE*, *MAE*, and *MSE* evaluation matrices were defined as follows (see Eq. (4.18) -(4.20)):

$$RMSE = \sqrt{\frac{\sum_i^n (Predicted_i - Actual_i)^2}{n}} \tag{4.18}$$

$$MAE = \frac{1}{n}\sum_i^n |Predicted_i - Actual_i| \tag{4.19}$$

$$MSE = \frac{1}{n}\sum_i^n (Predicted_i - Actual_i)^2 \tag{4.20}$$

where $n$ is the number of test samples; predicted is the predicted beach profile change at $t_4$=120 min, and actual denotes the measured $t_4$ from the hydraulic model experiment.

From the prediction accuracy comparison of using the activation function of LAF, RAF, and SAF cases, all three activation functions have not much differences of error since amount of the training data is not too much (Table 4.2-4.4); however ReLU activation function was chosen since ReLU is a faster learning AF, which has proved to be the most successful and widely used function (Ramachandran et al., 2017) and it's data sparsity which reduces the likelihood of the gradient to vanish.

Table 4.2: Results in RMSE, MAE, MSE (Linear activation function)

| SWL | CASE | RMSE | MAE | MSE |
|---|---|---|---|---|
| **SWL1** | 1 | 0.6663 | 0.6663 | 0.8736 |
| | 2 | 1.2512 | 1.2512 | 3.4243 |
| | 3 | 0.8655 | 0.8655 | 1.4636 |
| | 4 | 0.7411 | 0.7411 | 1.3602 |
| **SWL2** | 1 | 0.7467 | 0.7467 | 0.8849 |
| | 2 | 0.7956 | 0.7956 | 1.1911 |
| | 3 | 0.4788 | 0.4788 | 0.3683 |
| | 4 | 0.6418 | 0.6418 | 0.6751 |

Table 4.3: Results in RMSE, MAE, MSE (ReLU activation function)

| SWL | CASE | RMSE | MAE | MSE |
|---|---|---|---|---|
| **SWL 1** | 1 | 0.6141 | 0.6141 | 0.7235 |
| | 2 | 1.3004 | 1.3004 | 3.9409 |
| | 3 | 0.9777 | 0.9777 | 1.9097 |
| | 4 | 0.8903 | 0.8903 | 1.9033 |
| **SWL 2** | 1 | 0.7559 | 0.7559 | 0.9443 |
| | 2 | 0.8308 | 0.8308 | 1.2265 |
| | 3 | 0.5345 | 0.5345 | 0.4829 |
| | 4 | 0.6398 | 0.6398 | 0.7698 |

Table 4.4: Results in RMSE, MAE, MSE (Sigmoid activation function)

| SWL | CASE | RMSE | MAE | MSE |
|---|---|---|---|---|
| **SWL 1** | 1 | 0.6098 | 0.6098 | 0.6909 |
| | 2 | 1.2353 | 1.2353 | 3.6859 |
| | 3 | 0.9431 | 0.9431 | 1.9205 |
| | 4 | 0.8769 | 0.8769 | 1.7792 |
| **SWL 2** | 1 | 0.7633 | 0.7633 | 0.9537 |
| | 2 | 0.9091 | 0.9091 | 1.6425 |
| | 3 | 0.5691 | 0.5691 | 0.5491 |
| | 4 | 0.6394 | 0.6394 | 0.7830 |

## 4.6 Artificial Intelligence (ANN) model results

In this chapter, ANN was used to predict the future profile evolution of the sediment transport of the sand and gravel nourishment of test cases with sand berm and beach, gravel berm and sand beach, buried gravel layer, and buried gravel sill. After deciding to use the ReLU activation function for the final output, the final beach profile for $t_4$=120 min was compared with that of the hydraulic model experiment. Some drawbacks associated with the practical use of ANN include the possibly long time of the modeling process and the large amount of data required. Figure 4.6 shows the initial profile with SWL for each test cases. Figures 4.7- 4.14 show the predicted beach profile evolution compared to the measured profile from the hydraulic model experiment.

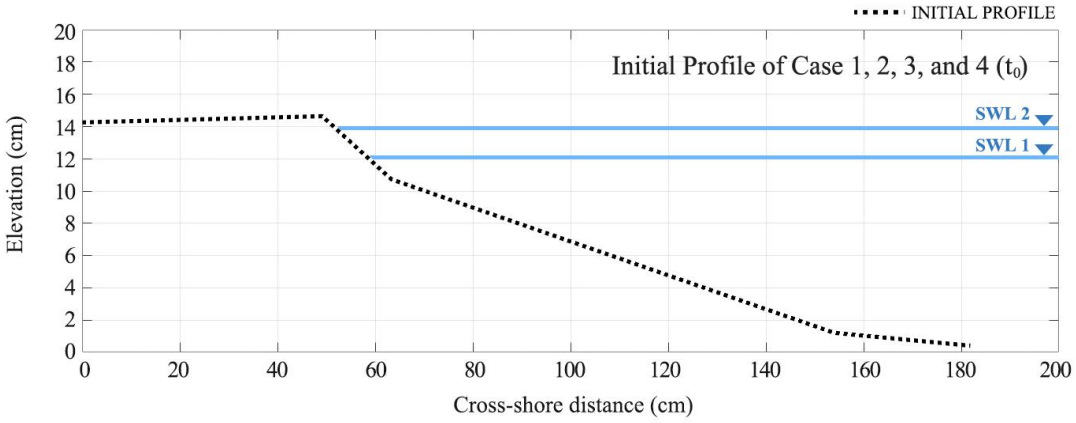


Figure 4.6: Case 1, 2, 3, and 4 initial profile

As shown in Figures 4.7 and 4.8, in test case 1, using only sand nourishment, with SWL 1 and SWL 2 were compared. This profile is the equilibrium beach profile where the ANN model predicted the foreshore very well; however, erosion on the backshore was not accurately predicted on SWL 1. For SWL 2, there was a scour hole

that occurred during $t_2$, and ANN used the previous training data to reproduce the scour. This was due to the lack of data to be trained except three-time steps $t_1$, $t_2$, and $t_3$. However, the overall profile appeared to be reasonable.

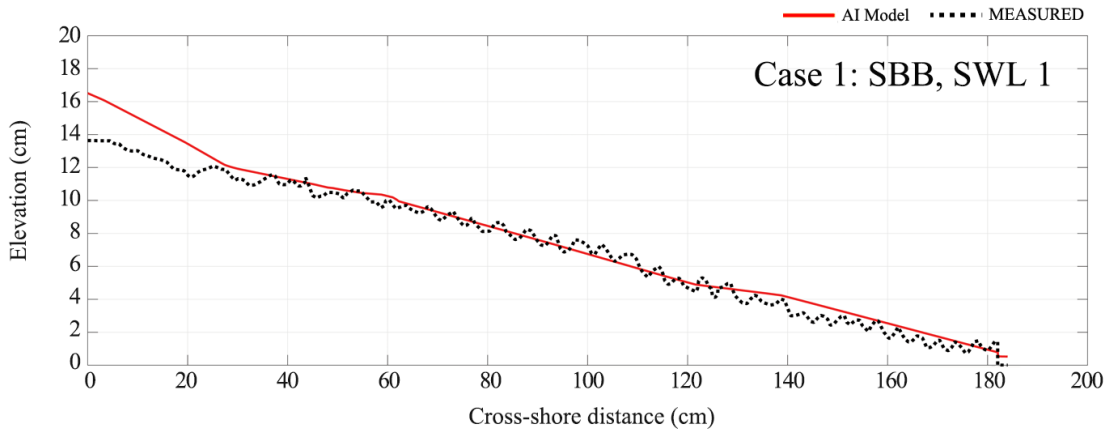


Figure 4.7: Case 1 SWL 1 comparison of ANN prediction and measured from the physical test

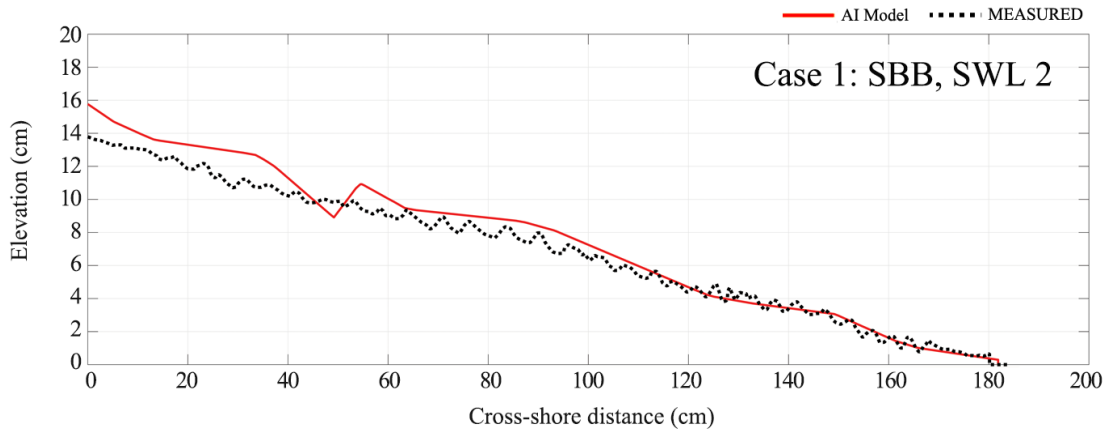


Figure 4.8: Case 1 SWL 2 comparison of ANN prediction and measured from the physical test

Typical gravel nourishment of Tuvalu was reproduced and tested through test case 2 with SWL 1 and SWL 2. Figures 4.9 and 4.10 show the results of the ANN model and compared with the measured profiles. From SWL 1, the ANN model produced the dune on top of the berm like the measured profile; however, the shape and location were not in the exact location. Nonetheless, for the tendency wise, creating the dune on top of the berm, and foreshore erosion were accurately reproduced through ANN. Measured profile of test case 2 with SWL 2 showed the dune forming on the backshore, and the ANN model also predicted the berm shape profile on the backshore. Although, overall tendency appeared to be reasonable, size and location of the dune were not precisely reproduced. One of the main reasons for this inaccuracy may be the lack of the data since only 8 test cases with $t_1$, $t_2$, and $t_3$ were used as the training dataset.

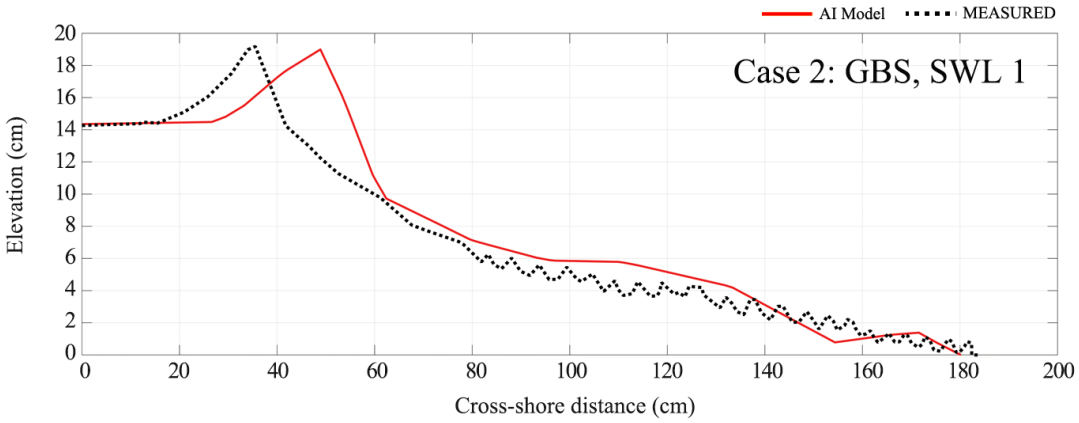


Figure 4.9: Case 2 SWL 1 comparison of ANN prediction and measured from the physical test

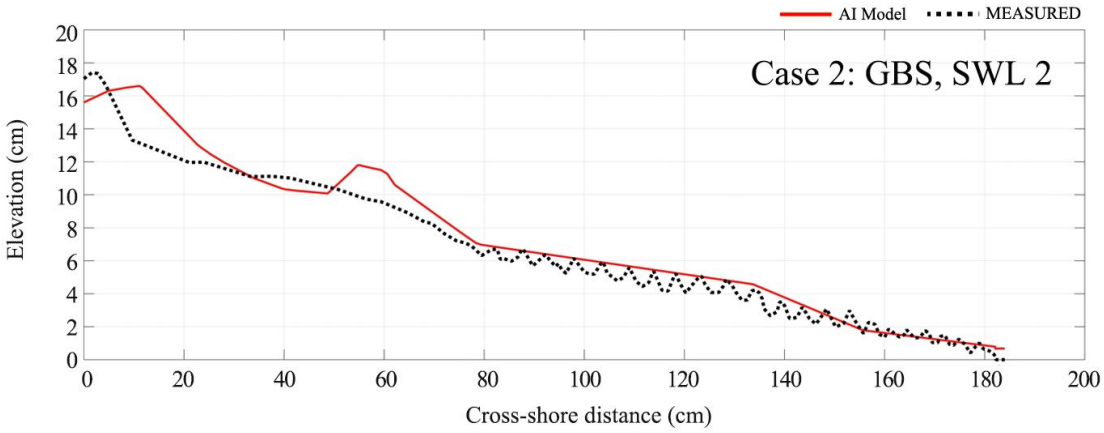


Figure 4.10: Case 2 SWL 2 comparison of ANN prediction and measured from the physical test

In test case 3 with SWL 1 shown in Figure 4.11, the ANN model predicted less erosion on the backshore compared to the measured profile evolution. Even though the overall tendency of beach profile becoming equilibrium was predicted, the amount of erosion was not precisely predicted. Nonetheless, the prediction of ANN on test case 3 with SWL2 in Figure 4.12 was accurate as compared to the measured data. Erosion was accurately predicted on both the berm and the foreshore.

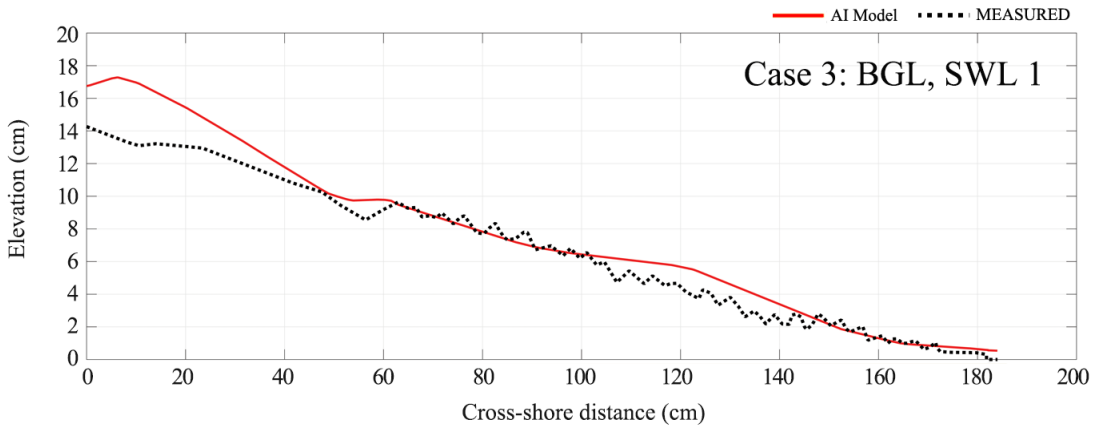


Figure 4.11: Case 3 SWL 1 comparison of ANN prediction and measured from the physical test

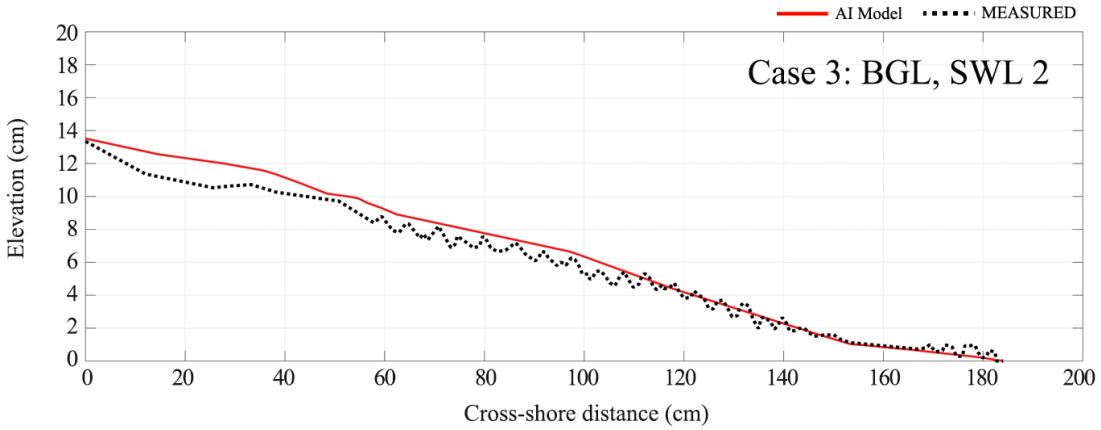


Figure 4.12: Case 3 SWL 2 comparison of ANN prediction and measured from the physical test

Finally, for the test case 4 with SWL 1, similarly to test case 2 with SWL2 in Figure 4.10, the scour hole was predicted on the berm, and less erosion was predicted on the backshore of the beach. As shown in Figure 4.14, foreshore prediction of cross-shore 60 to 180 cm prediction was accurate. Gravel sill did not move so much on the cross-shore 40 – 64 cm in the measured data; however, the tendency of ANN prediction on this section predicted well. The prediction had a dune shape formed on this section unlike measured data. Cross-shore 0 to 40 cm had a reasonable prediction as compared to the measured data.

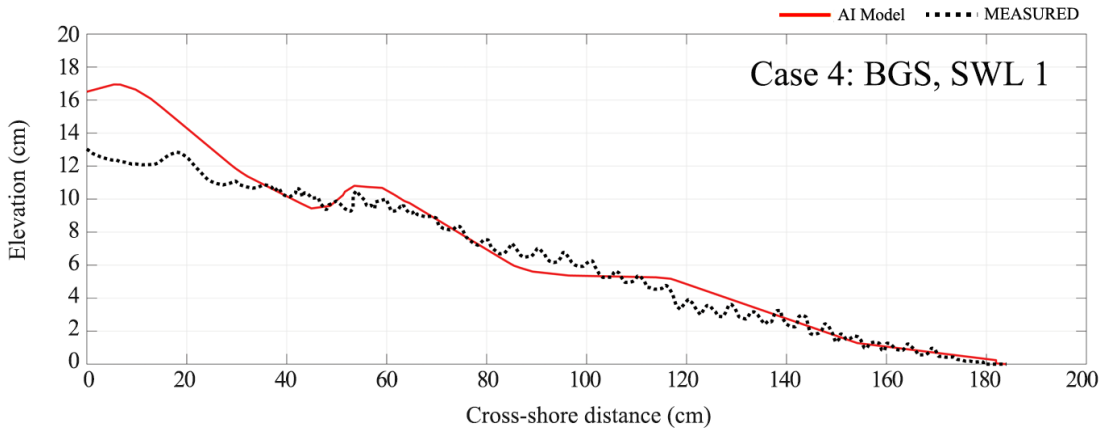


Figure 4.13: Case 4 SWL 1 comparison of ANN prediction and measured from the physical test.

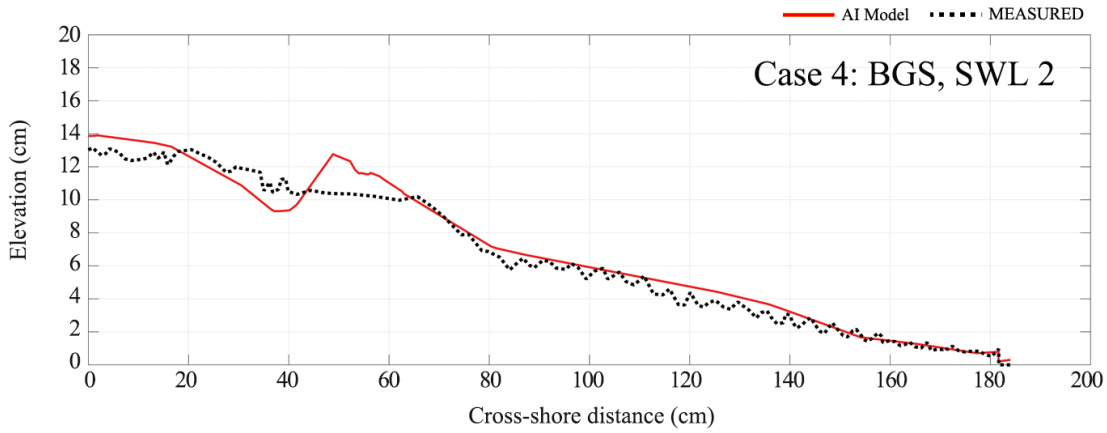


Figure 4.14: Case 4 SWL 2 comparison of ANN prediction and measured from the physical test

Artificial neural networks were used to predict the final profile of test cases 1, 2, 3, and 4 with SWL 1 and 2 (a total of 8 test cases) by training the test cases with time intervals 30 minutes ($t_1$=30 min, $t_2$=60 min, and $t_3$=90 min). For the activation function, the ReLU function was used for the prediction. Throughout the profile comparisons of ANN model and measured data for $t_4$ = 120 min, the ANN model was able to predict the tendency of the erosion quite well with forming the dune on the backshore when using gravel nourishment. However, the ANN model's prediction about the erosion amount of the measured data was reasonable but not precisely accurate. This limitation could have been caused by lack of the dataset used for model training. In the future analysis, more datasets with shorter timesteps should be trained on the model to increase the accuracy of the prediction. Moreover, various types of the initial profile should be trained in order to make the ANN model more robust and accurate. Further researches should be conducted in order to use the model practically.

## 4.7 Data Comparisons

Since the comparison of ANN model can be made with numerical simulation on only test case 1 using only the sand beach profile, three numerical simulation models (CSHORE, SBEACH, and XBEACH-G) were compared with the ANN model. As mentioned in Section 4.3.3, CSHORE most accurately predicted the profile evolution for measured profile at $t_4$=120 min. When comparing the result of CSHORE with that of the ANN model prediction (Figure 4.15), ANN model prediction was more accurate with same tendency of becoming equilibrium profile; however, on the backshore, less erosion has been predicted, and the tendency of the backshore erosion was similar to that of the XBEACH-G.

When the SWL increased to SWL 2 (Figure 4.16), the prediction of the numerical simulation was not very accurate. The ANN model prediction was not very precise as compared to CSHORE. The erosion was overestimated for the CSHORE; however, the ANN model less accurately estimated the erosion. XBEACH-G and SBEACH predictions on SWL 2 were not very accurate. SBEACH predicted too much deposition on the foreshore, while XBEACH-G predicted too much erosion as compared to other models. This may be a problem when the SWL is too high. The ANN model prediction's main focus is that it can be used in any profile without any limitations (e.g., gravel nourishment) so that ANN can be applied and compared with the test cases 2, 3, and 4. Using large amounts of small and field-scale data will increase the accuracy of the current ANN model, highlighting the potential of artificial intelligence applications on the sediment transport prediction of beaches where the numerical simulation cannot predict.

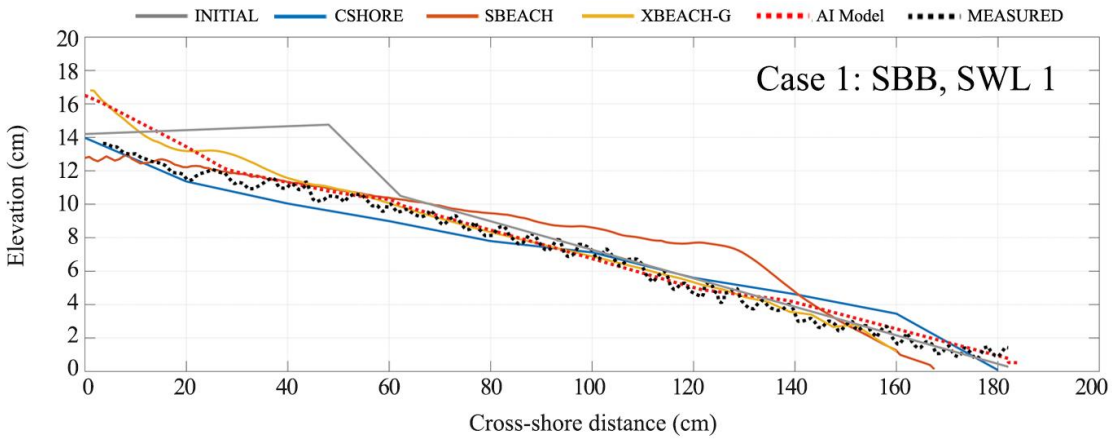


Figure 4.15: Case 1 SWL 1 comparison of numerical simulations and the ANN model

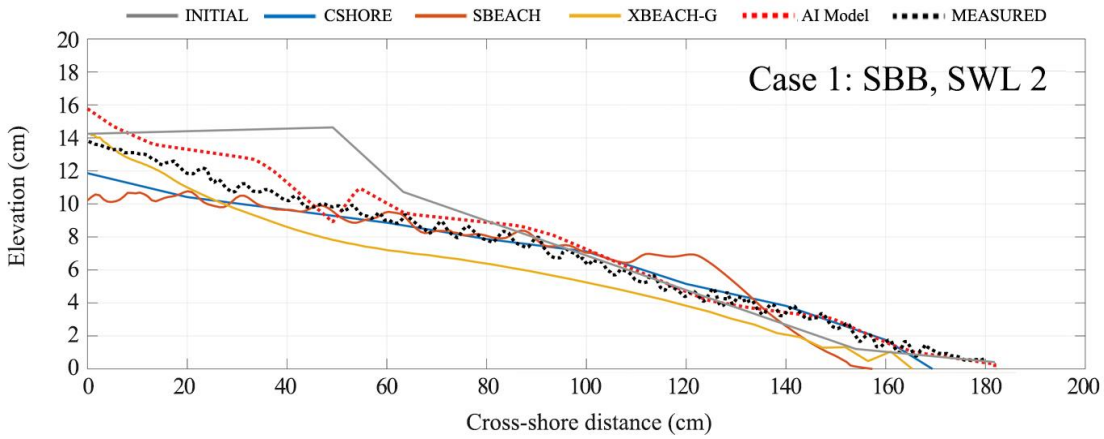


Figure 4.16: Case 1 SWL 2 comparison of numerical simulations and the ANN model

## 4.8 Conclusions

In this chapter, modeling and prediction of beach profile evolution on beaches with gravel nourishments using an artificial intelligence model was performed. The level of reflectivity of the beach is an important parameter to control the magnitude and distribution of the undertow velocity. Throughout the profile, the AI model less accurately estimated the erosion on the backshore; however, in some test cases, the prediction was noticeably accurate. Overall, the tendency for sediment transport was accurately predicted. Training limited dataset can cause less accurate predictions, as neural networks work better with a large amount of data. Therefore, training large amounts of both small- and large-scale data will increase the accuracy of the profile evolution prediction, which can then be applied to many beaches where numerical simulation cannot produce accurate predictions.

Despite the availability of useful numerical simulations, a novel insight provided in this chapter is supplementing the shortcomings of these numerical models by using artificial intelligence. Although the results were obtained through the use of a basic artificial deep learning model, in the future, the model can be upgraded by a comparative review of various artificial intelligence models to make a robust model using more data to be trained. Also, the importance of explainable AI, which can tell what the results mean, as well as create complex and good models, is increasing. At present, it remains challenging to explain what correlations exist and how these results are obtained in analyzing and predicting data using artificial neural networks. Therefore, future studies should contain Explainable AI so that the model can be practically used in coastal engineering.

# Chapter 5

# CONCLUSIONS

## 5.1 Experimental Findings

A laboratory experiment consisting of four test series: SBB, GBS, BGL, BGS and GBL with 40 runs in total (each run consist 30 min) was conducted in a wave flume with a sand beach and a nourished berm to compare the effectiveness of a sand berm and beach (SBB), a gravel berm and sand beach (GBS), a buried gravel layer (BGL), and a buried gravel sill (BGS). The still water level was increased to generate extreme conditions to create accretional profile changes on the foreshore and berm. While SBB test case was vulnerable to the extreme wave conditions and quickly become an equilibrium profile, GBS shows deposition of the berm appeared over time and found to have a good result as a countermeasure against erosion. For the aesthetic and environmental purposes, BGL and BGS cases were tested. Gravel underneath the berm acts as a filter for the permeable layer of gravel and keeps the sand inside the rear section unsaturated for a certain period of time. Scour appeared on BGS, and found to be less efficient compared to BGL. Although it is known fact that the water permeable layer is effective when there is no sea level rise, the gravel water permeable layer has a similar effect even when the sea level rises was confirmed through this research.

BGL was found to be an efficient method in slowing down erosion; however, if the duration of the high wave in an abnormal tide condition becomes longer, eventually, buried gravels were moving onshore and could interrupt the aesthetic view of the beach. Thus, gravel bags were substituted for the gravel layer from BGL, and the gravel bag layer (GBL) was tested to see the difference. No considerable difference was observed for SWL 1 (HHWL condition); however, when the still water level was increased, gravel

bag protected the berm from forming the scour hole, and In SWL 1, the erosion and deposition patterns of case 3 and case 5 were similar; however, in SWL 2 (abnormal tide condition), gravel bag layer was found to have superior erosion control ability as compared to buried gravel layer. This was so because, in the case of test case BGL, as time passed, the role of the gravel permeable layer was reduced by the scattering of some moving gravel into the surface layer. On the other hand, the results confirmed that the gravel bag demonstrated the ability to control erosion for a long time by sufficiently exerting the permeable layer's role despite the passage of time and preserve the aesthetic view at the same time.

## 5.2 Artificial Intelligence

Artificial neural networks were used to predict the final profile. For the activation function, the ReLU function was used for the prediction. Throughout the profile comparisons of artificial neural networks and measured data for the final profile, the artificial neural networks model was able to predict the tendency of the erosion quite well with forming the dune on the backshore even when using gravel nourishment.

When gravel and sand are mixed, such as gravel nourishment, it is challenging to draw results other than the hydraulic model experiment. Throughout the research, application of artificial intelligence in coastal engineering started with the question, ‘if one can create a robust artificial intelligence model by using various hydraulic model experiments and field data as big data, can it be possible to replace the limitations of the numerical simulations composed of mathematical formulas?’. The results showed in this study may be minimal; however, the results were good enough and thought to be the excellent baby step to deepen the convergence of artificial intelligence in coastal

engineering. However, the something to keep in mind is that artificial intelligence is a data-based predictive analyst, so it is essential to use enough data. The more data, the more accurate the prediction. Although, it is vital to verify availability through various model verification before being used practically.

The prediction of the artificial neural networks model about the erosion trend was accurate, but the amount was not so precise. This limitation could have been caused by a lack of the dataset used for model training. In the future analysis, more datasets with shorter timesteps, small- and large-scale experiments should be trained on the model to increase the accuracy of the prediction. Moreover, various tests with various types of beach profiles should be trained to make the AI model more robust and accurate to be used practically.

## REFERENCES


Abambres, M., and Ferreira, A. (2017) "Application of ANN in Pavement Engineering: State-of-Art", Hal-020066889v2.

Bagnold, R.A. (1996) "An Approach to the Sediment Transport Problem from General Physics", USGS Paper 422-I.

Bailard, J.A. (1982) "Modeling On-Offshore Sediment Transport in the Surfzone", 18th International Conference on Coastal Engineering.

Banihabib, M. E., Bandari, R., and Valipour, M. (2020) "Improving Daily Peak Flow Forecasts Using Hybrid Fourier-Series Autoregressive Integrated Moving Average and Recurrent Artificial Neural Network Models", AI 2020, I, 263-275.

Bruun, P. (1954) "Coastal Erosion and the Development of Beach Profiles", Beach Erosion Board Technical Memo, No. 44, US Army Engineer Waterways Experiment Station.

Cammelli, C., Jackson, N.L., Nordstrom, K.F., and Pranzini, E. (2006) "Assessment of a Gravel Nourishment Project Fronting a Seawall at Marina di Pisa, Italy".

Chaudhuri, T.B., and Ghosh, I. (2016) "Artificial Neural Network and Time Series Modeling Based Apporoach to Forecasting the Exchange Rate in Multivariate Framwork", Journal of Insurance and Financial Management, vol. 1, Issue 5, 92-123.

Cohen, O., and Antony, E.J. (2007) "Gravel Beach erosion and nourishment in Nice, French Riviera", Mediterranee,No 108-2007, 99-103.

Davis, R.A., Wang, P., and Silverman, B. (2000) "Comparison of the Performance of Three Adjacent and Differently Constructed Beach Nourishment Projects on the Gulf Peninsula of Florida, Journal of Coastal Research, Vol.16, pp.396-407.

Davison, A.T., Nichollas, R.J., and Leatherman, S.P. (1992) "Beach Nourishment as a Coastal Management Tool: An annotated Bibliography on Developments Associated with the Artificial Nourishment of Beaches", Journal of Coastal Research, (8)4, pp. 984-1022.

Fine, T.L (1999) "Feedforward Neural Network Methodology", Springer, New York

Galappatti, G., and Vreugdnhil, C.B. (1985) "A Depth-integrated Model for Suspended Sediment Transport", Journal of Hydraulic Research, Vol 23, pp. 359-277.

Goda, Y. (1985) “Random Seas and Design of Maritime Structures”, World Scientific, pp. 35.

Google Earth (2017). Fongafale, Tuvalu. 8 31 06.28 N 179 11 46.14 E Eye alt 3.37 km. Maxar Technologies 2017. Http://www.earth.google.com.

Havelin, J. (2012) “Low Cost Options for Shore Protection”, PFH online Course C223 (11 PDH), U.S. Army Corps of Engineers.

Houston, J,R. (1991) “Beachfill performance”, Shore and Beach, vol.59(3), pp. 15-24.

Ishikawa T., Uda, T., and Miyahara, S. (2012) “Moving Gravel Body Method to Control Downcoast Erosion”, Coastal Eng. Proc., 33 (2012), 1- 14.

JICA (2011). “The Study for Assessment of Ecosystem, Coastal Erosion and Protection Rehabilitation of Damaged Area in Tuvalu”, final report, Vol. 1.

Kim, H.D., Kim, K.H., Aoki, S., Koo, S., and Kwak, K. (2019) “Gravel Beach Nourishment at a Low-Wave Energy Environment to Control the Effects of Global Warming”, Coastal Sediment (19)., pp. 329-337.

Kim, H.D. (2017). “Coastal Protection Techniques for Storm Damage: Experimental and Numerical Study on Rock Seawall in Swash Zone to Reduce Wave Overtopping and Overwash of Sand Beach”, MCE thesis paper.

Kim, H.D., Aoki, S., Kim, K.H., and Sohn, J. (2019). “Effectiveness of Eco-Friendly Design Options in Pacific Island Nations”, APAC 2019.

Kim, H.D., Kobayashi, N., and Chávez Cárdenas, X. (2016). “Comparison of rock seawall and dune for storm damage reduction”, Coastal Eng. Proc., 35 (2016), 1-13.

Kobayashi, A., Uda, T., and Noshi, Y. (2016). “Monitoring of Gravel Nourishment on Makuhari Beach in Tokyo Bay”, Coastal Eng. Proc., 35 (2016), pp. 1-9.

Kobayashi, N. (2016). “Coastal sediment transport modeling for engineering applications.” J. Waterway, Port, Coastal, Ocean Eng., 10.1061/ (ASCE) WW.1943-5460.0000347, 03116001.

Kobayashi, N., and Kim, H.D. (2017). “Rock Seawall in the Swash Zone to Reduce Wave Overtopping and Overwash of a Sand Beach”, Journal of Waterway Port Coastal and Ocean Engineering 143(6).

Konate, A (2019) “Artificial Neural Network: a tool for approximating complex functions”, hal-020759

Koo, S. (2018) “A Study for Mitigation Plan and Characteristics of Lagoon Beach Erosion due to Sea Level Rising of Tuvalu at the South Pacific”, Doctoral Dissertation, CKU.

Kumada, T., T. Uda, Matsu-ura,T., and Sumiya, M. (2010) “Field experiment on beach nourishment using gravel at Jinkoji coast”, Proc. 32nd ICCE, sediment. 100, pp. 1-13.

Larson, M. (1996) “A Model of Beach Profile Cahnge under Random Waves”, Journal of Waterways, Port, Harbor, and Coastal Engineering.

Lopez, I., Aragones, I., Villacampa, Y., and Gonzalez, F.J. (2017) “Gravel beach nourishment: Modelling the equilibrium beach profile”, Science of the Total Environment, pp. 772-783.

Matuszewski, J., and Sikorska-Lukasiewicz, K. (2017) “Neural Network Application for Emitter Identification”, International Radar Symposium, pp.1-8.

McCall, R.T., Masselink, G., Poate, T.G., Roelvink, J.A., and Almeida, L.P. (2015) “Modelling the Morphodynamics of Gravel Beaches during Storms with XBEACH-G”, Coastal Engineering, 103(2015), p.52-66.

Ministry of Maritime Affairs and Fisheries. (2005) “Design Criteria for Harbors and Fishery Ports”

Muhajjir, (2019) “Wave-Induced Morphological Change of Composite Sand-Gravel Beach”, Doctoral Dissertation, Osaka University.

National Research Council. (1995) “Beach Nourishment and Protection”, National Academy Press.

Nicholas, R.J., and Cazenave, A (2010) “Sea-Level Rise and Its Impact on Coastal Zones”, Science 328(5985): 1517-1520.

Onaka, S., Ichikawa, S., Izumi, M., Uda, T., and Hirano, J. (2017) “Effectiveness of Gravel Beach Nourishment on Pacific Island”, world scientific, 2017.

Pilarczyk, K.W. (2012) “Impact of the Delta Works on the Recent Developments in Coastal Engineering”, World Scientific Publishing Company Incorporated.

Roelvink, D., Reneiers, A, Dongeren A., and Thiel de Vries, J. (2009) "Modelling Storm Impacts on Beaches, Dunes and Barrier Islands", Coast. Eng., 56(11-12, pp. 1133-1152.

Ramachandran, P., Zoph, B., and Le, Q. (2017) "Searching for Activation Functions", ArXiv, 2017.

Rossi, P., Mancini, F., Dubbini, M., Mazzone, F., and Capra, A. (2017) "Combining Nadir and Oblique UAV Imagery to Reconstruct Quarry Topography: Methodology and Feasibility Analysis", European Journal of Remote Sensing, vol. 50, No.1, pp.211-221.

Salahudeen, A.B., Ijimdiya, T.S., Eberemu, A.O., and Osinubi, K.J. (2018) "Artificial Neural Networks Prediction of Compaction Characteristics of Black Cotton Soil Stabilized with Cement Kiln Dust", Journal of Soft Computing in Civil Engineering, 2-3, 50-71.

Settlemaier, J., Gibbs, A., Santos, P., Freeman, T., and Gaer, D. (2011) "Simulating Waves Nearshore Modeling Efforts at the National Weather Service Southern Region Coastal Weather Forecast Offices", 91th AMS Annual Meeting, P13A.4.

Stive, M.J.F., and De Vriend, H.J. (1987) "Quasi-3D Nearshore Current Modelling: Wave-induced Secondary Current", Proceedings Coastal Hydrodynamics, ASCE, pp. 356-370.

Sumitomo Corporation Europe Limited (2017) "Kyowa Filter Unit", Subsea EXPO 2017, Aberdeen.

Tealab, A. (2018) "Time Series Forecasting using Artificial Neural Networks Methodologies: A Systematic Review", Future Computing and Informatics Journal 3, pp.334-340.

Wieser, W. (1953) "The Effect of Grain Size on the Distribution of Small Invertebrates Inhabiting the Beaches of Puget Sound", 181-194.

Yuan, F. (2017) "Cross-shore Beach Morphological Model for Beach Erosion and Recovery", Doctoral Dissertation, UNSW.